

Dissecting the Graphcore IPU Architecture via Microbenchmarking

Technical Report

December 7, 2019

Zhe Jia
Blake Tillman
Marco Maggioni
Daniele P. Scarpazza



High Performance Computing R&D Team
Citadel, 131 S. Dearborn St., Chicago.

Copyright © 2019, Citadel Enterprise Americas, LLC. All rights reserved.
Chicago, United States of America.

Edition	Date
First	December 7, 2019

The authors make this document available on the [arXiv.org](https://arxiv.org) e-print service owned and operated by Cornell University. Citadel grants arXiv.org a perpetual, non-exclusive license to distribute this manuscript.

Disclaimer. This presentation solely reflects the analysis and views of the authors. No recipient should interpret this presentation to represent the general views of Citadel or its personnel. Facts, analyses, and views presented herein have not been reviewed by, and may not reflect information known to other Citadel professionals.

Objectivity. This research aims at being objective and impartial. The authors strive to ensure that each claim is based on solid evidence. Results published here are meant to be reproducible by anybody who recreates the experimental conditions described by the authors, with the possible exception of good faith mistakes. No such mistakes are known to the authors at the time of publication.

Conflicts of interest. This research was supported entirely by Citadel. Citadel received no financial support from Graphcore or any other entity in connection with this work. Graphcore helped this work by providing an early-availability test system to Citadel, and by reviewing the contents of this manuscript for mistakes and omissions. The authors did not receive any consulting fees, research funding or reimbursement in conjunction with this work, and are not employed by Graphcore.

Acknowledgments. The authors thank their colleague Jeffrey Smith for his valuable input and assistance during the preparation of this manuscript.

All product names, trademarks and registered trademarks are property of their respective owners.

Contents

Contents	3
1 Architecture	7
1.1 Design Philosophy	7
1.2 Fine-grained Parallelism	9
1.3 Arithmetic Throughput	11
1.4 Memory Architecture	12
1.5 Interconnect Architecture	13
1.6 The Bulk Synchronous Parallel Model	15
2 Experimental Setup	17
2.1 System Configuration	17
2.2 Multi-IPUs	21
2.3 Methods	23
3 Local Memory	25
3.1 Latency	25
3.2 Bandwidth	26
4 Interconnect	31
4.1 Point-to-point Transfers	31
4.1.1 Congestion-free Latency	32
4.1.2 Latency between Tiles on a Chip by Proximity	33
4.1.3 Latency between IPUs by Proximity	34
4.1.4 Latency under Load	37
4.1.5 Congestion-free Peak Bandwidth	39
4.1.6 Peak Bandwidth under Load	41
4.1.7 Peak Bandwidth between IPUs by Proximity	43
4.1.8 Multi-threaded Peak Bandwidth	44
4.2 Broadcast	46
4.2.1 Congestion-free Broadcast Latency	47
4.2.2 Peak Broadcast Bandwidth	50
4.2.3 Effect of Message Size on Broadcast Bandwidth	51
4.3 Gather	54
4.3.1 Congestion-free Gather Latency	54

4.3.2	Peak Gather Bandwidth	56
4.4	Scatter	57
4.4.1	Congestion-free Scatter Latency	58
4.4.2	Peak Scatter Bandwidth	59
4.5	All to all	60
4.6	Reduction	60
4.6.1	Minimum Reduction Latency - Weak Scaling	61
4.6.2	Minimum Reduction Latency - Strong Scaling	64
4.6.3	Peak Reduction Bandwidth	64
4.7	Host Connectivity	67
4.7.1	Minimum Host-to-IPU Latency	67
4.7.2	Peak Host-to-IPU Bandwidth	67
5	Notable Arithmetic Primitives	71
5.1	Matrix Multiplication	71
5.2	Convolution	75
5.3	Pseudo-Random Number Generation	83
List of Figures		86
Bibliography		89

Abstract

This report focuses on the architecture and performance of the Intelligence Processing Unit (IPU), a novel, massively parallel platform recently introduced by Graphcore and aimed at Artificial Intelligence/Machine Learning (AI/ML) workloads.

We dissect the IPU’s performance behavior using microbenchmarks that we crafted for the purpose. We study the IPU’s memory organization and performance. We study the latency and bandwidth that the on-chip and off-chip interconnects offer, both in point-to-point transfers and in a spectrum of collective operations, under diverse loads. We evaluate the IPU’s compute power over matrix multiplication, convolution, and AI/ML primitives. We discuss actual performance in comparison with its theoretical limits.

Our findings reveal how the IPU’s architectural design affects its performance. Moreover, they offer simple mental models to predict an application’s performance on the IPU, on the basis of the computation and communication steps it involves.

This report is the natural extension to a novel architecture of a continuing effort of ours [1, 2] that focuses on the microbenchmark-based discovery of massively parallel architectures.

Chapter 1

Architecture

In this chapter, we introduce the reader to the fundamentals of the IPU's architecture and its programming paradigm.

1.1 Design Philosophy

The IPU architecture and its compute paradigm were co-designed from the ground up specifically to tackle machine intelligence workloads. For that reason, they incarnate certain design choices that depart radically from more common architectures like CPUs and GPUs, and might be less familiar to the reader. This section and the following ones discuss these choices and how they affect applications and application designers.

At the heart of any IPU-based system is the IPU processor, of which we offer a simplified block diagram in Figure 1.1. Its design aim is the efficient execution of fine-grained operations across a relatively large number of parallel threads. This means that the IPU, unlike other massively parallel architectures (e.g., the GPU) adapts well to fine-grained, irregular computation that exhibits irregular data accesses. The IPU offers true MIMD (Multiple Instruction, Multiple Data) parallelism and has distributed, local memory as its only form of memory on the device.

Each IPU contains 1,216 processing elements called *tiles*; a tile consists of one computing core plus 256 KiB of local memory. Except for the register file, the IPU offers no memory other than the distributed memories local to each tile.

In addition to the tiles, the IPU processor contains the *exchange*, an on-chip interconnect that allows for high-bandwidth, low-latency communication among tiles.

Each IPU also contains ten *IPU link* interfaces; the IPU link is a Graphcore-proprietary interconnect that enables low latency, high-throughput commu-

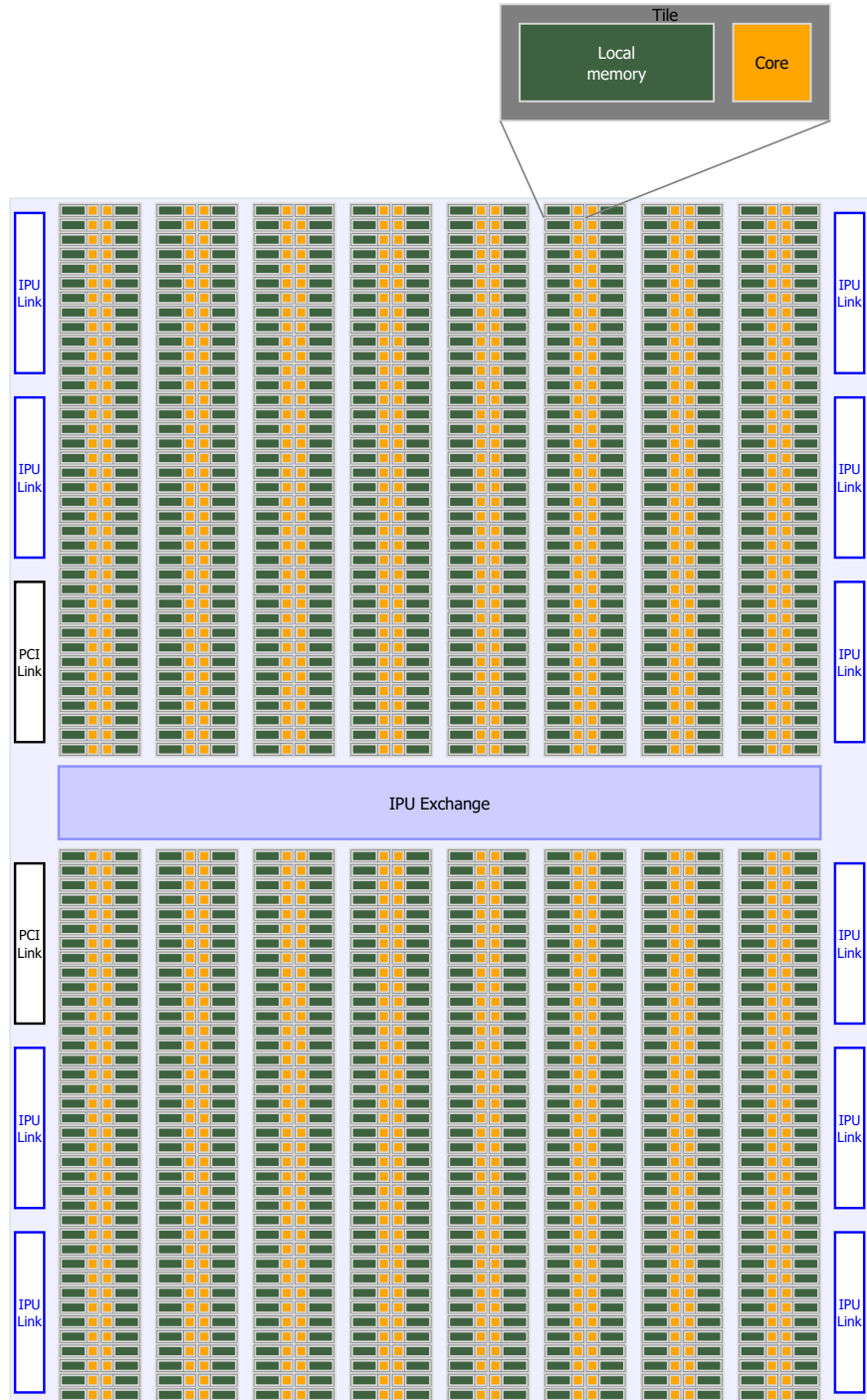


Figure 1.1: Simplified block diagram of an IPU processor: the processor features 1,216 tiles (each containing one core and its local memory), the exchange (an on-chip interconnect), IPU link interfaces that provide connectivity to other IPU chips, and PCIe interfaces for host connectivity.

nication between IPU processors. Because IPU links make transfers between remote tiles as simple to the programmer as between local tiles, they are the linchpin to the IPU paradigm’s scalability. Finally, the IPU contains two PCIe links for communication with CPU-based hosts.

Terminology. While Graphcore’s commercial literature uses the terms IPU-TilesTM, IPU-CoreTM, IPU-ExchangeTM and IPU-LinksTM, we refer to the same components as tiles, core, exchange and IPU links, respectively, with no risk of confusion.

Source. Information we report here on IPU architecture derives from Graphcore’s technical literature or from direct correspondence with Graphcore, and is republished with permission.

1.2 Fine-grained Parallelism

The IPU’s emphasis on *fine-grained* parallelism means that the IPU can efficiently run applications that have irregular and sparse data access patterns and control flow. Unlike SIMD/SIMT architectures, IPUs don’t need large warps of threads consuming contiguous vector data to achieve high efficiency. Instead, IPUs can run individual processing threads on smaller data blocks, in a highly parallel MIMD fashion. Each thread can have completely distinct code and execution flow without incurring performance penalties.

Architecturally, IPUs differ significantly from platforms commonly used to execute ML/AI workloads, namely CPUs and GPUs. We discuss those differences by comparing the fundamental approaches behind the design of CPUs and GPUs with those behind IPUs.

CPUs

CPUs tend to offer complex cores in relatively small counts. CPU cores feature sophisticated latency-reducing techniques like branch prediction, branch speculation, and out-of-order execution. These optimizations make CPUs excel at single-thread performance and control-dominated code, possibly at the expense of energy efficiency and aggregate arithmetic throughput per area of silicon.

Even if most modern CPUs offer vectorization (SIMD, Single Instruction, Multiple Data), they can’t match GPUs in aggregate floating-point arithmetic or in energy efficiency (performance per Watt) on large, regular, array-based workloads.

To hide memory latency, CPUs typically employ a deep memory hierarchy containing multiple levels of caches, together with prefetching and sophisticated prefetch predictors.

GPUs

GPUs, in contrast, feature smaller cores in a significantly higher count per device (e.g., thousands). GPU cores are architecturally simpler than those of CPUs and do not typically offer branch speculation, sophisticated branch prediction, out-of-order execution, or hardware prefetching.

GPUs arrange their cores into clusters that operate in lockstep; all cores in a cluster execute the same instruction at any point in time. Threads are grouped together in warps; warps are scheduled together to clusters. Threads in a warp will perform the same operation on independent data. This execution model is referred to as SIMT: Single Instruction, Multiple Threads.

Even though GPUs have evolved deep memory hierarchies featuring both cache and scratchpad memories [1, 2], their fundamental approach to hiding memory latency remains the oversubscription of threads to cores and the ability to inexpensively switch among threads. In this approach, when a warp of threads is awaiting operands from main memory, the hardware can suspend them and switch to another warp that has received its operands from memory and is ready to continue. The programming model explicitly encourages developers to expose sufficient thread parallelism so that a portion of the threads are always ready to execute, while the remainder await operands.

GPUs only access main memory at peak throughput when load/store operations within each warp involve contiguous regions of memory; that access is said to be *coalesced*. Uncoalesced memory accesses only achieve a fraction of the theoretical peak memory bandwidth. For best performance, developers must instantiate large blocks of threads that share the same program, attempt to consume input data (and produce output) in a coordinated, coalesced manner, and use control flow sparingly. Because of the SIMT model, GPUs pay a performance penalty when threads diverge in their control flow.

Because of their organization, GPUs excel at regular, dense, numerical, data-flow-dominated workloads that naturally lead to coalesced accesses and a coherent control flow. On these workloads, GPUs also tend to be more energy efficient than CPUs because they dedicate a higher fraction of their silicon to arithmetic units, rather than caches and latency-oriented features. Moreover, GPUs refactor instruction decoding circuitry outside of individual cores; this is possible because clusters of cores operate on the same instruction.

IPUs

IPUs provide large core counts (1,216 per processor) and offer cores complex enough to be capable of executing completely distinct programs. The IPU's approach to reducing memory latency is radical—it does away with shared memory entirely. The IPU only offers small, distributed memories that are local and tightly coupled to each core. Each tile contains 256 KiB of memory, totaling 304 MiB per device.

IPU memories are scratchpads, not caches. They are implemented as

SRAM and therefore offer much higher bandwidth (45 TB/s, aggregate) and lower latency (6 clock cycles) than DRAMs. Their performance is comparable to L2 CPU caches and superior to GPU shared memories (or L1 caches). Section 1.4 extends our discussion on memory.

IPU cores pay no penalty when their control flows diverge or when the addresses of their memory accesses diverge. In fact, they pay no penalty for running disjoint instruction flows that exhibit uncorrelated memory accesses. Cores access data from their respective local memory at a fixed cost that is independent of access patterns. This makes IPUs more efficient than GPUs at executing applications with irregular or random data access patterns and/or applications that are control-flow dominated, provided that working sets fit in IPU memory.

Similarly to CPUs and GPUs, IPUs achieve higher efficiency by oversubscribing threads to cores. Specifically, each IPU tile offers hardware support for 6 threads in a manner that is functionally similar to the SMT technique (Simultaneous MultiThreading, or Intel’s Hyper-Threading) commonly found on CPUs. Each IPU tile maintains 6 resident execution contexts and multiplexes them onto shared resources, thus hiding instruction latencies (dependency, memory access and branch latencies), reducing corresponding pipeline stalls, and increasing aggregate throughput. Each tile rotates among threads according to a static, round-robin schedule. The entire IPU supports therefore $6 \times 1,216 = 7,296$ threads. For maximum occupancy, software designers are encouraged to instantiate that many threads.

On the IPU, efficiency on irregular workloads does not come at the expenses of regular, numerical, array- or matrix-based workloads, which are known to run well on GPUs. In the next section we show that IPUs outperform GPUs on a per-board comparison when operands fit in memory.

1.3 Arithmetic Throughput

The IPU offers an impressive arithmetic throughput, up to 31.1 TFlops/s in single precision and 124.5 TFlops/s in mixed precision¹ per chip, surpassing contemporary GPUs in a comparison of theoretical limits.

In a per-board comparison, the IPU’s theoretical advantage over the GPU grows roughly by a factor of two, and so it does in an energy efficiency comparison.

This level of throughput is made possible by the use of specialized pipelines called *Accumulating Matrix Product* (AMP) units that are present in each IPU tile. AMP unit are used to accelerate matrix multiplication and con-

¹With *mixed precision* we denote operations in which multiplicands are in half precision (FP16) and their products are accumulated onto a single precision result (FP32).

volution operations. An AMP unit can finish 64 mixed-precision or 16 single-precision floating point operations per clock cycle.

However, actual arithmetic performance, both on IPUs and GPU, depends dramatically on the properties of the specific numerical workload at hand, and may significantly differ from theoretical limits. Evaluating the IPU’s arithmetic performance on a meaningful basket of real-world numerical workloads is far outside of the scope of a microbenchmarking report like this. However, we benchmark matrix multiplication performance as offered by Poplar’s linear algebra library (poplin) and we compare them with theoretical limits, and with respective performance numbers associated with NVidia’s V100 GPU.

The actual performance we measured shows the IPU as a clear winner in single precision against NVidia’s V100 GPU (per-chip comparison). In mixed precision, the comparison does not yield a clear winner and requires a more nuanced discussion. We postpone this discussion, together with experimental setup details and quantitative results to Section 5.1, which is entirely dedicated to the matrix multiplication workload.

1.4 Memory Architecture

In the IPU’s fine-grained processing philosophy, the role of local memories is fundamental. In fact, the very choice to adopt distributed SRAM memories located next to the cores is what allows threads to access data efficiently even when access patterns are irregular, sparse and incoherent at a fine grain.

Each tile contains 256 KiB, totaling 304 MiB on the entire processor. Each tile owns an independent, contiguous 21-bit address space that is shared among the 6 hardware execution contexts, where code executed locally and data processed locally must fit. The nominal aggregate bandwidth for the entire IPU memory is 45 TB/s, while the latency is 6 clock cycles.

While the IPU’s aggregate capacity is lower than the typical DRAM memory on a GPU (e.g., 32 GiB), IPU memories make up in speed what they lack in capacity; they have shorter latency than both L1 caches and shared memories on the NVidia Turing T4 GPUs, and comparable latency with L2 caches on Intel Skylake/Kaby Lake/Coffee Lake CPUs. See Table 1.1 for a quantitative comparison between IPU memory and SRAM memories with comparable latency on GPUs and CPUs.

As far as capacity is concerned, the aggregate IPU memory is larger than memory layers of equivalent latency on CPUs and GPUs, surpassing them by one to two orders of magnitude (see column *Per-chip Capacity* in Table 1.1). The aggregate size of the IPU’s memory removes the need for a cache hierarchy similar to those found on GPUs and CPUs.

We dedicate the entirety of Chapter 3 to studying the performance of the IPU’s local memory, which we measure via microbenchmarks.

Architecture	Memory	Per-chip Capacity (MiB)	Latency (ns)	Latency (cycles)	Clock Frequency (GHz)
Graphcore IPU	Tile-local	304	3.75	6	1.60
Nvidia T4 GPU	Shared	1.25 ... 2.5	11.94	19	1.59
	L1	1.25 ... 2.5	20.13	32	
Intel *-Lake CPU	L1D	0.25 ... 0.875	0.93 ... 1.92	4 ... 5	2.60 ... 4.30
	L2	4 ... 28	2.79 ... 4.62	12	

Table 1.1: Size and latency comparison between IPU memories and similar SRAM-based memory hierarchy levels on contemporary GPUs and CPUs. The IPU’s local memory has lower latency than the fastest memories on the Turing GPUs and is on par with the L2 cache in modern Intel CPUs. However, the IPU’s local memory is vastly larger than those memories in a per-chip comparison. (Intel data: from public sources; intervals range over the product offering at the time of the writing. GPU data: from our prior work [2].)

The IPU’s memory organization requires software designers to partition their working set across the tiles’ memories appropriately and make tiles exchange data with each other when they need non-local operands. The programming model, along with Graphcore’s Poplar language and associated compiler, allows for the automatic orchestration of these data transfers. Designers describe the operands’ flow but need not worry about explicit variable placement and transfer scheduling. Transient data that is only consumed once should be streamed into the device via PCI from the host.

Graphcore’s optimized machine-learning and linear algebra libraries adopt the data partitioning approach we described. Performance-sensitive software designers are encouraged to follow it as well.

The cumulative memory of 304 MiB per IPU (608 MiB per board) is typically sufficient for many models used in contemporary AI/ML applications to reside entirely on-chip. Models that fit entirely on chip benefit from the high bandwidth and low latency offered by local memory. Models of larger size can be sharded across IPU processors and IPU boards, thanks to the architectural and programming paradigm features described in the next section.

1.5 Interconnect Architecture

The IPU interconnect is what allows tiles on an IPU system to work tightly together and exchange data efficiently with each other. It is also what truly makes a system with multiple IPUs act as a single, coherent machine.

A system with multiple IPUs exposes the single IPU devices independently, but it also exposes *Multi-IPUs*. A Multi-IPU is a virtual IPU device that is comprised of multiple physical IPUs and offers all their memory and compute resources as if they belonged to a single device. The ability to federate multiple physical IPUs into a virtual, monolithic device is precisely what

allows users to train and infer models larger than a single IPU’s capacity, while also taking advantage of the cumulative compute power. Software designers can scale their applications to multiple IPUs with no additional development effort because the same APIs can target physical IPUs or Multi-IPUs indifferently. The tight cooperation between on-chip exchanges and IPU links is the crucial factor that allows Multi-IPUs to exist and put the cumulative memory capacity and compute resources of its participants at the developer’s disposal.

To study the IPU’s on-chip and off-chip interconnect performance, we adopt the terms, the methods and the interests of classic research focusing on the characterization of parallel systems and high-performance networks [3, 4, 5, 6].

On chip, the interconnect exhibits an impressive aggregate throughput of 7.7 TB/s (actual). We measured this throughput under load, with all tiles transferring data concurrently to randomly selected destinations, with a benchmark that is representative of all-to-all exchanges (Section 4.1.6). On a per-tile basis, each of the 1,216 tiles can simultaneously use 6.3 GB/s of bandwidth to transfer data to an arbitrary destination on chip. The latency of an on-chip tile-to-tile exchange is 165 nanoseconds or lower and does not degrade under load above that value.

In multiprocessor systems, the exchange and the IPU links work together to support tile-to-tile communication transparently to the user, regardless of where in the system the two endpoints are located; it is as easy to program a Multi-IPU as it is a single, physical IPU.

Each board is connected to peer boards via IPU links and to its host system via PCIe interfaces. The 2 IPUs on each board are connected by three links with a nominal bidirectional bandwidth of 64 GB/s each, two of which reserved for intra-board transfers. Our benchmarks achieved an actual bandwidth of 108 GB/s.

Connecting boards in an IPU-link network is the key to building larger IPU-based systems. While our study is limited to a single-host configuration featuring 8 boards, much larger systems can be built, including hostless systems. They are beyond the scope of this report. Although different network topologies are possible, our experimental evaluation focuses on the concrete configuration adopted in the test system provided to us by Graphcore; we describe it in detail in Chapter 2.

Then, we dedicate the entirety of Chapter 4 to the study of the IPU’s interconnect performance, both on chip and across chips.

In summary, we remark two general observations:

- **performance:** the aggregate arithmetic resources of the virtual IPU scale linearly, and the overall interconnect performance scales relatively well.

For example, communication latencies degrade gracefully with system diameter, as our benchmarking results show in Sections 4.1.1 and 4.1.3;

- **programmability:** the Multi-IPU programming model is transparent to the developer. The underlying hardware makes the abstraction efficient and, in practice, no extra development effort is needed to scale applications onto large IPU systems. In contrast, CUDA applications do require extra development effort and complexity to parallelize across multiple GPUs, and even more to parallelize across hosts. The same is true for CPU parallel applications, especially across hosts.

1.6 The Bulk Synchronous Parallel Model

An important design factor that underlies the IPU programming paradigm is the Bulk Synchronous Parallel (BSP) model [7]. BSP is the very approach that IPUs use to organize their compute and exchange operations.

Proposed in the 1980s, the BSP model is an abstraction for parallel computation that facilitates expressing parallel algorithms and reasoning on the performance they achieve as they execute on parallel computers.

The BSP model organizes computation in multiple sequential *supersteps*; a superstep is composed of a local computation phase, followed by a communication phase and a barrier synchronization:

- in the **local computation** phase, every process performs computation that operates solely on local memory. No communication between processes occurs in this phase;
- in the **communication** phase, processes exchange data; each process may send a message to each desired destination counterpart (all-to-all personalized exchange). No computation occurs in this phase;
- a **barrier** synchronization phase follows; no process continues to the next superstep till all processes have reached the barrier. Neither computation nor communication occurs in this phase except for that strictly required by the barrier itself.

Processes can use the communication phase not only to send each other intermediate computation results, but also to request and (at a later communications stage) receive data from remote memories. This mechanism allows each process to use any other's local memory as a remote memory and to ultimately access the entire aggregate system memory as one larger store.

Parallel algorithms of arbitrary complexity can be described in the BSP model without restriction of generality.

The IPU is a true BSP machine. It faithfully incarnates hardware support, enforcement and optimization for the three phases of each BSP superstep. Its programming model lets programmers specify processes in terms of graph vertices that compute on local data (and local data *only*).

Input operands are brought to each process by the run-time system before the computation begins, in the communication step associated with the previous superstep.

The programming model and the hardware jointly enforce the separation between phases:

- IPU cores can only access directly local memories; this organization naturally enforces the *local* restriction of the computation phase;
- the on-chip exchange provides native hardware support and acceleration for the all-to-all exchanges of the communication phase ...
- and for the barrier synchronization as well.

In the IPU paradigm supported by the Poplar SDK, programmers describe computation as vertices, data as tensors and data exchanges as static edges, without having to worry about allocation of data at rest in local memories, allocation of input/output transfer buffers, or scheduling of transfers. All these tasks are carried out by the Poplar compiler. The compiler organizes the processing of machine intelligence models exclusively using this BSP paradigm.

Because the IPU implements the BSP model using its exchange and IPU links, the interconnect's performance is the primary factor that determines the performance of BSP communication and synchronization phases and ultimately affects overall application performance. We dedicate Chapter 4 to study the performance of intra- and inter-IPU transfers via benchmarks. Those benchmarks are, in fact, compiled into and executed as BSP communication and barrier synchronization phases.

Chapter 2

Experimental Setup

In this chapter, we specify the experimental system setup we use in our benchmarks. Of particular interest to the reader is the IPU link network topology, which determines the IPUs' relative proximity to each other and influences the performance of data transfers across IPUs.

2.1 System Configuration

All results in this report derive from benchmarks that we ran on a test system provided by Graphcore and equipped with 8 Graphcore C2 PCIe boards. Each C2 board hosts 2 IPU processors running at 1.6 GHz. While this test system was configured for 1.6 GHz IPU operation, production systems may differ in configuration and performance; contact Graphcore directly for inquiries.

We show a simplified representation of the server's topology and its connections in Figure 2.1. The system features two Intel Xeon Platinum 8168 CPUs, each containing 24 cores, with 33 MiB of L3 cache and a clock frequency of 2.70 GHz.

IPUs are connected to each other via IPU links, organized in a ladder network (thin and thick blue arrows in the figure). The network topology directly explains the interconnect performance that we measured (Chapter 4).

In this ladder-shaped topology,

- each vertical “side rail” represents one single-link chain connecting either all even or all odd IPUs; each such link has a nominal 64 GB/s bandwidth;
- each horizontal “rung” (thick, horizontal, blue arrow) represents a triple-link, bundled connection between the two IPUs on each C2 board. The three links offer a nominal bidirectional bandwidth of 64 GB/s each, or 192 GB/s aggregate.

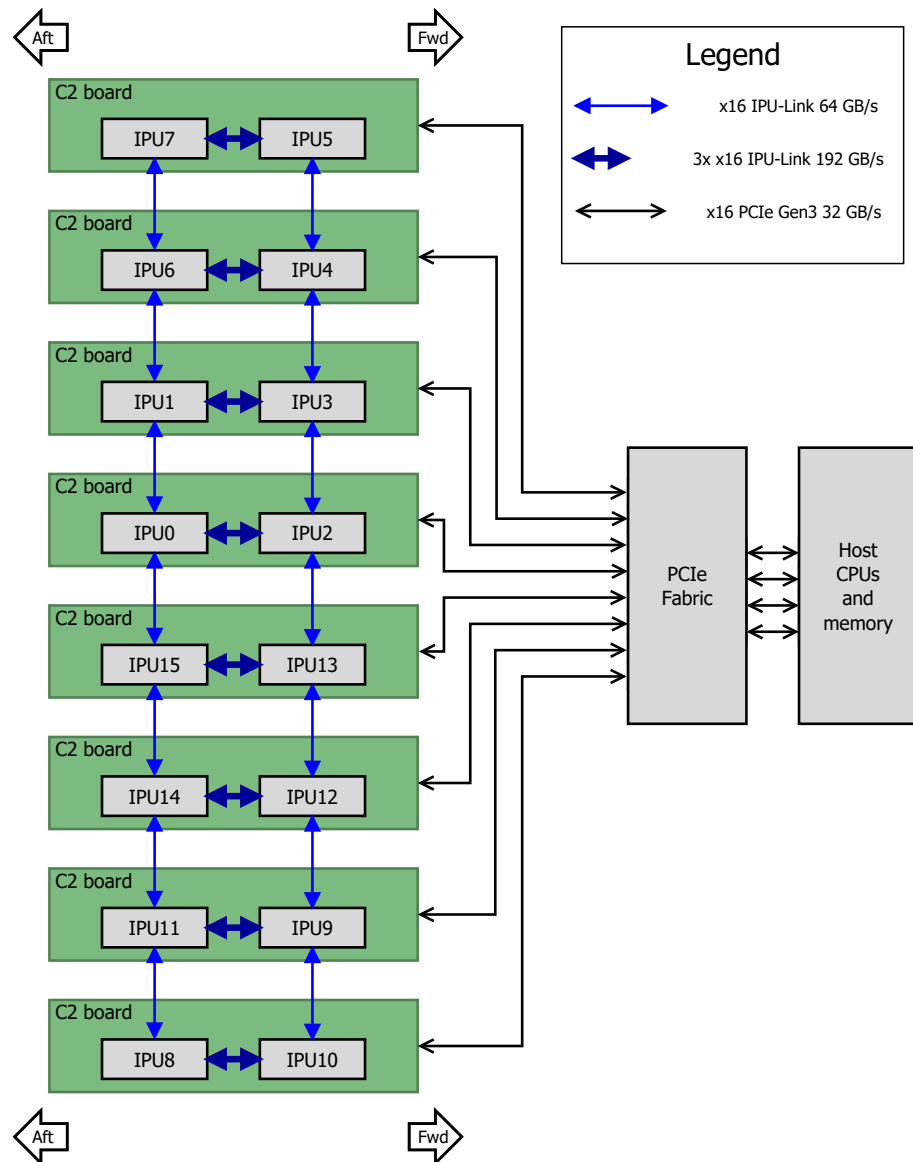


Figure 2.1: Topology and interconnection of C2 boards and IPU processors in the system that we employed in all our experiments. All IPU numbers in this figure are *Device IDs*. Board placement in the chassis is depicted accurately (see Fwd and Aft arrows).

The routing of traffic along the bundled on-board IPU links is statically configured so that:

- two links are reserved for data transfers where the two IPUs on a board are the source and destination; this yields a 128 GB/s nominal aggregate bidirectional bandwidth between the two IPUs of each board;
- one link is reserved for *pass-through* transfers, where either the source or the destination IPU belongs to another board and has a different parity.

In the topology, each board has exactly two neighbors, with the exception of the first and last boards, which only have one neighbor. Each IPU is connected directly to the other IPU on the same C2 board and up to two other IPUs located on neighboring boards. For example, IPU1 is connected directly to IPU3 (on the same board), and to IPU0 and IPU6 (on different boards). IPU0 is not directly connected to IPU3; each data transfer from IPU0 to IPU3 uses either IPU1 or IPU2 as a relay.

For the avoidance of doubt, the ladder structure is not a torus, i.e., it does not wrap around at the edges. The card hosting IPUs 7 and 5 is not a neighbor of the card hosting IPUs 8 and 10. A transfer from IPU7 to IPU8 must traverse the entire ladder vertically.

All the IPU numbers we use here are *Device ID* numbers as exposed and used by the Poplar SDK and by the IPU's command-line tools. Device IDs reflect the lexicographic order of the respective devices' PCI domains, not their physical placement in the server. For these reasons, Device IDs do not respect proximity in the network topology. IPUs with consecutive Device IDs are not on the same board or, in general, neighbors. For example, consider IPU pair 7 and 8. On the other hand, Poplar provides a mapping (DNC IDs) that accounts for the IPU's network proximity. We discuss that in the next section.

Our microbenchmarks reveal that proximity matters. Specifically, tile proximity directly affects the latency between pairs of tiles in on-chip communication, and network proximity between IPUs directly affects inter-IPU latency.

Neighboring IPUs experience the lowest round-trip latency when communicating with each other, whereas marginal latency increases progressively when the endpoint IPUs are farther and farther away. For example, the two IPUs on a board can typically perform a minimum data transfer in 0.63...0.83 microseconds, and two neighboring IPUs of same parity can perform a transfer in 0.54...0.77 microseconds; any addition hop costs on average 0.16 microseconds (varying between 0.145 and 0.174); we present these results in Section 4.1.3 and Figure 4.4. IPUs 7 and 10 are the farthest pair and experience a latency of approximately 1.76 microseconds.

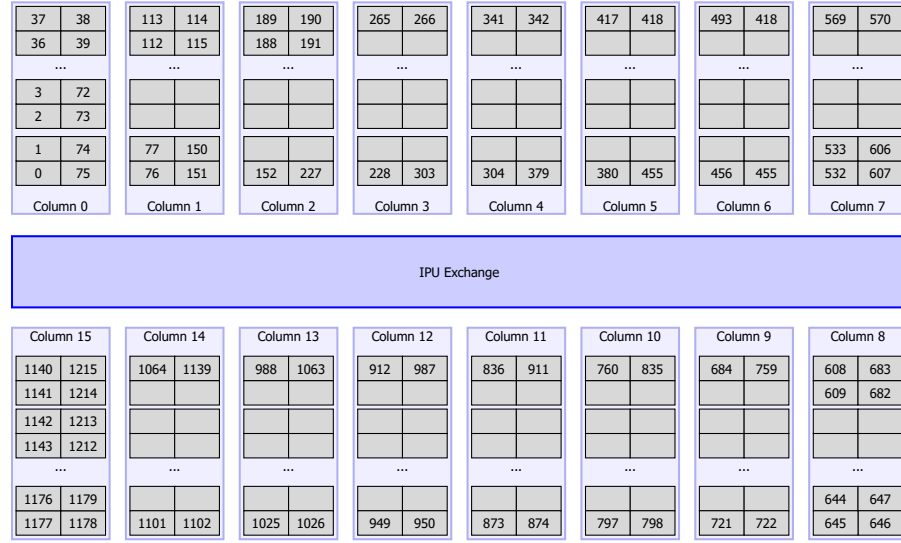


Figure 2.2: Detailed tile layout within an IPU processor, including tile numbering. The logical tile IDs depicted are those exposed to the programmer. Tiles topologically close to each other actually experience shorter communication latencies than tiles farther away (see Section 4.1.2). Source: direct communication with Graphcore.

On the other hand, peak bandwidth between two endpoint IPUs is not affected by their proximity (Figure 4.6) as the topology suggests. Also in accordance with topology are our findings on bidirectional communications between the IPUs on each board: we achieved 108 GB/s, or 84% of the nominal peak bandwidth (Section 4.1.6, Table 4.6). We find that monodirectional bandwidth achieves almost exactly half that much bandwidth.

The cursory results we just listed are only examples of our findings; the next chapter is entirely dedicated to studying the IPU's interconnect performance in diverse communication patterns and under different loads, as measured with our benchmarks.

Tile numbering. The on-chip interconnect among tiles within an IPU is represented in Figure 2.2, where the actual logical tile ID numbering is shown. Tiles are arranged in columns containing 76 total tiles. These 76 tiles are organized in 19 *islands* containing four tiles each. Our benchmarks shows that proximity affects latency and that neighboring tiles within the same island experience a marginally shorter latency between each other than tiles further away within the same column. Tiles in different columns experience a marginally higher latency.

A developer who is strongly focused on latency could, at the extreme, manually place compute vertices on tiles in order to take advantage of the

respective proximities.

2.2 Multi-IPUs

This section discusses how the platform groups physical IPUs into virtual Multi-IPU devices and how IPU tiles are numbered within each Multi-IPU device. All details reflect the concrete configuration of the Graphcore evaluation system we benchmarked.

On our evaluation system, the drivers and SDK expose the exact set of Multi-IPU devices of Figure 2.3. Each Multi-IPU possesses a unique Device ID; their numbering resumes from where physical ID numbering ends. On our system, the highest-numbered physical IPU has Device ID 15, and the first Multi-IPU (virtual) has Device ID 16.

For performance reasons, Multi-IPU are constructed only out of neighboring IPUs and only in powers of two (2, 4, 8, and 16 IPUs). All 2-IPU devices contain a pair of IPUs residing on the same board. For example, IPU16 contains IPU7 and IPU5. All 4-IPU devices contains the IPU from a pair of C2 cards that are neighbors in the ladder network topology, and so on.

Multi-IPUs correspond to partitions of the following sequence of Device IDs into equally-sized, contiguous sub-sequences with power-of-two lengths:

$$5, 7, 4, 6, 3, 1, 2, 0, 13, 15, 12, 14, 9, 11, 10, 8.$$

Trivially, this sequence corresponds to a front-to-back, left-to-right enumeration of IPUs in the chassis. For the complete avoidance of doubt, chassis front and back are denoted in the picture by the Fwd and Aft arrows, whereas left and right are as seen by an observer placed at the back of the chassis and looking forward (Fwd direction).

Within each Multi-IPU device, the run-time numbers IPUs according to the sequence just reported. This 0-based index of each physical IPU within a Multi-IPU is called a *DNC ID*. For example, IPU16 is composed of IPUs 5 and 7 (5 and 7 are their Device IDs); their DNC IDs are trivially 0 and 1, respectively. Consider IPU30, the device containing all IPUs in the system, whose Device IDs are 5, 7, 4, 6 ... 10; their respective DNC IDs are 0,1,2,3 ... 15.

To avoid confusion between Device IDs and DNC IDs, the reader only needs to remember that:

- **Device IDs** reflect PCI device enumeration; consecutive Device IDs do not indicate IPU proximity;

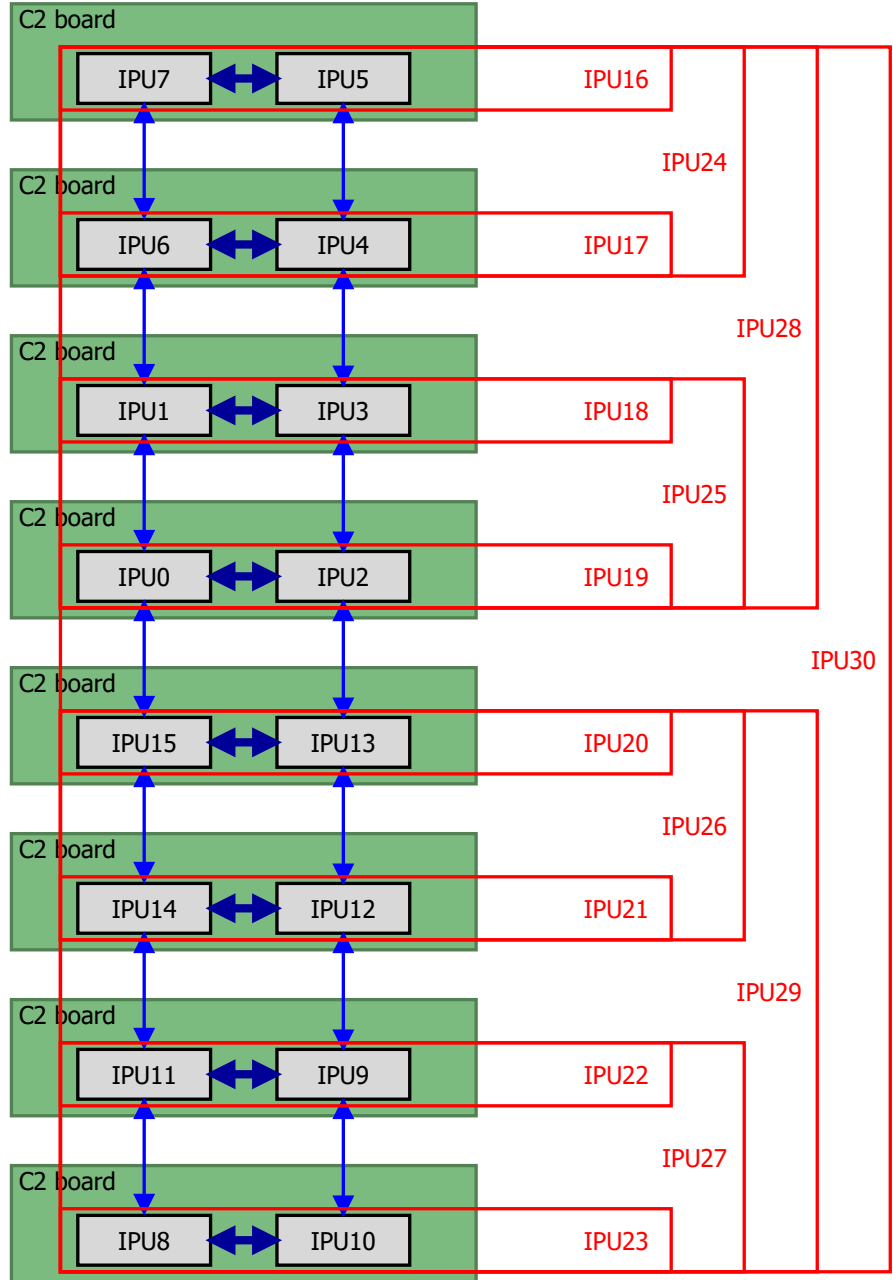


Figure 2.3: Topology of Multi-IPU virtual devices (depicted in red) with respect to the physical IPUs (in black). All numbers are Device IDs. For example, IPU16 is a virtual device containing physical IPUs 5 and 7. IPU30 is a virtual device containing all 16 physical IPUs in the server.

- **DNC IDs** reflect actual IPU proximity in the IPU Link topology; consecutive DNC IDs denote IPUs that are close to each other.

DNC IDs matter to the final user because they also reflect the order in which tiles are ordered within the Multi-IPU. Tiles are ordered sequentially according to the DNC IDs: tiles 0...1,215 belong to IPU with DNC ID 0, tiles 1,216 ... 2,431 belong to DNC ID 1, and so on.

A user employing a different system than the one we evaluated can obtain an explicit enumeration of all IPU devices (physical, and virtual) and their topology, including DNC numbering, by using command line tool `gcinfo --list-all-devices`.

2.3 Methods

Software SDK version. At the time this report is written, the IPU is a novel architecture and Graphcore is refreshing its Poplar SDK and its IPU drivers with relative frequency. Because subsequent releases include incremental optimizations, the choice of any one SDK version in conjunction with a benchmark affects the benchmark’s performance results. We used SDK version 1.0.49. Researchers intending to duplicate our results should employ the same version.

Whenever meaningful, we timed the latency of each operation with care for the following concerns:

- **Single-IPU measurements.** In benchmarks involving a single IPU, we timed operations on the IPU, via the cycle-accurate primitive `popsys::cycleStamp()`. The use of this primitive isolates measurements from CPU-IPU communication overheads and IPU program launch overheads.
- **Multi-IPU measurements.** Benchmarks involving multiple IPUs can not practically use `popsys::cycleStamp()`. We time them instead from the host system. We time multiple iterations of each benchmark in order to amortize overheads, making their impact negligible. To remove spurious overhead between one iteration and the next, we use the Poplar primitive `program::Repeat()`, which excludes the host from having any role in the repetition.
- **Warm up.** Whenever we desire steady-state measurements, we take appropriate countermeasures to exclude warm-up overheads from the results. For example, whenever benchmarks involve the host, we typically execute an untimed warm-up iteration of the benchmark before we start timing.

Units. In this paper we prefer harmonized ISO/IEC 80000-13:2008 standard to denote data sizes and capacities: 1 KiB = 1,024 bytes; 1 MiB = 1,024 KiB; 1 GiB = 1,024 MiB; 1 TiB = 1,024 GiB. When units of capacity are used to express throughputs, we use customary 1,000-based prefixes (k,M,G,T —thus, kB/s, MB/s, GB/s, TB/s) for consistency with the literature and ease of calculation.

Chapter 3

Local Memory

We start our analysis from the basic constituents of an IPU system and proceed outward. In this chapter, we focus on the performance of the memories located within each tile.

On an IPU, each tile possesses 256 KiB of memory that it can access directly via instructions. (For a tile to access memory that is local to another tile, it must use the exchange; we characterize the exchange's performance in the next chapter.)

We find that the performance of each local memory is fixed (6 cycles latency, 31.1 TB/s aggregate peak read bandwidth); local memories are completely decoupled from each other, in function and performance, as architectural considerations suggest. Pressure on the local memory in one tile does not affect memory performance in any other tile.

3.1 Latency

The latency experienced by a tile reading a value from its local memory is 6 clock cycles. Our experiments show that this latency is fixed and does not depend on access patterns, stride, working set size, number of threads used on each tile (1 ... 6), number of concurrent tiles running the same benchmark simultaneously, or size of the target working set accessed by the benchmark.

A minimal benchmark suitable to demonstrate latency invariance follows, courtesy of Graphcore. The code implements a pointer chase that scans an array of configurable size. The array is pre-populated with indices that realize a linked-list visit with configurable stride.

```
template <const int unroll_factor>
class PChaseVertex : public poplar::Vertex {
public:
    poplar::Input<Vector<uint32_t>> in;
    poplar::Input<uint32_t> start;
    poplar::Input<bool> flag;
```

```

poplar::Output<uint32_t>          out;

bool compute() {
    uint32_t index = start;
    for (int i = 0; i < unroll_factor; i += 1)
        index = in[index];
    if (flag)
        *out = index;
    return true;
}
};

template class PphaseVertex<1000>; // explicit instantiation

```

In the listing, variable `flag` presents the compiler with a possible side effect; its purpose is to prevent the compiler from detecting the entire benchmark as dead code and optimizing it out.

Experimental results confirm that neither size nor stride affect memory access latency.

3.2 Bandwidth

We measure the aggregate read bandwidth available to user code on the entire IPU and compare it with theoretical limits derived from hardware specifications (31.1 TB/s). We achieved bandwidths closely matching theoretical values only with a benchmark written in assembly language containing a zero-overhead loop of 128-bit loads. Experiments show that Poplar load-dense code with narrower loads, 32- and 64-bit wide, access roughly a quarter and half of the theoretical bandwidth, respectively. Code with lower-than-perfect load instruction density may achieve even lower bandwidth. However, naive code consisting of array-based, single-precision read loops without hand optimizations emits relatively dense 32-bit loads, achieving a quarter of the theoretical limit. Finally, we show how developers can use the `float2` vector types to increase access width, roughly doubling their bandwidth, without resorting to assembly code. All these results are presented in detail in this section.

Theoretical limit. The theoretical aggregate read bandwidth derives from the following assumptions: each tile can read 16 bytes per clock cycle, the clock frequency is 1.6 GHz, and the tile count is 1,216. The result, 31.1 TB/s, is the product of these three factors. (Top row in Table 3.1.)

Multi-threading. All benchmarks in this section use six identical threads per tile in order to achieve complete hardware thread occupancy. Using a smaller amount of threads yields proportionally lower bandwidth.

Naive code. To measure the performance limits of loop-based code written in Poplar/C++, we use a benchmark specifically designed to generate long sequences of load instructions. This benchmark delivers 7.59 TB/s, roughly a quarter of the theoretical limit. (Bottom row in Table 3.1.) Real-world user

Approach	Language	Load width (bits)	Bandwidth (TB/s)	Fraction of Theoretical
Theoretical limit	–		31.13	100 %
Best actual	assembly	128	30.70	98.6%
float2	Poplar	64	15.30	49.2%
64-bit loads	assembly	64	15.26	49.0%
float4	Poplar	64	15.02	48.3%
Naive, float (upper limit)	Poplar	32	7.59	24.4%

Table 3.1: Theoretical and actual aggregate read bandwidths available on the entire IPU chip, as measured via diverse benchmarks written in assembly or in Poplar.

code will see even lower performance than 7.59 TB/s if it exhibits a lower load instruction density. An excerpt of the benchmark source code follows, courtesy of Graphcore.

```
#define UNROLL 256

class AccaddVertex32 : public poplar::Vertex {
public:
    Input<Vector<float>>           in;
    poplar::Input<uint32_t>           size;

    bool compute() {
        for (int i = 0, e = size ; i < e; i += UNROLL) {
            float* base = &in[i];

            #pragma unroll UNROLL
            for (int j = 0; j < UNROLL; j++)
                asm volatile("": "r"(base[j]));
        }
        return true;
    }
};
```

The listing contains the array-based loop, with an inner loop containing an inline assembly block accompanied by an unroll pragma directive. The inner loop instructs the compiler to generate an unrolled sequence of load instructions.

We verify by inspection that the corresponding emitted code contains an unrolled sequence of 256 load instructions, each 32-bit wide.

Best actual bandwidth. To determine the absolute highest bandwidth achievable by user code, we benchmark hand-written assembly code that features zero-overhead loops of 128-bit wide memory accesses. The details of this code are beyond the scope of this document. It achieves a bandwidth closely matching the theoretical: 30.7 TB/s, or 98.6% of the theoretical limit. (“Best actual” in Table 3.1.) We know of no other means to emit 128-bit load instructions than resorting to assembly.

Vector types. Applications loading 32-bit words can achieve the higher 64-bit bandwidth by loading two words at a time if the source data is contiguous.

This avenue benefits developers who desire higher performance but are not willing to write assembly code. They can instruct the compiler to generate wider loads by using vector type `float2` and explicitly aligning their input arrays, as we illustrate in the listing below. Vector type `float2` expresses an array of two 32-bit floating point values intended to be handled together by the hardware. This code will emit 64-bit load instructions and achieve the same performance as a hand-written assembly loop of 64-bit loads (rows labeled “`float2`” and “64-bit loads” in Table 3.1), which is roughly half of the theoretical limit.

```
#define UNROLL 256

class AccaddVertex64 : public poplar::Vertex {
public:
    Input<Vector<float, VectorLayout::SPAN, 8>> in;
    poplar::Input<uint32_t> size;

    bool compute() {
        float2 *f2in = reinterpret_cast<float2 *>(&in[0]);
        for (int i = 0, e = size / 2; i < e; i += UNROLL) {
            float2* base = &f2in[i];
            #pragma unroll UNROLL
            for (int j = 0; j < UNROLL; j++)
                asm volatile("") :: "r"(base[j]);
        }
        return true;
    }
};
```

The crucial aspects of this listing are the alignment directives associated with input tensor `in` and the `reinterpret_cast` syntax necessary to access `in` via vector type `float2`. The inline assembly loop at the bottom is not part of the technique we propose, and it is just intended to achieve perfect load instruction density (forcing the compiler to generate an unrolled sequence of load instructions), as in an example we presented earlier.

This vector type approach does not extend to `float4`, which does not cause the compiler to emit 128-bit loads. We find that a benchmark based on `float4` roughly achieves the same performance as the code just illustrated (“`float4`” in Table 3.1). We omit its listing.

Sensitivity to block size. We show how the aggregate local memory bandwidth seen by a workload varies according to the size of blocks it accesses. Our benchmark scans a block of configurable size. We instantiate the workload six times per tile to optimally occupy the six hardware threads. We vary block sizes from a single word to 200 KiB, which is close to the user-available capacity. Our results are in Figure 3.1; for sufficiently large blocks, the bandwidth saturates smoothly. Accessing memory in blocks of 8 KiB is sufficient to achieve 95% of peak bandwidth.

No congestion occurs as more and more tiles use the respective memories. This finding is consistent with the operation of completely distributed local memories.

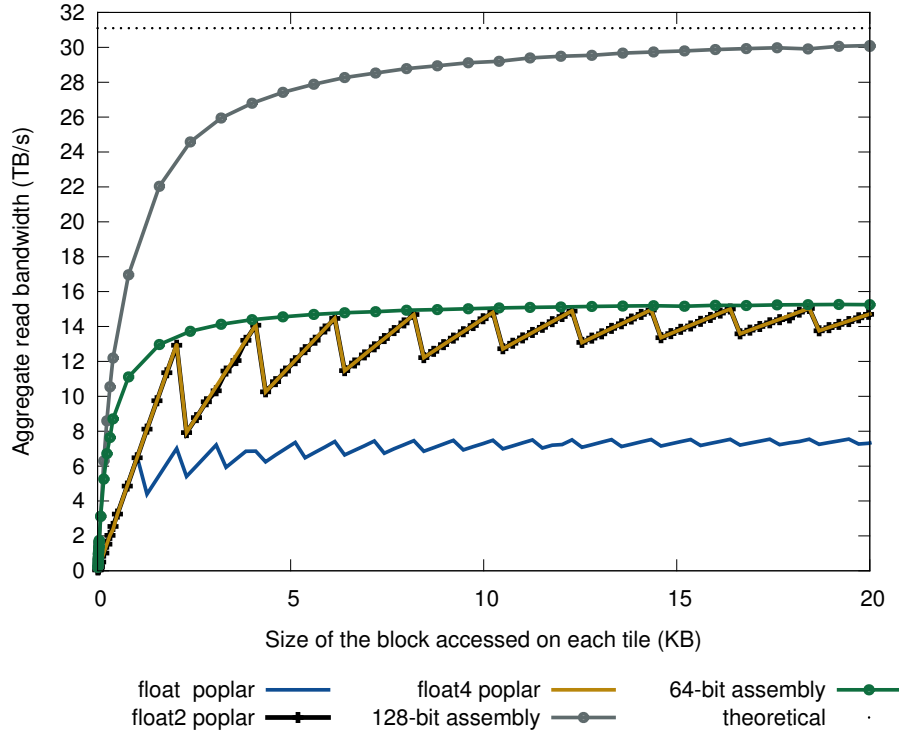


Figure 3.1: Aggregate local memory bandwidth on the entire IPU as a function of block size.

Write bandwidth. The theoretical limit is 15.5 TB/s, derived from each tile’s ability to write 8 bytes per clock cycle. Naive, array-based, single-precision write loops achieve the same performance as the corresponding read loops (“float poplar”) in Figure 3.1. That code benefits from the use of vector types in the same manner as illustrated above and with the same performance benefits. The following listing, courtesy of Graphcore, illustrates how to instruct the compiler to emit 64-bit wide, aligned write instructions for single precision (32-bit) elements.

```
#define UNROLL 8
using namespace poplar;
class AccaddVertex : public poplar::Vertex {
public:
    Input<Vector<float, VectorLayout::SPAN, 8>> in;
    // Request 8-byte alignment (SPAN) for variable 'in'

    poplar::Input<uint32_t> size;
    poplar::Input<bool> flag;
    poplar::Output<float> out;

    bool compute() {
        float2 *f2in = reinterpret_cast<float2 *>(&in[0]);
        float tmp = 0.0;
```

```
// loop limit is size/2 because each element consists of 2 floats
for (int i = 0; i < size/2; i+= UNROLL ){
    float2 tmps[UNROLL];
    #pragma unroll UNROLL
    for (int j = 0; j < UNROLL; j++)
        tmps[j] = f2in[i+j];
    if (flag)
        for (int j = 0; j < UNROLL; j++)
            tmp += tmps[j][0] + tmps[j][1];
}

if (flag)
    *out = tmp;
return true;
};
```

Using an unroll factor equal to 8 achieves the highest bandwidth. This code achieves the same bandwidth as the corresponding code that we illustrated above for array reads.

Chapter 4

Interconnect

We evaluate the IPU interconnect’s performance by benchmarking point-to-point and collective operations. We analyze whether and how latency and bandwidth degrade as the scale of the communication operation increases, involving on-chip and off-chip interconnects.

We selected a sufficiently broad set of primitives for benchmarking that represent communication patterns commonly found in parallel applications. Our results are intended to help software designers derive early performance estimates for their applications.

Our choice of microbenchmarks and metrics conforms with publicly available benchmarking suites for parallel computing, such as the *OSU Micro-benchmarks*[8] by the Ohio State University’s Network-based Computing Laboratory.

The first section of this chapter focuses on point-to-point transfers; the remaining sections each focus on one collective operation.

4.1 Point-to-point Transfers

In this section, we study the performance of IPU systems when engaged in point-to-point communications (data transfers from one source tile to one destination tile) under diverse load conditions.

Our results draw a map of the relative proximity of the constituents of an IPU system (specifically, how quickly tiles can reach each other in terms of latency and bandwidth, depending on relative distance in the system) that is predictable and consistent with the known topology of the system presented in Figures 2.1 and 2.2.

Software designers can take advantage of our results to gain an understanding of the latency penalty and bandwidth associated with traversing the

on-chip interconnect, crossing IPU links on a board, and crossing IPU links across boards.

We benchmark latency and bandwidth in a spectrum of congestion conditions ranging from global silence (the system is idle, with the only exception of the one transfer benchmarked) to full load (all tiles are engaged in communication with the same pattern as the one benchmarked).

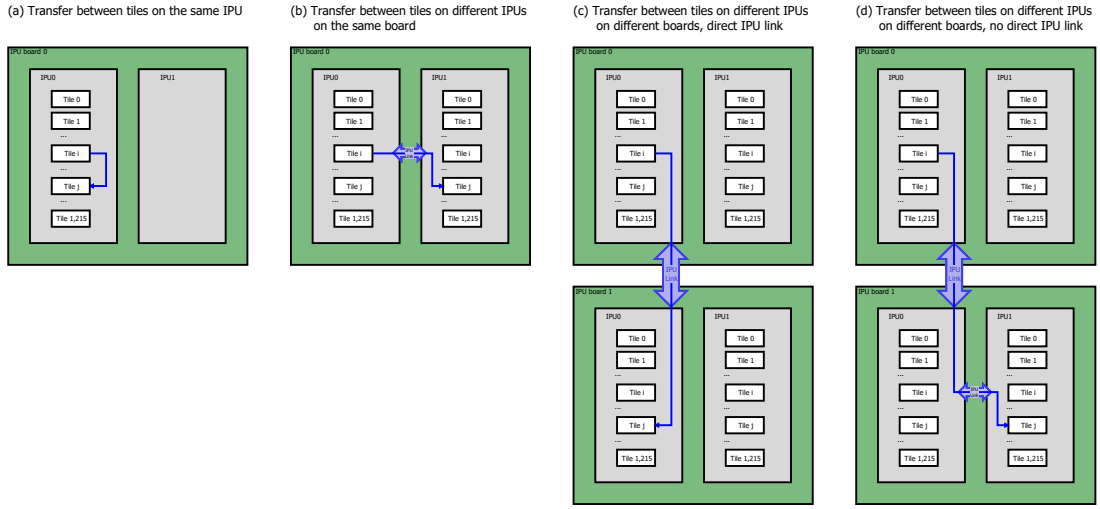


Figure 4.1: Communication topologies we evaluate in point-to-point latency benchmarks. Data transfers between the source and the destination tiles are depicted with blue arrows. The experiments are designed to exercise both on-chip (a) and off-chip (b,c,d) interconnects.

4.1.1 Congestion-free Latency

We study the latency incurred by a single, minimum-size transfer between two tiles while the rest of the system is idle (global silence on the interconnects).

The latencies we measure are consistent with the topology of the experiment. On chip, a source tile can reach any destination tile on the same IPU within 0.13 microseconds on average. As soon as a message needs to cross an IPU link to reach its destination, a penalty of approximately 0.5 microseconds applies. Surprisingly, reaching a tile on the second IPU located on the same board as the source is marginally more expensive than reaching a directly connected IPU on a different board. Detailed results are in Table 4.1.

Detailed descriptions of the experimental topologies we benchmarked follow, matching the corresponding illustrations in Figure 4.1 and corresponding results of Table 4.1:

- in experiment (a) we exercise the on-chip interconnect; the source and destination tiles (i and j) reside on the same IPU. We obtain the average latency value over a large number of experiments. In each such experiment, i and j are chosen randomly;
- in experiment (b) we exercise the off-chip IPU Link interconnect between two IPUs on the same board;
- in experiment (c) we exercise the off-chip IPU Link interconnect between two IPUs on different boards when those IPUs are directly connected via an IPU link. Surprisingly, this latency is marginally lower than that of experiment (b);
- in experiment (d) we exercise the off-chip IPU Link interconnect in conditions where the two IPUs involved are not directly connected via an IPU link and communication requires traversing more than one IPU link.

Experiment		Latency
On-chip	(a)	0.133 μ s
Off-chip, on board	(b)	0.633 μ s
Off-board, direct IPU link	(c)	0.524 μ s
Off-board, indirect IPU link	(d)	0.779 μ s

Table 4.1: Point-to-point latency for small messages under no load. Experiments labeled (a)...(d) correspond to the illustration in Figure 4.1 and are described above.

4.1.2 Latency between Tiles on a Chip by Proximity

We study how the physical proximity between pairs of tiles on a chip affects their communication latency in congestion-free conditions.

We measure latency between all pairs of tiles and depict our results in Figures 4.2 and 4.3. The first figure focuses on tiles within a column; the second shows the entire IPU. In both figures, the main diagonal (in white) corresponds to local transfers, which are carried out in local memory and do not involve the exchange. Latencies reflect tile topology (Figure 2.2).

Latency measurements. The reader should pay attention to the fact that the latency measurements presented within this section may differ from those of other sections, e.g., Table 4.1. The discrepancy is due to the use of different timing methods. Specifically, experiments in this section use the on-IPU, fine-grained profiling facilities offered with the Poplar SDK (that we described under “Single-IPU measurements” in Section 2.3) which do not include the cost of the on-IPU synchronization phase that precedes the transfer, whereas other sections typically use host-based “Multi-IPU measurements” that include that cost. Both measurements are meaningful when appropriately characterized.

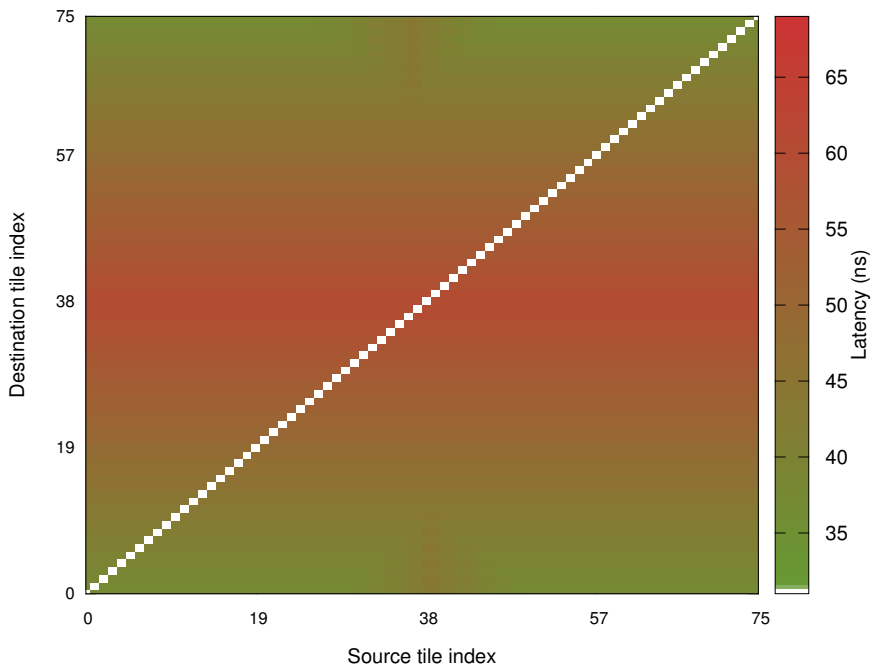


Figure 4.2: Minimum latency between all tiles belonging to the same Column on an IPU processor (we first presented columns in Figure 2.2).

Within a column. Data transfers within the same column take 37...59 ns (59...95 clock cycles); see Figure 4.2. Intra-column latency primarily depends on what island the destination tile belongs to; transfers to the same island have same latency, no matter the source island. Latency is minimal when transferring to a tile belonging to the island closest to the IPU Exchange (e.g., for Column 0, that's island of tiles 0, 1, 74 and 75). Latency increases by 1.25 ns (2 clock cycles) for every island the destination moves away from the exchange.

Across columns. Latency is 98 ns (the highest) in transfers from Column 8 to 0 (tile 646 to 0). Transfers from the rightmost columns (column 7 and 8) to the leftmost columns (0 and 15) take more than 63 ns. Transfers in the opposite direction have lower latency.

4.1.3 Latency between IPUs by Proximity

We measure and chart the minimum latency between pairs of IPUs across the entire 16-IPU experimental system. Latencies correlate directly with the distance between source and destination IPUs along the network topology of Figure 2.1. We chart our results in Figure 4.4.

Numbering. In this section we only refer to IPUs by *DNC IDs* (as opposed to

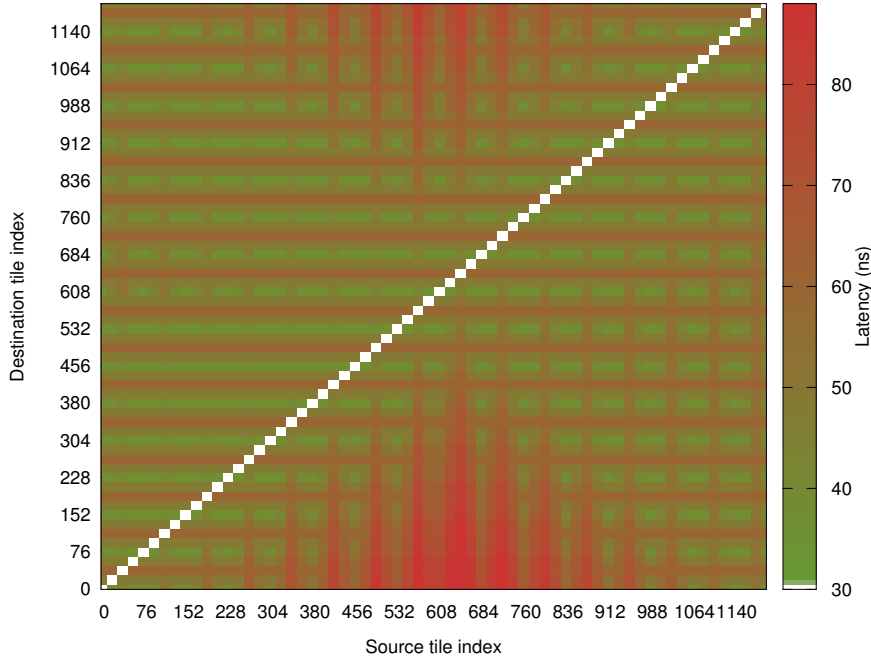


Figure 4.3: Minimum latency between all pairs of tiles on an IPU processor.

Device IDs—recall the distinction from Section 2.2). This is precisely because DNC IDs account for the proximity between pairs of IPUs, whereas Device IDs don’t.

Results. We find that:

- the lowest latency is between IPU with DNC IDs i and $i \pm 2$, i.e., each even-numbered IPU reaches the fastest those even-numbered IPUs that are facing it on the neighboring boards. The same applies to odd-numbered IPUs. These links are visible in the matrix as the two diagonal lines with the most intense shade of green; they are two cells above the main diagonal and two cells below the main diagonal;
- pairs of IPUs located on the same board see the second-best latencies across the system;
- there is no wrap-around. The IPUs with DNC IDs 0 and 14 are not neighbors; neither are 1 and 15. These four IPUs suffer from edge effects in the sense that they only have one neighbor of same parity. This reflects the IPU Link network shape (i.e., not a torus).

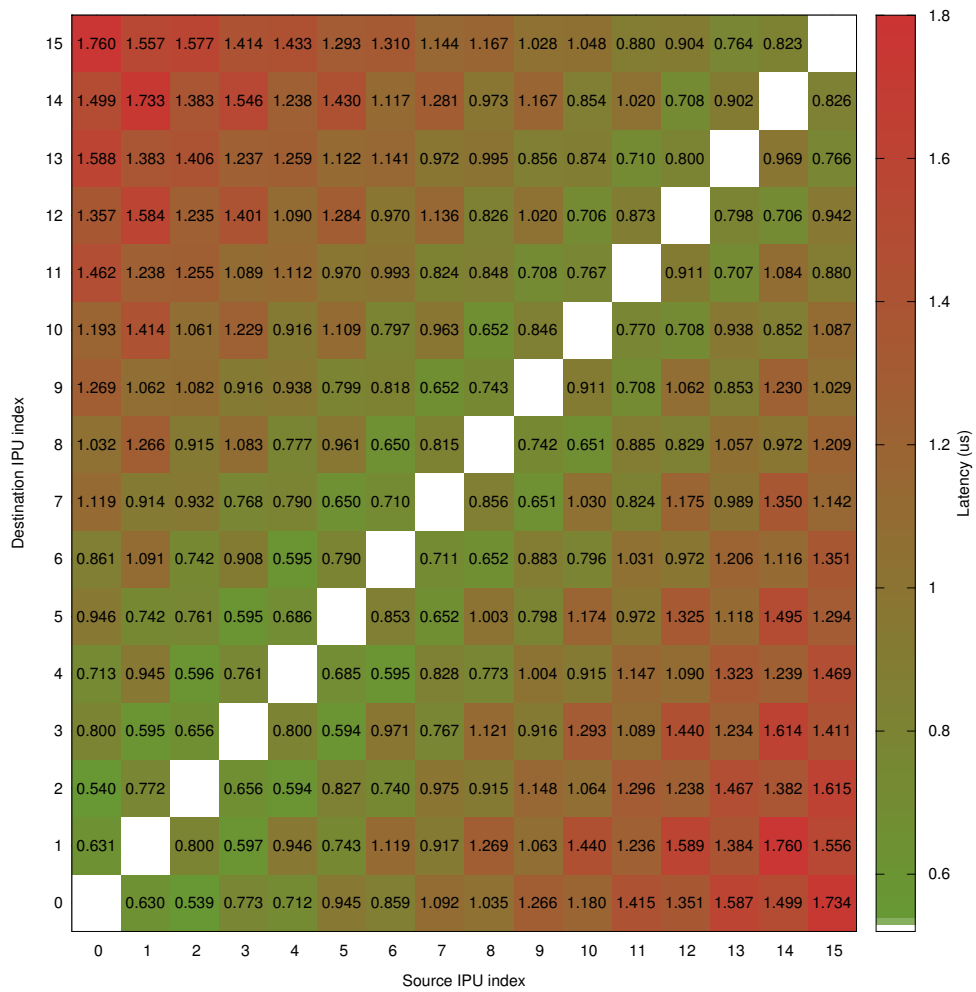


Figure 4.4: Minimum latency between each pair of IPUs in our experimental 16-IPU system, measured in zero-congestion conditions. IPUs are numbered according to their *DNC IDs*, as discussed in Section 2.2.

4.1.4 Latency under Load

In this section, we investigate the impact of congestion on point-to-point latency. We simulate traffic conditions by instantiating identical point-to-point transfers that occur concurrently.

We compare latencies in the congestion-free scenario and under load in Table 4.2. In the table, experimental conditions (a)...(d) refer to same topologies we considered in our congestion-free study (Section 4.1.1). In summary, congestion increases on-chip latency only marginally (+24%), but it affects off-chip IPU link latency significantly, with slowdowns of 4.0...7.7 \times .

We also find that the average per-message latency in a multi-IPU system is remarkably scalable: randomized concurrent transfers across a 16-IPU system experience a latency that is minimally higher (1.93 ns/message) than on a single-board 2-IPU system (1.76 ns/message).

The methods we used to put the interconnect under load are described below.

Experiment		Congestion-free Latency	Latency under load	Congestion degradation
On-chip	(a)	0.133 μ s	0.165 μ s	1.2 \times
Off-chip, on board	(b)	0.633 μ s	2.521 μ s	4.0 \times
Off-board, direct IPU link	(c)	0.524 μ s	2.524 μ s	4.8 \times
Off-board, indirect IPU link	(d)	0.779 μ s	5.989 μ s	7.7 \times

Table 4.2: Effect of congestion on point-to-point latency. This is a short summary that compares congestion and no-congestion results in conditions (a)...(d) corresponding to the previous section. More detailed experiments are in the next table.

Experiments (a)...(d) in presence of congestion match the corresponding congestion-free experiments (described in the previous section), with the following additional details:

- in experiment (a), each tile on an IPU performs one transfer to one randomly selected tile on the same IPU; as many transfers occur concurrently as there are tiles on one IPU (1,216). Each tile participates in exactly one transfer as a source and in exactly one (other) transfer as a destination;
- in experiment (b), we exercise the off-chip IPU Link interconnect between two IPUs on the same board. Each tile on one IPU performs one transfer to one randomly selected tile on the other IPU on the same board. As many transfers occur concurrently as there are tiles on one IPU. Each tile on the first IPU participates in exactly one transfer as a source, and each tile on the second IPU participates as a destination. All cross-IPU traffic is monodirectional;

- in experiment (c), we exercise the off-chip IPU Link interconnect between two IPUs on different boards when those IPUs are directly connected via an IPU link (e.g., each tile on IPU5 performs one transfer to one randomly selected tile on IPU4; see Figure 2.1). As many transfers occur concurrently as there are tiles on one IPU. Each tile on the source IPU participates in exactly one transfer as a source, and each tile on the destination IPU participates in exactly one transfer as a destination. All cross-IPU traffic is monodirectional;
- in experiment (d) we exercise the off-chip IPU Link interconnect in conditions where the two IPUs involved are not directly connected via an IPU link and communication requires traversing more than one IPU link (e.g., each tile on IPU5 performs one transfer to one randomly selected tile on IPU6; see Figure 2.1). All other conditions are the same as in experiment (c).

For a finer-grained characterization of congestion impact, see the augmented results of Table 4.3 and our observations that follow.

Scale (IPUs)	Experiment	Concurrent transfers	Total latency	Avg. latency per message
On-chip: source and destination tiles are on the same IPU				
		1	0.123 μ s	122.565 ns
		2	0.130 μ s	65.040 ns
		4	0.157 μ s	39.253 ns
		8	0.152 μ s	18.994 ns
	...	16	0.160 μ s	10.009 ns
	...	38	0.148 μ s	3.884 ns
	...	76	0.165 μ s	2.173 ns
1/8	...	152	0.163 μ s	1.070 ns
1/4	... a quarter of one IPU	304	0.165 μ s	0.541 ns
1/2	... half IPU	608	0.165 μ s	0.272 ns
1	... the entire IPU	(a)	1,216	0.165 μ s
Cross-IPU experiments - 2 IPUs - monodirectional traffic				
2	... both IPUs on the same board	(b)	1,216	2.521 μ s
	... across boards, direct IPU link	(c)	1,216	2.524 μ s
	... across boards, no direct IPU link	(d)	1,216	5.980 μ s
Cross-IPU experiments - random system-wide destinations				
2	... both IPUs on the same board	2,432	4.282 μ s	1.761 ns
2	... across boards, direct IPU link	2,432	2.572 μ s	1.058 ns
2	... across boards, no direct IPU link	2,432	6.030 μ s	2.480 ns
4	4 IPUs on two boards	4,864	5.981 μ s	1.230 ns
8	8 IPUs on four boards	9,728	16.532 μ s	1.699 ns
16	16 IPUs, entire system	19,456	37.611 μ s	1.933 ns

Table 4.3: Fine-grained and larger-scale detailed results on the effect of congestion on latency.

In the on-chip experiments, we vary congestion by varying the number of concurrent transfers from 1 to 1,216. In each transfer, a randomly selected set of tiles (of count 2, 4, 8 ... 1,216) transfer to as many destination tiles on the

same IPU. At the upper extreme, this coincides with experiment (a) as already described.

The middle band of the table contains results of experiments (b), (c) and (d) involving 2 IPUs where the source tiles are segregated on one IPU and all the destination tiles are on another. All cross-IPU traffic in these experiments is monodirectional. We have described these experiments earlier in this section.

In the bottom band of the table, we present results corresponding to desegregated destinations. We consider varying system scales (from 2 to 16 IPUs) and, at every scale, all the tiles in the system are the source of one transfer. The destination of each transfer is chosen randomly among all tiles in the system. The destination tile can be on the same IPU as the source or on any other IPU. This communication scheme is representative of parallel applications using a domain decomposition that requires uniformly spread communication. Results show good scalability across system sizes. The average per-message latency does not seem to grow significantly in a 16-IPU system compared to smaller systems.

4.1.5 Congestion-free Peak Bandwidth

We study the peak bandwidth available to a single point-to-point transfer between pairs of tiles in different topologies in congestion-free conditions (no other operations occurring in the rest of the system; global silence on all interconnects except for the transfer being benchmarked).

Peak. Everywhere in this paper, the term *peak bandwidth* denotes the bandwidth seen by transfers of sufficiently large messages (we use the terms *block* and *message* equivalently). On most interconnect architectures, peak bandwidth values are achieved with larger messages. That happens because transfers both of large and small blocks tend to incur similar communication setup overheads, but with larger blocks those overheads are amortized on higher byte counts, thus yielding higher throughput values. This property holds on the IPU too, for both the on-chip IPU interconnect and the off-chip IPU Link network. We verify this claim experimentally in Section 4.2.3.

Our experiments cover the same topologies already described in Section 4.1.1 and depicted in Figure 4.1.

All results follow in Table 4.4. There is a 14% decrease in point-to-point bandwidth when moving from on-chip to off-chip, on-board communication. There is an additional 9% penalty when moving from on-board to inter-board communication with source and destination IPU linked directly. When IPUs are not connected directly, bandwidth decrease marginally (less than 2%).

Tile proximity on chip. Physical proximity between the source tile and destination tile on a chip does not affect the peak bandwidth available between the two tiles. We compare the bandwidth accessible between physically near

Experiment		Peak Bandwidth
On chip	(a)	6.34 GB/s
Off chip, on board	(b)	5.46 GB/s
Off board, direct IPU link	(c)	4.99 GB/s
Off board, indirect IPU link	(d)	4.91 GB/s

Table 4.4: Point-to-point peak bandwidth under no load. Experiments labeled (a)...(d) correspond to the topologies in Figure 4.1.

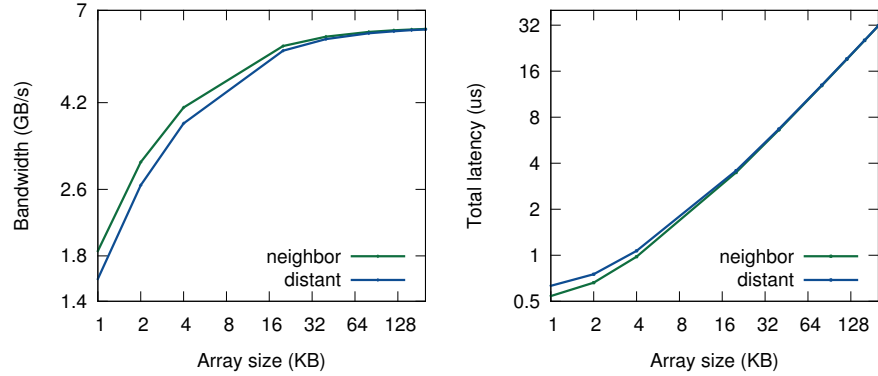


Figure 4.5: The effect of physical proximity on tile-to-tile transfer bandwidth within an IPU is negligible, especially with large messages. In our experiments, the chosen pair of neighboring tiles is (0,1) and the chosen pair of far tiles is (0,644), consistent with the tile enumeration of Figure 2.2.

and far tiles at various block sizes; results are in Figure 4.5. Performance is indistinguishable for sufficiently large data blocks. When blocks are smaller than 32 KiB, far tile pairs suffer a slightly longer transfer setup time.

Experiment		Congestion-free Bandwidth (GB/s)	Bandwidth under load (GB/s)	Degradation
On chip	(a)	6.34	6.21	1.02 ×
Off chip, on board	(b)	5.46	0.0436	125.2 ×
Off board, direct IPU link	(c)	4.99	0.0224	222.8 ×
Off board, indirect IPU link	(d)	4.91	0.0224	219.2 ×

Table 4.5: Effect of congestion on point-to-point bandwidth. This is a short summary that compares congestion and no-congestion results in conditions (a)...(d) corresponding to the previous section. Extended results are available in the next table.

4.1.6 Peak Bandwidth under Load

We study the peak bandwidth available to concurrent point-to-point transfers between pairs of tiles in different topologies and under different loads. We consider the same topologies as in the previous sections (Figure 4.1). We compare our results against congestion-free ones (Table 4.5).

On chip. The aggregate bandwidth available on the on-chip interconnect scales virtually perfectly with the number of concurrent transfers. As concurrent transfers grow in number, the bandwidth seen by each transfer remains virtually constant at 6.3 GB/s; see the first band of Table 4.6, culminating in experiment (a).

Off chip. The off-chip bandwidth offered by IPU links is lower than that offered on chip by the exchange. An intra-board IPU link connection offers 55 GB/s in each direction. IPU Link connections between different boards offer approximately half that much bandwidth per direction, 28 GB/s, regardless of whether the pair of IPUs is directly or indirectly connected via IPU links. Bidirectional bandwidth under load effectively doubles the monodirectional values.

Our extended results of Table 4.6 provide a finer-grained characterization of congestion.

Experiments (b),(c) and (d) focus on the measurement of monodirectional inter-IPU bandwidth in the same topologies depicted in Figure 4.1. They all involve 1,216 concurrent transfers, arranged so that each tile on the source IPU is the source of exactly one transfer directed at exactly one randomly selected tile located on the destination IPU.

Results show that the on-board, inter-IPU monodirectional bandwidth is roughly twice as high as across boards (55 vs 28 GB/s).

Additionally, we measure bidirectional inter-IPU bandwidth with experiments (b*),(c*) and (d*), which are the bidirectional extension of (b), (c), and (d), respectively. Experiments (b*),(c*) and (d*) all involve 2,432 transfers, of

Scale (IPUs)	Experiment	Concurrent transfers	Aggregate bandwidth (GB/s)	Bandwidth per transfer (MB/s)
On-chip: source and destination tiles are on the same IPU				
	One tile to one tile	1	6.34	6,341.
	2 tile to 2 tiles	2	12.65	6,323.
	...	4	25.29	6,323.
	...	8	50.58	6,323.
	...	16	101.06	6,316.
	...	38	240.12	6,319.
	...	76	480.32	6,320.
1/8	...	152	959.89	6,315.
1/4	... a quarter of one IPU	304	1,919.68	6,315.
1/2	... half IPU	608	3,839.22	6,315.
1	... the entire IPU	(a)	1,216	7,679.01
Cross-IPU experiments - 2 IPUs - monodirectional				
2	... both IPUs on the same board	(b)	1,216	55.00
	... across boards, direct IPU link	(c)	1,216	27.72
	... across boards, no direct IPU link	(d)	1,216	27.71
Cross-IPU experiments - 2 IPUs - bidirectional				
2	... both IPUs on the same board	(b*)	2,432	108.09
	... across boards, direct IPU link	(c*)	2,432	54.86
	... across boards, no direct IPU link	(d*)	2,432	55.02
Cross-IPU experiments - randomized system-wide destinations - no segregation				
2	to 2 IPUs			
2	... both IPUs on the same board	2,432	109.57	45.05
2	... across boards, direct IPU link	2,432	54.86	22.56
2	... across boards, no direct IPU link	2,432	55.02	22.62
4	to 4 IPUs on two boards	4,864	109.72	22.56
8	to 8 IPUs on four boards	9,728	111.13	11.42
16	to 16 IPUs, entire system	19,456	111.28	5.72

Table 4.6: Point-to-point peak bandwidth: bandwidth available to concurrent transfers under load.

which 1,216 go from one IPU to another and 1,216 go in the opposite direction. Each tile on the first IPU is involved in exactly two transfers: in one as a source tile, and in the other as a destination tile. In both such transfers, the other endpoint is on the other tile. The same is true for the second IPU. All transfers are across IPUs. No transfers are IPU-local.

These experiments' results show that bidirectional aggregate bandwidth is twice as high as the corresponding monodirectional values (108 GB/s vs. 55, and 55 GB/s vs 28).

The bottom band in the table studies per-transfer bandwidth degradation as the system size scales up. We instantiate Multi-IPUs comprising growing physical IPU counts (2, 4, 8, and 16), and in each experiment we originate exactly one transfer from each tile in the Multi-IPU system toward a randomly selected tile in the system (uniform distribution). Source and destination tiles may or may not be on the same IPU or C2 board.

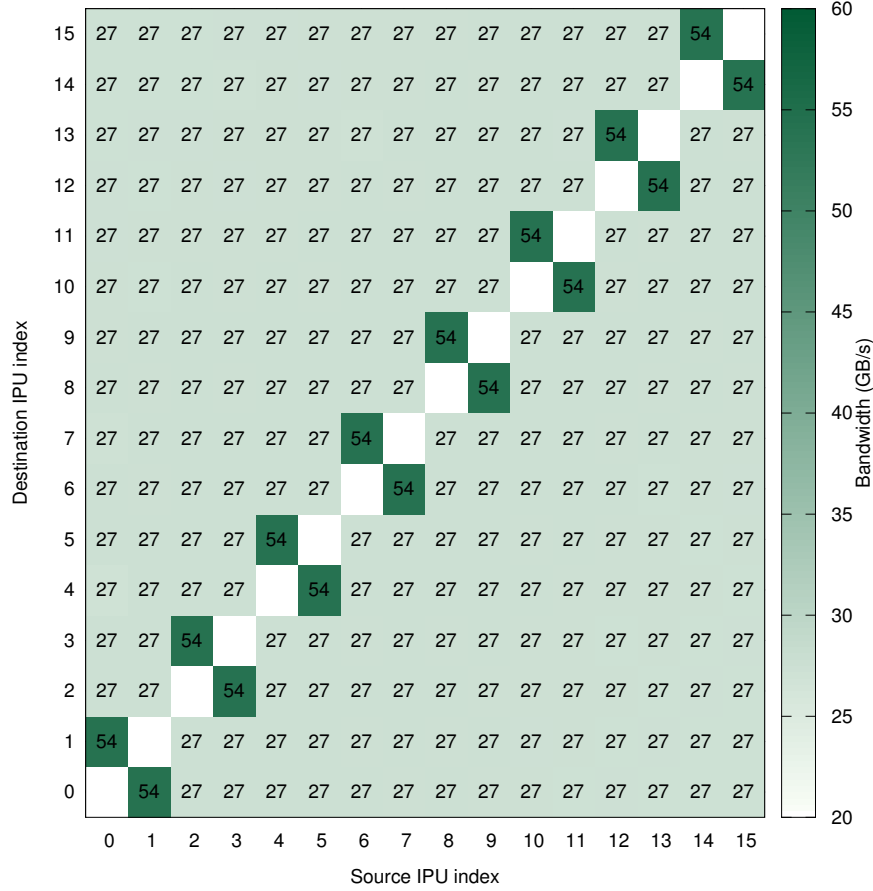


Figure 4.6: Peak monodirectional bandwidth between pairs of IPUs, in congestion-free conditions. IPUs are numbered according to their *DNC IDs*, as discussed in Section 2.2.

In a 16-IPU system, the average per-tile bandwidth degrades to approximately 5.72 MB/s, which is 25% of the monodirectional aggregate per-tile bandwidth available when the system involves a pair of IPUs (not on the same board).

4.1.7 Peak Bandwidth between IPUs by Proximity

We study how IPU proximity in a multi-IPU system affects monodirectional peak bandwidth in congestion-free conditions. We find that it does not—a randomly selected pair of IPUs not located on the same board can transfer data at 27 GB/s (monodirectional) regardless of their respective position in the ladder network (Figure 4.6).

Benchmark. Our benchmark considers all (source,destination) pairs of IPUs.

We number IPUs according to their DNC IDs. In each experiment, we create exactly 1,216 transfers. Each tile in the source IPU transfers a 4 KiB message to a distinct, randomly selected tile on the destination IPU. No other transfers are occurring in the system.

4.1.8 Multi-threaded Peak Bandwidth

We study the effect of multi-threading on the peak bandwidth available on-chip and off-chip. We find the following:

- a single thread is sufficient to achieve full bandwidth;
- the use of multiple threads is not necessary to achieve peak values;
- if used (potentially for other purposes), multi-threading will not cause any bandwidth degradation.

This investigation is motivated by the fact that tiles support executing instructions from up to six concurrent thread contexts in an SMT-like fashion. It is legitimate for a software designer to wonder whether the use of multiple threads to initiate concurrent transfers will achieve a higher aggregate bandwidth.

Results show that the use of additional threads causes no material change in performance, neither on chip nor across chips.

Experiment	Aggregate bandwidth (GB/s)					
	1 thread	2 threads	3 threads	4 threads	5 threads	6 threads
On-chip: source and destination tiles are on the same IPU						
One tile to one tile	6.14	6.13	6.13	6.13	6.13	6.13
2 tiles to 2 tiles	12.22	12.27	12.24	12.26	12.07	12.29
4 tiles to 4 tiles	24.45	24.52	24.48	24.54	24.51	24.49
8 tiles to 8 tiles	48.96	48.95	48.92	48.94	48.92	48.93
16 tiles to 16 tiles	97.85	97.86	97.87	97.94	97.89	97.76
38 tiles to 38 tiles	232.54	232.44	232.37	231.96	232.03	232.15
76 tiles to 76 tiles	464.62	464.59	464.32	464.76	464.60	464.49
152 tiles to 152 tiles	928.64	927.85	928.49	928.49	928.41	928.19
304 tiles to 304 tiles	1,857.74	1,855.70	1,856.45	1,856.45	1,857.36	1,856.30
608 tiles to 608 tiles	3,713.81	3,712.90	3,712.75	3,712.45	3,712.90	3,702.61
1,216 tiles to 1,216 tiles	7,425.80	7,427.92	7,425.80	7,425.80	7,426.41	7,428.22
Cross-IPU experiments - 2 IPUs - monodirectional						
... both IPUs on the same board	54.99	54.99	54.99	54.90	54.88	54.91
... across boards, direct IPU link	27.71	27.71	27.71	27.67	27.66	27.67
... across boards, no direct IPU link	27.71	27.71	27.66	27.63	27.66	27.66

Table 4.7: Multi-threaded point-to-point peak bandwidth: the use of different threads per tile does not affect the bandwidth available to concurrent transfers.

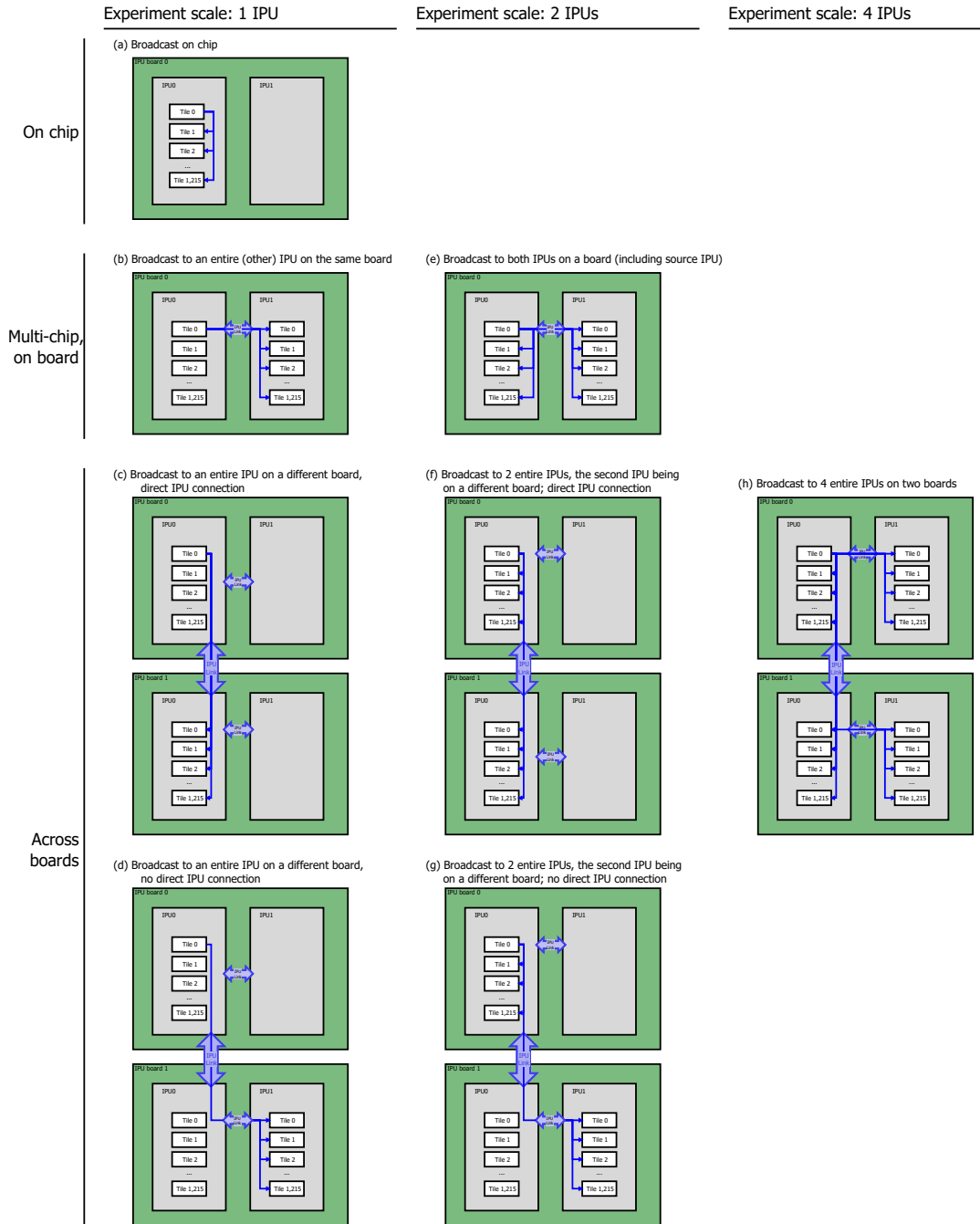


Figure 4.7: Topologies we benchmark in our broadcast and scatter experiments. Different topologies have different connectivity between source and destination tiles and perform differently. We depict data flows from the source to the destination tiles with blue arrows. Reversing all blue arrows depicts the data flows in the gather experiments.

4.2 Broadcast

This is the first section in this chapter dedicated to studying the performance of collective operations. Specifically, this section focuses on latency and bandwidth available to broadcast operations at different scales and for different topologies.

Broadcast. In a broadcast operation, one tile sends the same message to multiple destination tiles. Each destination tile receives an identical copy of the data. The source tile maintains a source buffer available to the operation, in local memory, for the entire duration of the operation. Correspondingly, each destination tile maintains a local destination buffer available to the operation. In benchmarks involving whole IPUs, the source tile is also among the destinations, and maintains both a source and a destination buffer in its local memory. This limits the largest block size available for this benchmark to approximately 100 KiB.

Scale. By scale we mean the destination tile count, or the IPU count if whole IPUs are involved (Table 4.7). We vary scale from one tile to the entire test system, which includes 16 IPUs on 8 boards. When using 2 IPUs, we study the impact of topology and source-destinations proximity: we place the source and destinations on the same board (experiment (b)) and on different boards. We consider pairs of boards directly or indirectly connected with IPU Links (experiments (c) and (d), respectively).

No load. Experiments in this section study load conditions in which no other operation is in progress. Each transfer’s performance is affected only by the load caused by the remainder of the collective operation.

Topologies. We benchmark the topologies of Figure 4.7, where thin blue arrows depict the data flows from the source to the destination tiles. Experiments at different scales are illustrated in different columns of the figure: sub-figures in the first column illustrate experiments where the destination tiles belong to 1 IPU; the second column illustrates experiments where destination tiles span 2 IPUs; and the third column illustrates experiments where the destination tiles span 4 IPUs. We omit experiments involving 8 and 16 IPUs for brevity.

In the figure, experiments on different rows involve different portions of the interconnect. In the first row, only the on-chip interconnect is involved. Experiments in the second row also involve the IPU Link connection between two IPUs located on the same board. Experiments in the lower rows involve IPU Links across multiple boards.

Experiments (b) and (e) study the cost of performing a broadcast between IPUs when both IPUs reside in the same tile. The difference between (b) and (e) is that in (e), the tiles on the first IPU are also broadcast destinations, while in (b), no tiles of the first IPU are destinations.

The same difference appears between experiments (c) and (f). Again, the same difference appears between experiments (d) and (g). This is symbolized in the picture by additional blue arrowheads in (f) and (g) that point to tiles on the source IPU.

Experiments (c) and (f) involve 2 IPUs that are not on the same board but are connected directly via IPU Links. In contrast, experiments (d) and (g) involve 2 IPUs that are not connected directly via IPU Links.

4.2.1 Congestion-free Broadcast Latency

We focus first on the minimum latency associated with a broadcast operation. To do that, we transfer a message of minimum size, i.e., a word of 32 bits. We vary the experiment's scale from one tile to the whole system. We find that the system displays remarkable scalability, with a 16-IPU broadcast taking less than 2 microseconds. Our results are in Table 4.8.

The first experiment in the table (not labeled) is a mere transfer from a tile to itself. It results in a local memory copy that doesn't involve the exchange or IPU links. We report it (12 nanoseconds) only for reference; the reader can subtract this value from subsequent result values to separate the local and interconnect contributions to latency.

In the experiments described in the following rows, the set of destination tiles grows till it reaches the entire IPU.

One tile can broadcast one word to the entirety of its IPU in less than 0.2 microseconds. The additional penalty to perform an off-chip broadcast involving 2 IPUs is approximately 0.5 microseconds. The total latency of a broadcast targeting all 16 IPUs in the test system is below 2 microseconds.

Observations:

- the latency of a broadcast operation involving the entire chip roughly grows logarithmically with tile count (Figure 4.8, left);
- similarly, the latency of a broadcast operation spanning across multiple IPUs roughly grows logarithmically with IPU count (Figure 4.8, right);
- performing a broadcast across 2 IPUs takes approximately 0.7 microseconds; that is approximately 0.5 microseconds more expensive than a single-IPU broadcast;
- the cost of performing an off-chip broadcast is dominated by the cost of traversing an IPU Link; the latency we measure in experiments (b) and (e) is identical. This suggests that in experiment (e), the on-chip broadcast involving the source IPU occurs in parallel with the sequence of operations comprising the transfer to across the IPU link followed by the on-chip broadcast on the destination IPU. The latter sequence

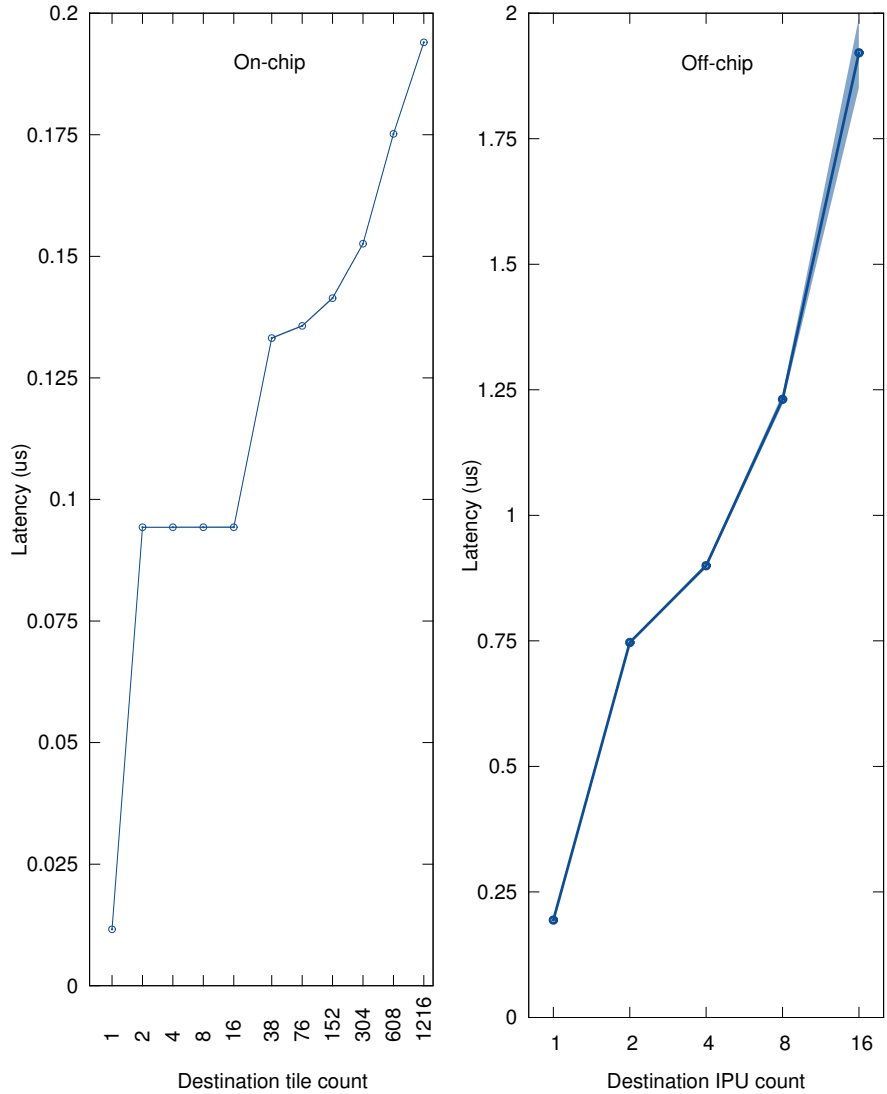


Figure 4.8: Broadcast latency scaling. Left: scaling within an IPU (on chip). Right: scaling and across multiple IPUs (off chip).

Scale (IPUs)	Experiment	Destination tile count	Total latency
	Transfer to self (via local memory)	1	0.012 μ s
	On-chip: source and destination tiles are on the same IPU		
	One tile to n tiles	1	0.094 μ s
	...	2	0.094 μ s
	...	4	0.094 μ s
	...	8	0.094 μ s
	...	16	0.094 μ s
	...	38	0.134 μ s
	...	76	0.136 μ s
1/8	...	152	0.142 μ s
1/4	... a quarter of one IPU	304	0.153 μ s
1/2	... half IPU	608	0.176 μ s
1	... the entire IPU	(a)	1,216
			0.194 μ s
1	to an entire IPU, different than that of source tile		
	... both IPUs on the same board	(b)	1,216
	... across boards, direct IPU link	(c)	1,216
	... across boards, no direct IPU link	(d)	1,216
2	to 2 IPUs		
	... both IPUs on the same board	(e)	2,432
	... across boards, direct IPU link	(f)	2,432
	... across boards, no direct IPU link	(g)	2,432
4	to 4 IPUs on two boards	(h)	4,864
8	to 8 IPUs on four boards	(i)	9,728
16	to 16 IPUs, entire system	(j)	19,456
			1.921 μ s

Table 4.8: Broadcast minimum latency: latency necessary to broadcast one value from one tile to a set of tiles. We study destination sets of varying size and location. System scale and respective location of source and destination tiles affect latency. Experiments labeled (a)-(j) benchmark the topologies of Figure 4.7.

takes longer than the local broadcast and determines the overall latency. Intuitively, once the penalty to reach remote tiles across the IPU Link is paid, the marginal cost of also reaching local tiles is null.

- same considerations apply between pair of experiments (c,f), and pair (d,g);
- unexpectedly, a broadcast between two IPUs on the same board (e) takes marginally more time than between the IPUs located on different boards (f,g). This result is consistent with our gather results (see Section 4.3.1).

4.2.2 Peak Broadcast Bandwidth

In this section we study the peak bandwidth available to broadcast operations of different scales. As in the previous section, we study the effect of source-destination IPU proximity in the topologies (a)...(j) of Figure 4.7. Our results are in Table 4.9.

The message size we employ in these experiments is 100 KiB. It is sufficiently large to saturate the aggregate bandwidth per tile, and at the same time, it is close enough to the maximum size that allows for two copies (source and destination buffer) to exist simultaneously in each tile’s local memory (248 KiB are available to the user). Fitting both buffers in local tile memory allows us to run experiments where the source tile is also among the destinations.

No other traffic is occurring in the system except for that created by the broadcast operation itself.

Scale (IPUs)	Experiment	Concurrent transfers	Aggregate bandwidth (GB/s)	Bandwidth per transfer (GB/s)
On-chip: source and destination tiles are on the same IPU				
	Point to point	1	6.35	6.35
	One tile ... to 2 tiles	2	12.70	6.35
	... to 4 tiles	4	50.49	12.62
	...	8	100.92	12.61
	...	16	201.58	12.60
	...	38	477.10	12.56
	...	76	954.17	12.55
1/8	...	152	1,906.51	12.54
1/4	... to a quarter of one IPU	304	3,808.50	12.53
1/2	... to half IPU	608	7,595.88	12.49
1	... to the entire IPU (same as source tile)	(a)	1,216	15,134.80
1	to an entire IPU, different than that of source tile			
	... both IPUs on the same board	(b)	1,216	6,871
	... across boards, direct IPU link	(c)	1,216	6,433
	... across boards, no direct IPU link	(d)	1,216	6,427
2	to 2 IPUs			
	... both IPUs on the same board	(e)	2,432	9,440
	... across boards, direct IPU link	(f)	2,432	9,051
	... across boards, no direct IPU link	(g)	2,432	9,034
4	to 4 IPUs on two boards	(h)	4,864	25,437
8	to 8 IPUs on four boards	(i)	9,728	36,756
16	to 16 IPUs, entire system	(j)	19,456	47,343

Table 4.9: Peak bandwidth available to broadcast operations of varying scale. Experiments labeled (a)-(j) correspond to the topologies illustrated in Figure 4.7; we describe them in detail.

On-chip performance. As the scale of the broadcast increases within an IPU, the bandwidth per tile achieved by the operation saturates around 12 GB/s. 12 GB/s seems to be the on-chip average per-transfer peak. Saturation occurs with small destination sets: a destination set of 4 tiles is sufficient to achieve

peak per-tile bandwidth.

Off-chip performance. A direct comparison between experiments (a) and (b), that have identical destination count, reveals the penalty for extending the broadcast off chip: a drop in average per-transfer bandwidth from 12.4 to 5.6 GB/s. The performance difference between on-board and inter-board communication is negligible.

Scaling. The results of experiments (h)-(j) show that larger system scales benefit from a monotonically increasing aggregate broadcast bandwidth. The growth trend is, however, not linear, and not trivially explained.

4.2.3 Effect of Message Size on Broadcast Bandwidth

We study broadcast bandwidth performance below peak, i.e., when smaller messages are transferred. We find that smaller messages achieve a fraction of peak bandwidth depending on system scale (e.g., 1 KiB messages achieve 15-30% peak bandwidth). Moreover, as system scale grows, larger message sizes are needed to achieve close-to-peak performance. These observations are not surprising and apply similarly to most parallel systems. We summarize them quantitatively in Table 4.10. We also chart in detail the effects of message size on broadcast bandwidth in Figures 4.9 and 4.10. The charts' data refer to the same scales (1-16 IPUs) and experimental topologies (a)-(j) already discussed.

In almost all experimental conditions, bandwidth saturates smoothly, increasing monotonically with block size and suffering no degradation. Minor exceptions are topologies (c) and (d) (broadcasting to a whole IPU across boards), where block sizes larger than 64 KiB seem to experience slightly lower bandwidths than at 64 KiB.

Scale (IPUs)	Experiment		% peak at 1 KiB message	90% peak message size (KiB)	Peak bandwidth (GiB/s)
1	... the entire IPU (same as source tile)	(a)	30.3 %	13.2	15,134
1	to an entire IPU, different than that of source tile				
	... both IPUs on the same board	(b)	18.9 %	5.7	6,871
	... across boards, direct IPU link	(c)	22.1 %	5.4	6,433
	... across boards, no direct IPU link	(d)	16.4 %	4.8	6,427
2	to 2 IPUs				
	... both IPUs on the same board	(e)	25.2 %	7.3	9,440
	... across boards, direct IPU link	(f)	31.4 %	7.5	9,051
	... across boards, no direct IPU link	(g)	29.5 %	7.4	9,034
4	to 4 IPUs on two boards	(h)	16.5 %	22.2	25,437
8	to 8 IPUs on four boards	(i)	15.2 %	33.6	36,756
16	to 16 IPUs, entire system	(j)	14.6 %	41.2	47,343

Table 4.10: Summary of aggregate broadcast bandwidth below peak.

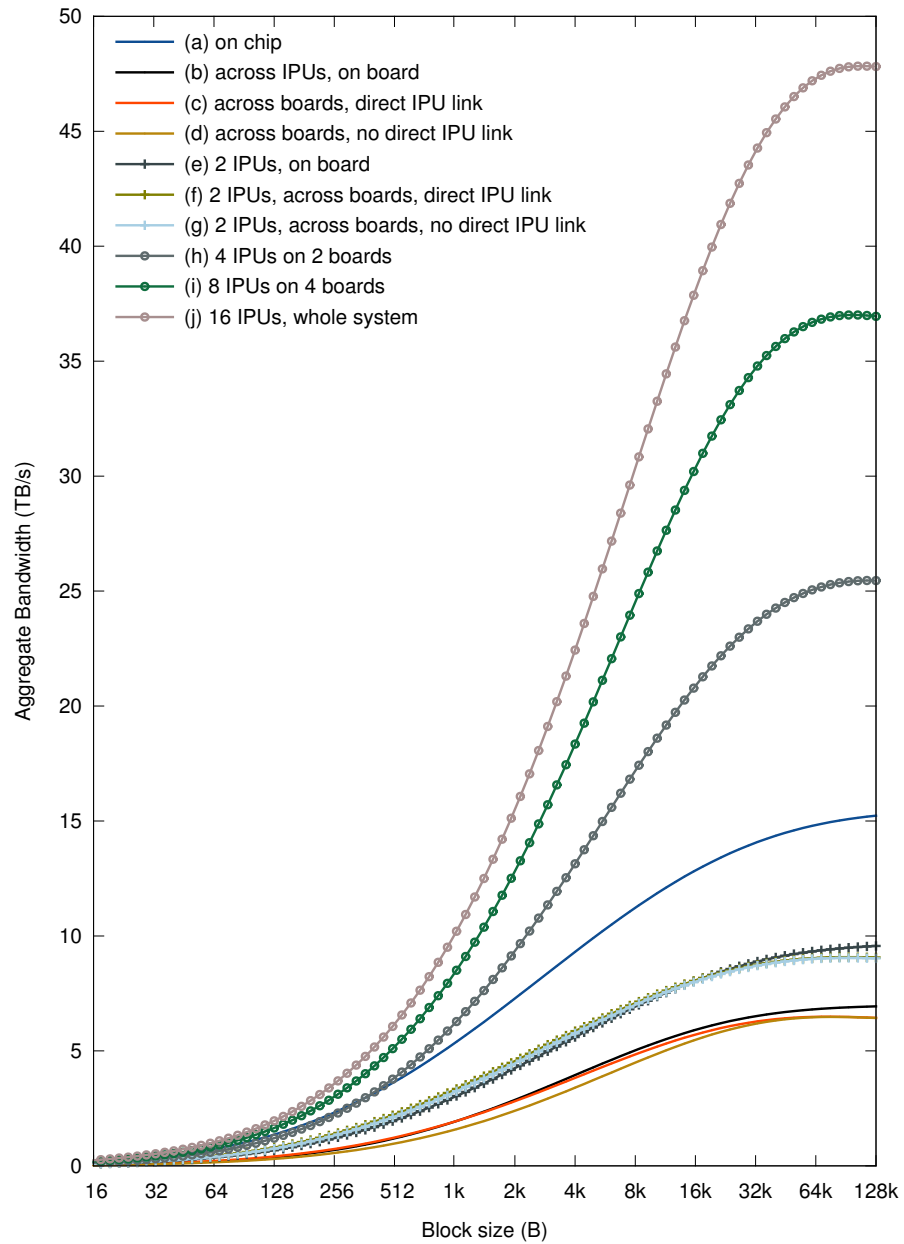


Figure 4.9: Impact of block size on aggregate broadcast bandwidth. Each line represents a different experiment topology (a)-(j) as illustrated in Figure 4.7.

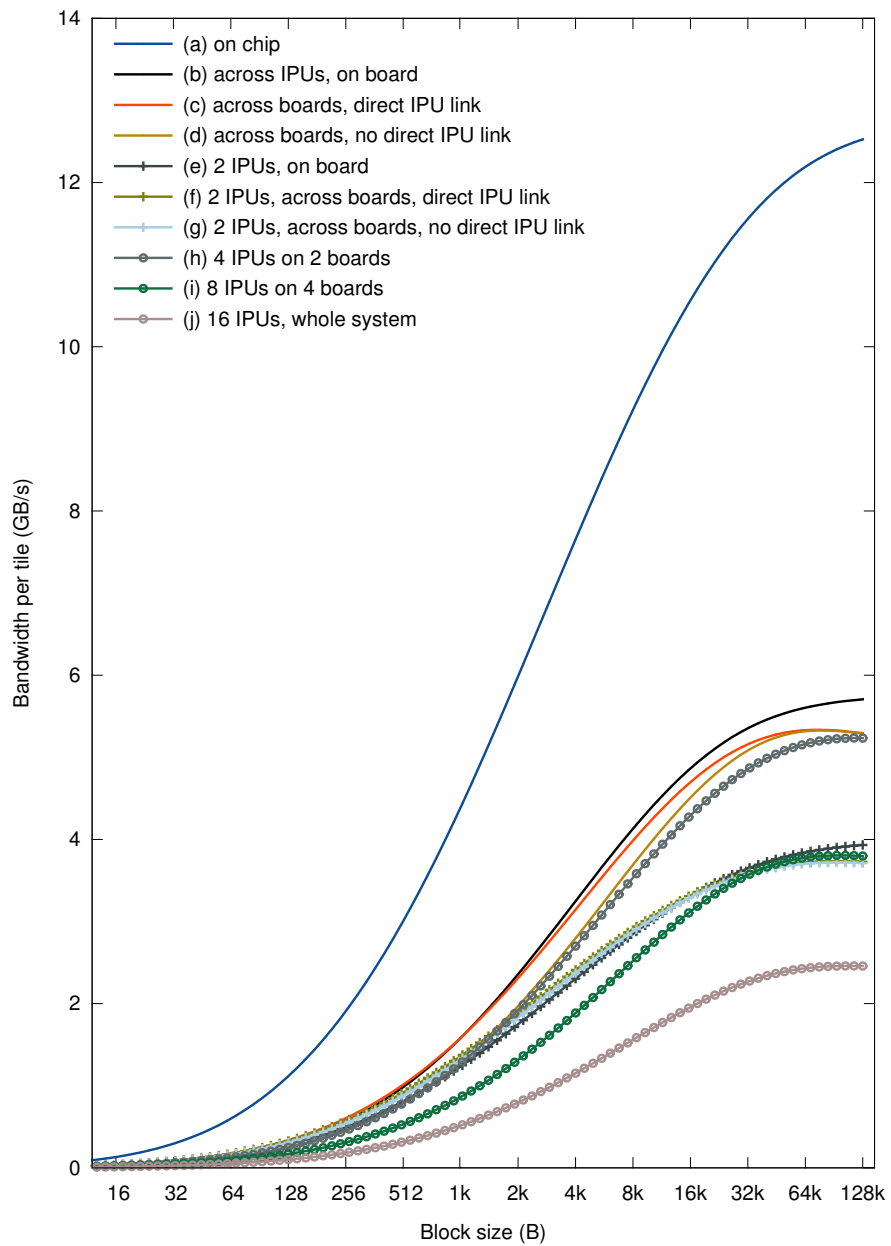


Figure 4.10: Impact of block size on broadcast bandwidth per tile. Each line represents a different experiment topology (a)-(j) as illustrated in Figure 4.7.

IPU systems behave well at scale, with bandwidth growing smoothly with scale as the number IPUs increases to 2, 4, 8, and 16 (experiments (g),(h),(i) and (j) respectively). We see no saturation at scale, and larger scales benefit from higher aggregate bandwidths. Per-tile bandwidths decrease smoothly, roughly with the logarithm of the system size.

4.3 Gather

In this section we study the latency and bandwidth performance available to gather operations.

Gather. For the complete avoidance of doubt, a gather is a collective operation in which one tile receives one message from multiple source tiles. The destination tile receives a distinct message from each source, and must maintain a destination buffer available to the operation, in its local memory, as large as the product of message size and source count. Each source only needs to maintain one destination buffer as large as the message size. In benchmarks involving whole IPUs, the source tile is also among the destinations, and must maintain in its local memory one source buffer plus multiple destination buffers.

Scale. We benchmark the same scales as in our broadcast experiments described in Section 4.2.

No load. Experiments in this section study load conditions in which no other operation is in progress. Each transfer’s performance is affected only by the load caused by the remainder of the collective operation.

Topologies. We benchmark the topologies discussed in the previous section and illustrated in Figure 4.7, with the notable difference that data flows are **reversed** with respect to those of a broadcast operation, depicted in the figure and described in Section 4.2.

Message size. The destination tile must dedicate to the operation one buffer per source tile in its local memory. This constraint limits the maximum message size usable in a gather operation. In turn, the limited message size is the primary factor limiting the aggregate bandwidth available to the operation. A complete discussion follows.

In benchmarks involving whole IPUs, the destination tile is also among the sources, and maintains at the same time one output buffer and multiple input buffers in its local memory.

4.3.1 Congestion-free Gather Latency

We study the minimum latency associated with a gather operation. To do that, we transfer a message of minimum size, i.e., a word of 32 bits. A gather involving an entire IPU completes in 0.8 microseconds. Gather latencies in

Scale	Experiment	Source tile count	Total latency (μ s)	Avg. latency per transfer (ns)
	Transfer to self (via local memory)	1	0.012	11.557
	On-chip: source and destination tiles are on the same IPU			
	... from 2 tiles	2	0.094	47.142
	...	4	0.094	23.567
	...	8	0.094	11.784
	...	16	0.094	5.892
	...	38	0.097	2.563
	...	76	0.121	1.595
1/8	...	152	0.169	1.111
1/4	... from a quarter of one IPU	304	0.264	0.869
1/2	... from half IPU	608	0.455	0.748
1	... from the entire IPU	(a)	1,216	0.835
1	from an entire IPU to a destination tile located on a different IPU			
	... both IPUs on the same board	(b)	1,216	4.929
	... across boards, direct IPU link	(c)	1,216	3.205
	... across boards, no direct IPU link	(d)	1,216	6.693
	Multi-IPU experiments			
2	IPUs on the same board	(e)	2,432	5.708
2	IPUs on different boards, direct IPU link	(f)	2,432	3.983
2	IPUs on different boards, no direct IPU link	(g)	2,432	7.472
4	IPUs on two boards	(h)	4,864	8.995
8	IPUs on four boards	(i)	9,728	12.377
16	IPUs, entire system	(j)	19,456	25.159
				1.293

Table 4.11: Minimum gather latency in experiments of varying scale and topology. The topology of experiments (a)-(j) is as illustrated in Figure 4.7, but with reversed data flow directions.

Multi-IPUs of increasing size grow sub-linearly, with 16 IPUs completing a whole-system gather in 25 microseconds. Our results are in Table 4.11.

As we did for the broadcast operation, we first report the latency (12 nanoseconds) of a trivial gather operation involving the same tile as source and destination. It results in a local memory copy, and we only report it for comparison and latency breakdown.

Latency off chip. The direct comparison between experiments that involve a pair of IPUs, connected directly vs. indirectly by IPU links, reveal that gather latency depends directly on the number of hops between source and destination IPUs in the ladder network.

Specifically, experiment (d) results in approximately twice as much latency as experiment (c). Similarly, experiment (g) exhibits roughly twice as much latency as (f). This is intuitively consistent with the fact that experiments (g) and (d) involve two hops in the IPU link network, whereas experiments (c) and (f) only involve one hop (see Figure 4.7, but assume the reverse data flow direction).

A gather operation involving two IPUs on the same board exhibits slightly longer latency when the IPUs are across boards and directly connected. This is evident by direct comparison between (c) and (b) in the table and also by comparison between (f) and (e). This result is consistent with our results for the broadcast and scatter operations, which we report in Tables 4.8 and 4.13, respectively.

Latency at scale. Results show that a doubling of system size roughly corresponds to a doubling of network diameter, which causes in turn an approximate doubling of total latency.

4.3.2 Peak Gather Bandwidth

Scale	Experiment	Source tile count	Message size (bytes)	Aggregate bandwidth (GB/s)	Bandwidth per transfer (MB/s)
	Transfer to self (via local memory)	1	160	0.571	570.61
1/8	On-chip: source and destination tiles are on the same IPU				
	To one tile ... from 2 tiles	2	160	0.580	290.07
	... from 4 tiles	4	160	1.258	314.47
	...	8	160	2.105	263.16
	...	16	160	3.148	196.75
	...	38	160	4.465	117.51
	...	76	160	5.260	69.22
	...	152	160	5.759	37.89
	1/4 ... from a quarter of one IPU	304	160	6.063	19.94
	1/2 ... from half IPU	608	160	6.219	10.23
1	... from the entire IPU	(a)	1,216	160	6.303
1 from an entire IPU, different than that of the destination tile					
... both IPUs on the same board					
(b) 1,216					
... across boards, direct IPU link					
(c) 1,216					
... across boards, no direct IPU link					
(d) 1,216					
Multi-IPU experiments					
2	on the same board	(e)	2,432	80	5.829
2	across boards, direct IPU link	(f)	2,432	80	5.685
2	across boards, no direct IPU link	(g)	2,432	80	5.677
4	two boards	(h)	4,864	40	5.856
8	four boards	(i)	9,728	20	5.743
16	eight boards, entire system	(j)	19,456	4	5.520

Table 4.12: Peak gather bandwidth: bandwidth available to gather operations that use the largest message size allowed by local memory capacity, in varying scales and topologies. We explicitly report the message used in each experiment, as different scales correspond to different maximum message sizes. Experiments labeled (a)-(j) use topologies corresponding to those illustrated in Figure 4.7, but with reversed data flow directions.

In this section we study the peak bandwidth available to gather operations at different scales and in different topologies. As we did in the previous sections, we study the effects of source-destination IPU proximity in topologies (a)...(j) of Figure 4.7, with the caveat that gather operations involve data flows of the reverse direction than that depicted in the figure. At each scale we use the largest message size allowed by local memory capacity. Results show that the operation’s performance is primarily limited by the small message size and is less sensitive to scale. Aggregate gather bandwidth degrades very

gracefully with scale, with 16-IPU systems experiencing an aggregate bandwidth that is only 5.3% lower than that available on a 2-IPU board. Our results are in Table 4.12.

Small messages. Local memory capacity on the source tile is *the* limiting factor for message size. As scale increases, the maximum usable message size decreases from 160 to 4 bytes. Small message size limits, in turn, available aggregate bandwidth. The bandwidth decrease is consistent with that already benchmarked in Section 4.2.3.

Off chip. Scatter operations exhibit minimal degradation of performance when moving from on chip to off chip: aggregate bandwidth decreases from 6.3 to 5.6...5.2 GB/s. The aggregate bandwidth at scales of 2...16 IPUs is virtually identical for gather and scatter operations.

4.4 Scatter

In this section we study the latency and bandwidth performance available to scatter operations.

Scatter. A scatter operation is similar to a broadcast in the sense that both operations involve one source and multiple destination tiles. The two operations differ in the scatter sending a distinct message to each destination, whereas a broadcast sends the same message to all destination. Moreover, a scatter is the reverse operation of a gather.

Scale. We benchmark the same scales as in our broadcast and gather experiments. We described it in Section 4.2.

No load. Experiments in this section study load conditions in which no other operations are in progress. Each transfer's performance is affected only by the load caused by the remainder of the collective operation.

Topologies. We benchmark the same topologies discussed in the previous sections, and illustrated in Figure 4.7. Scatter data flow directions are correctly depicted in the figure (thin blue arrows) and also match those described in Section 4.2 for broadcast operations.

Message size. The source tile must dedicate to the operation one buffer per destination in its local memory. This constraints limits the maximum message size usable in a scatter operation. In turn, the limited message size is the primary factor limiting the aggregate bandwidth available to the operation. A complete discussion follows.

In benchmarks involving whole IPUs, the source tile is also among the destinations, and maintains at the same time one input buffer and multiple output buffers in its local memory.

Scale	Experiment	Destination tile count	Total latency (μ s)	Avg. latency per transfer (ns)
	Transfer to self (via local memory)	1	0.012	11.542
	On-chip: source and destination tiles are on the same IPU			
	... to 2 tiles	2	0.181	90.713
	...	4	0.183	45.823
	...	8	0.186	23.237
	...	16	0.191	11.927
	...	38	0.205	5.384
	...	76	0.226	2.973
1/8	...	152	0.273	1.795
1/4	... to a quarter of one IPU	304	0.367	1.207
1/2	... to half IPU	608	0.555	0.913
1	... to the entire IPU	(a)	1,216	0.927
1	to an entire IPU, different than that of the source tile			
	... both IPUs on the same board	(b)	1,216	1.361
	... across boards, direct IPU link	(c)	1,216	1.275
	... across boards, no direct IPU link	(d)	1,216	1.404
	Multi-IPU experiments			
2	IPUs on the same board	(e)	2,432	2.268
2	IPUs on different boards, direct IPU link	(f)	2,432	2.181
2	IPUs on different boards, no direct IPU link	(g)	2,432	2.181
4	IPUs on two boards	(h)	4,864	3.707
8	IPUs on four boards	(i)	9,728	7.115
16	IPUs, entire system	(j)	19,456	13.729
				0.706

Table 4.13: Minimum scatter latency in experiments of varying scale and topology. The topology of experiments (a)-(j) is as illustrated in Figure 4.7.

4.4.1 Congestion-free Scatter Latency

We study the minimum latency associated with scatter operations of varying scale and in different topologies. We transfer a message of minimum size, i.e., a word of 32 bits. We vary the experiment’s scale from one tile to the whole system. We find that a whole-IPU scatter completes in 0.9 microseconds, only marginally slower than the gather operation of equal scale. Scatter operations show remarkable scalability, with latencies in Multi-IPUs growing sub-linearly as a function of the number of hops in the ladder network. A whole-system gather completes in 14 microseconds. Interestingly, off-chip scatter operations are significantly faster than gathers of equal scale. Quantitative results are in Table 4.11.

As we did in earlier tests, we report first the latency (12 nanoseconds) of a trivial operation involving the same tile as source and destination. It results in a local memory copy, and its latency is only intended for comparison and contribution breakdown.

Latency off chip. Results collected over experiments at scale show that scatter latencies also depend on the number of hops between sources and destination

in the ladder network, but the off-chip penalty going from a single-IPU to a 2-IPU test is much smaller for scatter than for gather operations (0.4 vs. 3.1 microseconds).

Comparisons between 2-IPU, direct-vs-indirect topologies yield somewhat similar considerations as gathers: directly connected pairs of IPUs on different boards see a marginally better latency pairs of IPUs located on the same board which, in turn, see a better latency than pairs of IPU not directly connected via IPU links. The latency differences between the respective topologies are, however, much smaller than those seen in the gather experiments.

At scale. Similarly to what we found for gather operations, a doubling of system size roughly corresponds to a doubling of network diameter, which causes in turn an approximate doubling of total latency. Scatter operations complete, however, almost twice as quickly as gathers of equal scale.

4.4.2 Peak Scatter Bandwidth

Scale	Experiment	Destination tile count	Message size (bytes)	Aggregate bandwidth (GB/s)	Bandw. per tile (MB/s)
	Transfer to self (via local memory)	1	160	13.884	13883.50
On-chip: source and destination tiles are on the same IPU					
	One tile ... to 2 tiles	2	160	1.728	864.10
	... to 4 tiles	4	160	2.706	676.54
	...	8	160	3.812	476.55
	...	16	160	4.770	298.12
	...	38	160	5.592	147.15
	...	76	160	5.971	78.56
1/8	...	152	160	6.175	40.62
1/4	... a quarter of one IPU	304	160	6.279	20.65
1/2	... half IPU	608	160	6.332	10.41
1	... the entire IPU	(a)	1,216	160	6.360
1	to an entire IPU, different than that of source tile				
	... both IPUs on the same board	(b)	1,216	80	5.633
	... across boards, direct IPU link	(c)	1,216	80	5.229
	... across boards, no direct IPU link	(d)	1,216	80	5.217
Multi-IPU experiments					
2	IPUs on the same board	(e)	2,432	80	5.899
2	IPUs on different boards - direct IPU link	(f)	2,432	80	5.685
2	IPUs on different boards - no direct IPU link	(g)	2,432	80	5.677
4	IPUs on two boards	(h)	4,864	40	5.855
8	IPUs on four boards	(i)	9,728	20	5.743
16	IPUs, entire system	(j)	19,456	4	5.514

Table 4.14: Peak scatter bandwidth: bandwidth available to scatter operations that use the largest message size allowed by local memory capacity, in varying scales and topologies. We explicitly report the message used in each experiment, as different scales correspond to different maximum message sizes. Experiments labeled (a)-(j) use the corresponding topologies illustrated in Figure 4.7 and described in Section 4.2.

In this section we study the peak bandwidth available to scatter operations of different scales. As we did in the previous sections, we study the effect of source-destination IPU proximity in topologies (a)...(j) of Figure 4.7.

At each scale we use the largest message size allowed by local memory capacity. Results show that the operation’s performance is primarily limited by the small message size, and is less sensitive to scale. Aggregate scatter bandwidth degrades very gracefully with scale, with 16-IPU systems experiencing an aggregate bandwidth that is only 6.6% lower than that available on a 2-IPU board. Our results are in Table 4.14.

Small messages. We remark that local memory capacity on the source tile is *the* limiting factor for message size. As scale increases, the maximum usable message size decreases from 160 to 4 bytes. Small message size is, in turn, the primary factor for the low aggregate available bandwidth. Results are consistent with the findings already presented in Section 4.2.3.

Off chip. Scatter operations exhibit minimal degradation of performance when moving from on chip to off chip: aggregate bandwidth decreases from 6.3 to 5.6...5.2 GB/s. The aggregate bandwidth at scales 2...16 IPUs is virtually identical for gather and scatter operations.

4.5 All to all

In this section we study the performance of all-to-all collective operations on the IPU. Because of the number of distinct personalized transfers involved in this operation and the associated local memory footprint, we were unable to scale our benchmark to multiple IPUs, or even to an entire IPU. For that reason, results in this section will be incomplete. We report latency results up to half IPU (609 tiles). Half an IPU completes an all-to-all in 0.55 microseconds. Our results are in Table 4.15.

All to all. In an all-to-all operation, each tile in a group sends one distinct message to each tile in the group, itself included. If the group contains n members, each participant concurrently sends n distinct messages. The whole operation involves transferring n^2 distinct messages.

Message size. Each tile must dedicate to the operation n output buffers and n input buffers. This constraint limits the maximum message size usable in the operation. Specifically, we only consider messages consisting of a single word, because they allow us to benchmark the largest scale (1/2 IPU).

Scale. Because of the aforementioned considerations, we were unable to benchmark a whole-IPU all-to-all operation, or one involving multiple IPUs.

4.6 Reduction

We investigate the performance of reduction operations at different scales and in different topologies.

Reduction. A reduction involves a variable number of source tiles (depending

Scale	Experiment	Total tile count	Concurrent transfers	Total latency (μ s)	Avg. latency per transfer (ns)
	Transfer to self (via local memory)	1	1	0.012	11.542
	On-chip: all tiles are on the same IPU				
	between 2 tiles	2	4	0.131	32.816
		4	16	0.125	7.812
	...	8	64	0.143	2.227
	...	16	256	0.163	0.637
	...	38	1,444	0.182	0.126
	...	76	5,776	0.215	0.037
1/8	...	152	23,104	0.256	0.011
1/4	... a quarter of one IPU	304	92,416	0.355	0.004
1/2	... half IPU	608	369,664	0.552	0.001
1	... the entire IPU	1,216	1,478,656	-	-

Table 4.15: Minimum all-to-all latency: latency of all-to-all communications in different scales.

on scale) plus one destination tile. The operation takes one input numerical array on each source tile, and returns one output numerical array on the destination tile. (For the avoidance of doubt, we are describing the equivalent of an `MPI_Reduce` primitive, not an `MPI_Allreduce`.)

Weak vs. Strong Scaling. As we vary the scale of the experiment, we consider two scenarios: one in which the total amount of input operands grows linearly with parallelism (weak scaling) and one in which it remains constant (strong scaling).

Benchmark. The Poplar SDK offers `popops::reduce`, a library primitive that performs the reduction. Our experiments simply benchmark this primitive's performance. We use sum as a reduction operation.

No load. Experiments in this section study load conditions in which no other operation is in progress. Each transfer's performance is affected only by the load caused by the remainder of the collective operation.

SDK version. Actual performance depends on the library function implementation provided with the specific version of SDK employed. Our results are only representative of SDK 1.0.49.

4.6.1 Minimum Reduction Latency - Weak Scaling

We study how the latency of one reduction scales (first weakly, then strongly) as it extends across tiles, then across IPUs on one board, then across boards, finally spanning an entire 16-IPU system. Interestingly, we find the latency associated with completely distributed reduction is comparable (11...16% more expensive) than a sequential operation of equal input size entirely performed on one tile. Detailed results are in Table 4.16.

Intent The purpose of this experiment is to understand how larger scale and parallelism affect the overall latency and the per-operand latency of the operation. In this context, we are especially interested in the data transfer component, and not in the arithmetics involved in the reduction. Specifically, the larger is the scale, the higher is the fraction of messages occurring over slower interconnects, i.e., IPU link vs. exchange, or more vs. fewer hops.

Input size: in this section, all parallel experiments intentionally use the smallest inputs, i.e., one single-precision floating point value (32 bits) per tile. This choice exposes primarily the cost of data transfers, as opposed to that of arithmetic computation or local memory access.

For comparison against the parallel experiments, we also perform single-tile baseline experiments of equal input size as the parallel ones (i.e., 1,216, then 2,432, ... finally 19,456 operands). These measurements serve as a baseline for the cost of a reduction when no parallelism is involved.

Experiment	Operands per tile	Tiles involved	Total latency (μs)	Avg. latency per input operand (ns)
Baseline sequential				
1 tile	1,216	1	1.69	1.39
1 tile	2,432	1	2.44	1.00
1 tile	4,864	1	3.97	0.82
1 tile	9,728	1	7.02	0.72
1 tile	19,456	1	13.10	0.67
Increasing system diameter				
1 IPU, 1 tile	1	1	0.44	0.44
2 IPUs on the same board	1	2	1.13	0.57
4 IPUs on two PCI boards	1	4	1.48	0.37
8 IPUs on four PCI boards	1	8	2.02	0.25
16 IPUs, entire system	1	16	3.16	0.20
Increasing scale				
1 IPU, all 1,216 tiles	1	1,216	1.97	1.62
2 IPUs on the same board	1	2,432	5.32	2.19
2 IPUs on different boards, direct IPU link	1	2,432	3.60	1.48
2 IPUs on different boards, no direct IPU link	1	2,432	7.09	2.92
4 IPUs on two PCI boards	1	4,864	7.18	1.48
8 IPUs on four PCI boards	1	9,728	7.68	0.79
16 IPUs, entire system	1	19,456	14.51	0.74

Table 4.16: Reduction, weak scaling: Latency of one reduction as it scales up from a single tile to an entire 16-IPU system.

Experiment	Operands per tile	Tiles involved	Total latency (μs)	Avg. latency per input operand (ns)
Baseline - one tile	19,456	1	13.1	0.67
1 IPU, all 1,216 tiles	16	1,216	2.1	0.11
2 IPUs on the same board	8	2,432	5.4	0.28
2 IPUs on different boards, direct IPU link	8	2,432	3.7	0.19
2 IPUs on different boards, no direct IPU link	8	2,432	7.20	0.37
4 IPUs on two PCI boards	4	4,864	7.28	0.37
8 IPUs on four PCI boards	2	9,728	7.78	0.40
16 IPUs, entire system	1	19,456	14.51	0.75

Table 4.17: Reduction, strong scaling: Latency of one reduction as it scales up from a single tile to an entire 16-IPU system.

4.6.2 Minimum Reduction Latency - Strong Scaling

We benchmark reduction latency once more, but in a strong scaling scenario: problem size is kept constant across experiments at different scales, in order to expose the cost of parallelization. We choose the smallest input size that would place one operand per tile on the largest system considered, i.e., 19,456 operands. Reducing 19,456 single-precision values on one IPU takes 2.1 microsecond. Performing the same reduction on a 16-IPU system costs 14.51 microseconds.

4.6.3 Peak Reduction Bandwidth

We measure the throughput achieved by reductions of different sizes and scale. As a measure of reduction throughput, we adopt the input operand size consumed in the unit of time. In this section, all experiments study weak scaling. For simplicity, we report quantitative results for only two choices (1,000 and 25,000 operands per tile) of input size, in Table 4.18. In Figure 4.11 we chart the effect of operand size on reduction bandwidth in a broader and more detailed spectrum of input sizes.

On-chip scaling. In weak scaling conditions, on-chip aggregate reduction bandwidth grows remarkably well with system size. The aggregate per-chip throughput reaches 6.76 TB/s, with a parallel efficiency equal to 92.2%.

Off-chip scaling. For larger inputs (25,000 values per tile), the aggregate throughput grows by a factor of 9.4 \times as the system scales up from 1 to 16 IPUs. The peak aggregate throughput of a 16-IPU system reaches an impressive 64.7 TB/s. The per-tile bandwidth degradation is approximately 41%; the parallel efficiency is 59%.

Operand size. The effect of operand size on performance is evident by direct comparison between the third and fourth band of the table, which report results of experiments with 1,000 and 25,000 values per tiles, respectively.

Experiment	Operands per tile	Tiles involved	Aggregate bandwidth (GB/s)	Bandw. per tile (GB/s)
Single-IPU baseline performance				
Baseline - 1,000 tiles	1,216	1,000	1,671	1.67
Baseline - 1,000 tiles	2,432	1,000	2,657	2.68
Baseline - 1,000 tiles	4,864	1,000	3,747	3.75
Baseline - 1,000 tiles	9,728	1,000	4,729	4.73
Baseline - 1,000 tiles	19,456	1,000	5,432	5.43
Large operands - Single-IPU Weak scaling				
Running on ... one tile	25,000	1	6	6.03
... 2 tiles	25,000	2	12	5.97
... 4 tiles	25,000	4	24	5.91
...	25,000	8	47	5.86
...	25,000	16	92	5.72
...	25,000	38	224	5.90
...	25,000	76	448	5.89
...	25,000	152	890	5.85
... a quarter of one IPU	25,000	304	1,769	5.82
... half IPU	25,000	608	3,481	5.73
... the entire IPU	25,000	1,216	6,756	5.56
Smaller operands - Multi-IPU Weak scaling				
1 IPU, all 1,216 tiles	1,000	1,216	1,636	1.34
2 IPUs on the same board	1,000	2,432	1,540	0.63
2 IPUs on different boards, direct IPU link	1,000	2,432	2,090	0.86
2 IPUs on different boards, no direct IPU link	1,000	2,432	1,230	0.51
4 IPUs on two PCI boards	1,000	4,864	2,381	0.49
8 IPUs on two PCI boards	1,000	9,728	4,512	0.46
16 IPUs, entire system	1,000	19,456	5,016	0.26
Larger operands - Multi-IPU Weak scaling				
1 IPU, all 1,216 tiles	25,000	1,216	6,756	5.56
2 IPUs on the same board	25,000	2,432	11,399	4.69
2 IPUs on different boards, direct IPU link	25,000	2,432	12,400	2.55
2 IPUs on different boards, no direct IPU link	25,000	2,432	10,485	2.16
4 IPUs on two PCI boards	25,000	4,864	20,965	4.31
8 IPUs on two PCI boards	25,000	9,728	41,128	4.23
16 IPUs, entire system	25,000	19,456	63,724	3.28

Table 4.18: Reduction bandwidth available at different scales (sequential, 1-16 IPUs) and for different input sizes, in weak scaling conditions.

Larger operands achieve a substantially higher bandwidth at any scale, and better scalability overall: the large-vs-small operand speedup is $4.1 \times$ on a single IPU, but it grows to $12.7 \times$ on a 16-IPU system. We chart a broader set of results describing the same trends in Figure 4.11.

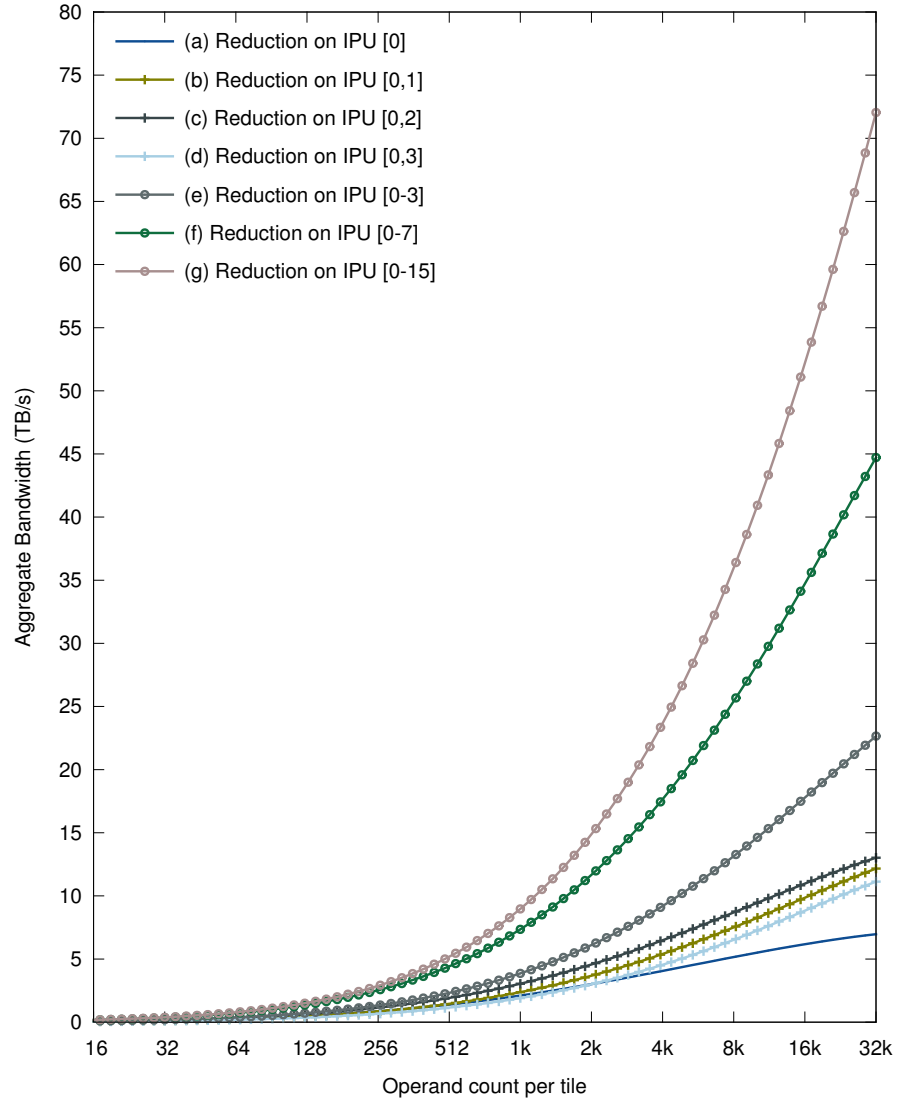


Figure 4.11: Effect of operand size on reduction bandwidth in weak scaling conditions. IPU identifiers are DNC IDs.

4.7 Host Connectivity

In this section we present bandwidth and latency associated with host-to-IPU data transfers. These metrics are relevant to evaluate potential bottleneck in achieving high performance in hybrid CPU/IPU applications where the PCI-express bus lies in the critical path. Bandwidth is important for streaming applications where CPU data are continuously offloaded to the IPU, and latency is important for inference applications where the output is produced in a ping-pong fashion across CPU and IPU. The reader should pay consideration to fact that PCI-express is an industry-standard I/O technology; the results presented here are meant to be compared against the theoretical limit.

SDK version. Performance depends on the version of SDK and drivers employed. Our results are only representative of SDK 1.0.49. We expect Graphcore to further optimize host-to-IPU connectivity performance in future releases.

4.7.1 Minimum Host-to-IPU Latency

Benchmark description: we use a benchmark that sends data from the host to a tensor on IPUs using the `graph::DataStream` mechanism with an empty callback to minimize overhead associated with the software stack. Depending on the benchmark scale and IPU count, the tensor is distributed across local memories such as each tile receives exactly 4 byte data. The latency measurements are taken on the host side as average over multiple multiple synchronous transfers.

Observations: as shown in Table 4.19, the latency to transfer data to an IPU is at least 8.81 μ s and is stable across the PCI-express topology. Sending data to different destination IPUs doesn't show obvious differences in latency. Data transfer latency also doesn't increase when communicating with multiple IPUs. We only notice a slight increase in latency as destination tile count increases. This, however, is a consequence of moving a tensor large enough to fit the maximum PCI-express payload size, requiring multiple transactions to complete the transfer.

4.7.2 Peak Host-to-IPU Bandwidth

Benchmark description: we measure aggregate bandwidth with a benchmark that transfers data from the host to a tensor on IPUs via `graph::DataStream`. The destination tensor is partitioned linearly across all involved tiles and IPUs. The benchmark sends 40 KB data to each tile, and up to 778.24 MB to all 16 IPUs. We report results in Table 4.20.

Observations: the achieved aggregate bandwidth increases with the growth of involved PCIe lane count. Since each IPU is connected to the PCIe switch via 8 PCIe Gen3 lanes, transfers to one IPU reaches up to \sim 6 GB/s. Every

Scale (IPUs)	Experiment	Destination tiles	Total latency (μs)
Destination tiles are on IPU 0			
	From CPU ... to 1 tile	1	8.81
	... to 2 tiles	2	8.84
	...	4	8.89
	...	8	8.31
	...	16	8.81
	...	38	8.81
	...	76	9.01
1/8	...	152	8.80
1/4	... to a quarter of one IPU	304	8.95
1/2	... to half IPU	608	9.56
1	... to the entire IPU	1,216	9.87
1 Single destination IPU			
	... to 1 tile on IPU 0	1	8.87
	... to 1 tile on IPU 1	1	8.89
	... to 1 tile on IPU 2	1	8.83
	... to 1 tile on IPU 3	1	8.80
	... to 1 tile on IPU 4	1	8.82
	... to 1 tile on IPU 5	1	8.81
	... to 1 tile on IPU 6	1	8.83
	... to 1 tile on IPU 7	1	8.85
	... to 1 tile on IPU 8	1	8.84
	... to 1 tile on IPU 9	1	8.80
	... to 1 tile on IPU 10	1	8.82
	... to 1 tile on IPU 11	1	8.81
	... to 1 tile on IPU 12	1	8.80
	... to 1 tile on IPU 13	1	8.81
	... to 1 tile on IPU 14	1	8.88
	... to 1 tile on IPU 15	1	8.82
Multiple destination IPUs, 1 tile each IPU			
2	... to 2 IPUs on the same board	2	8.88
2	... to 2 IPUs across boards, direct IPU link	2	8.83
2	... to 2 IPUs across boards, no direct IPU link	2	8.84
4	... to 4 IPUs on two boards	4	8.83
8	... to 8 IPUs on four boards	8	8.82
16	... to 16 IPUs, entire system	16	8.83

Table 4.19: Minimum host-to-IPU latency in experiments of different scale and topology.

Scale (IPUs)	Experiment	Destination tiles	PCIe lanes	Aggregate bandwidth (GB/s)	Bandw. per tile (MB/s)
Destination tiles are on IPU 0					
	From CPU to 1 tile	1	8	2.57	2,565.29
	... to 2 tile	2	8	3.54	1,768.85
		4	8	4.41	1,103.05
		8	8	5.07	634.30
		16	8	5.43	339.50
		38	8	5.85	154.04
		76	8	5.74	75.50
1/8	...	152	8	5.80	38.17
1/4	... to a quarter of one IPU	304	8	5.82	19.15
1/2	... to half IPU	608	8	5.87	9.66
1	... to the entire IPU	1,216	8	5.86	4.82
1	Single destination IPU				
	... to all tiles on IPU 1	1,216	8	5.84	4.80
	... to all tiles on IPU 2	1,216	8	5.85	4.81
	... to all tiles on IPU 3	1,216	8	5.87	4.82
	... to all tiles on IPU 4	1,216	8	5.84	4.80
	... to all tiles on IPU 5	1,216	8	5.84	4.80
	... to all tiles on IPU 6	1,216	8	5.84	4.80
	... to all tiles on IPU 7	1,216	8	5.84	4.80
	... to all tiles on IPU 8	1,216	8	5.97	4.91
	... to all tiles on IPU 9	1,216	8	6.02	4.95
	... to all tiles on IPU 10	1,216	8	6.03	4.96
	... to all tiles on IPU 11	1,216	8	6.02	4.95
	... to all tiles on IPU 12	1,216	8	6.03	4.96
	... to all tiles on IPU 13	1,216	8	6.03	4.96
	... to all tiles on IPU 14	1,216	8	6.03	4.96
	... to all tiles on IPU 15	1,216	8	6.03	4.96
Multiple destination IPUs					
2	... to 2 IPUs on the same board	2,432	16	11.35	4.67
2	... to 2 IPUs across boards, direct IPU link	2,432	16	11.36	4.67
2	... to 2 IPUs across boards, no direct IPU link	2,432	16	11.35	4.67
4	... to 4 IPUs on two boards	4,864	16	13.78	2.83
8	... to 8 IPUs on four boards	9,728	32	27.55	2.83
16	... to 16 IPUs, entire system	19,456	64	55.04	2.83

Table 4.20: Peak host-to-IPU bandwidth available to concurrent transfers in different transfer topologies.

four IPUs share the same 16 PCIe lanes, thus the transfer to 4 IPUs (h) can only achieve 13.78 GB/s. The transfer to all 16 IPUs (j) enjoys a bandwidth of 55.04 GB/s.

Chapter 5

Notable Arithmetic Primitives

5.1 Matrix Multiplication

Dense matrix multiplication (matmul) is a workload of such pervasive presence in HPC and AI/ML applications that its performance on a computing architecture is frequently used (and sometimes abused) as a singular proxy for an architecture’s overall performance. In this section, we report and discuss IPU dense matrix multiplication performance as offered by poplin, Graphcore’s linear algebra library, at the time of writing. We compare the IPU’s matmul performance with contemporary GPUs in terms of aggregate throughout and energy efficiency. We find that the IPU offers an impressive arithmetic throughput, up to 31.1 TFlops/s in single precision and 124.5 TFlops/s in mixed precision per chip, surpassing the GPU’s theoretical limits. Actual performance measured on GEMM benchmarks show the IPU as a clear winner in single precision against NVidia’s V100 GPU. In mixed precision, the comparison does not yield a clear winner and requires a more nuanced discussion that follows.

IPU-GPU comparisons. The IPU offers impressive theoretical compute power thanks to its specialized hardware called *Accumulating Matrix Product* (AMP) units. These units are similar in purpose to the GPU’s TensorCore units. In the comparisons that follow, the reader should pay consideration to the fact that while one C2 IPU board contains two IPU processors, a Volta GPU board (either PCI or SXM2) only contains one GPU processor; we focus on the per-chip comparisons as of interest to architecture designers.

Theoretical limits. Each IPU tile contains one AMP unit. An AMP unit can finish 64 mixed-precision or 16 single-precision floating point operations per clock cycle. At a 1.6-GHz clock rate, the 1,216 tiles on one IPU deliver 31.1 and 124.5 TFlops/s in single and mixed precision, respectively. In single precision, one IPU processor offers almost twice as much single-precision theoretical throughput as one V100 GPU: 31.1 vs. 15.7 TFlops/s. This result also reflects the fact that on the GPU, TensorCores do not support single precision,

Arithmetic		Graphcore C2 IPU		NVidia Volta V100 (SXM2)	
Precision		Units	1 IPU	Units	1 GPU
Single (FP32)	Theoretical	AMP	31.1	TensorCores	N/A
	Theoretical	Vector	7.8	FP cores	15.7
	Actual GEMM % Theor.	AMP	18.9 60.7%	FP cores	15.5 98.7%
Mixed (FP16.32)	Theoretical	AMP	124.5	TensorCores	125.0
	Theoretical	Vector	15.6	FP cores	31.4
	Actual GEMM % Theor.	AMP	58.9 47.3%	TensorCores	90.0 72.0%

Table 5.1: Arithmetic throughput per-chip comparison between IPUs and GPUs. We offer theoretical upper bounds and actual peak performance that we benchmarked on matrix-matrix multiplication (GEMM). Both platforms offer specialized units; we offer independent theoretical upper bounds for specialized and non-specialized units on both platforms. Benchmarks used the respective vendors’ optimized GEMM functions.

and single-precision computation uses regular FP cores. In mixed precision, one IPU processor roughly matches one V100 GPU (124.5 vs. 125.0 TFlops/s). Rows labeled as “Theoretical” in Table 5.1 report these numbers side to side, offering separate limits for specialized and non-specialized units.

Benchmark. Our experiments benchmark each device’s performance as all of the chip’s resources are used to perform one, large, matrix-matrix multiplication. We study performance sensitivity to input size. For simplicity, we only consider square input matrices, i.e., matmul of A and B , both of size $n \times n$. We vary n from 16 to the largest size fitting matrices.

Version sensitivity. Because we are benchmarking library functions, performance is also a factor of code optimization, not just hardware compute power. We report actual GEMM performance delivered on each device by the respective manufacturers’ optimized linear algebra libraries: Graphcore’s poplin and NVidia’s cuBlas. Our IPU results only describe SDK version 1.0.49, and may differ significantly from future, more optimized poplin versions. Same considerations apply to the GPU, where we used cuBLAS version 10.1.0.105.

Single precision. We measured 18.9 TFlops/s per IPU at peak, which is 60% of the theoretical limit. The two IPUs on a C2 board can deliver twice as much performance (37.8 TFlops/s) if used in parallel on independent matrix operands. The IPU outperforms the GPU in a per-chip comparison. This result reflects the fact that the GPU’s specialized TensorCore units do not support pure single precision. In Table 5.1, “Actual GEMM” rows report these results, also specifying what hardware units the library’s GEMM implementation uses at each precision and what fraction of theoretical throughput they achieve.

	Precision	
	Single	Mixed
Theoretical arithmetic throughput	31.1 TFlops/s	124.5 TFlops/s
Actual, Peak	18.9 TFlops/s	58.2 TFlops/s
Actual/theoretical fraction	60.7 %	46.7%

Table 5.2: Theoretical arithmetic throughput compared to the actual peak throughput we measured on dense matrix multiplication on one IPU.

While the IPU delivers higher throughput, the GPU supports larger operands thanks to its higher device memory capacity. In our experiments, the largest square matrix operands fitting one IPU are $2,944 \times 2,944$, while on a 32-GB GPU they are roughly $\sim 50,000 \times \sim 50,000$.

Mixed precision. On both devices, specialized hardware (TensorCores and AMP units) supports matrix multiplication in mixed precision. Despite one IPU delivering roughly the same theoretical throughput as one GPU, in GEMM benchmarks the IPU yields lower performance than a V100 GPU: 58.9 TFlops/s vs. 90.0 TFlops/s, respectively. The IPU uses a lower fraction of its theoretical limit (47.3%) than the GPU (72.0%). See the lower half of Table 5.1.

In mixed precision as well, the GPU supports larger operands. The largest square matrix operands fitting an IPU are $2,688 \times 2,688$, while on a 32-GB GPU they are roughly $\sim 72,000 \times \sim 72,000$.

Tile mapping. We benchmark two mappings of input operands to tile memory:

- **basic:** this benchmark invokes function `poplin::matMulAcc`, mapping matrices to tiles linearly via function `poputil::mapTensorLinearly`. Specifically, input matrices are spread evenly over tiles in a linear lexicographic manner, with the indices of the flattened matrix mapped across increasing tile IDs;
- **optimized:** this benchmark includes an optimization that preconditions the two input operands via functions `poplin::createMatMulInputLHS` and `...RHS`. It then uses `poplin::matMul` and `popops::scaledAddTo`.

Comparison with GPUs. We compare IPUs and GPUs in terms of throughput and energy efficiency in single and mixed precision. This is a measurement of how well a platform can minimize the latency to complete matmuls when the entirety of the processor is available for a single task. We offer comparisons on a per-chip and per-board basis. Since the IPU board has two chips, we consider a library-based matmul benchmark that extends the matmul operation

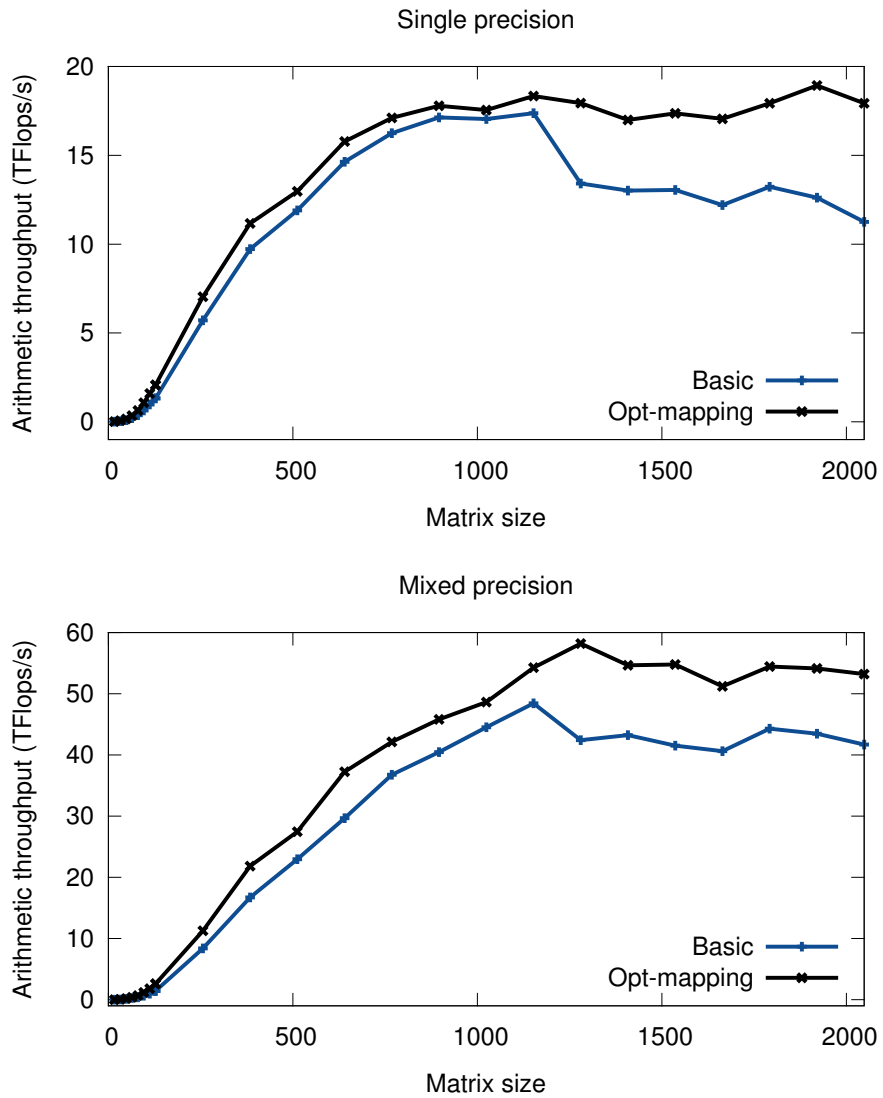


Figure 5.1: Floating-point arithmetic throughput achieved by dense matrix multiplication on one IPU. For simplicity, we use square inputs ($n \times n$) \times ($n \times n$); the horizontal axis varies n .

to both IPUs on a C2 board. The GPU we consider is NVidia’s V100. Table 5.2 summarizes our findings.

We chart results in Figure 5.1, where the horizontal axis represents n , one side of each square input operand matrix. Performance varies with input size, with smaller matrices unable to achieve sufficient occupancy of the device.

This is a common occurrence among massively parallel computing platform and is of little consequence in most cases. In our benchmark using optimized tile mapping, performance saturates around 18 and 55 ... 58 TFlops/s in single and mixed precision, respectively.

We also compare the devices in terms of energy efficiency by charting throughput values divided by nominal power absorbed by each board in Figure 5.3. Results are expressed in units of TFlops/s per Watt (TFlops/s/W). For the V100 GPU, we use nominal power, 250 W.

In both single and mixed precision cases, a single IPU delivers higher efficiency than two IPUs and higher efficiency than the V100 GPU.

5.2 Convolution

We dedicate this section to studying the IPU’s convolution performance. For our benchmarking suite, we selected a basket of 6 commonly used CNNs in image classification according to our survey of recent literature [9, 10, 11, 12, 13, 14]. We compare the IPU’s and the V100 GPU’s forward-pass performances, on a per-chip basis, first in terms of arithmetic throughput (TFlops/s), and then in terms of throughput normalized per nominal power consumption (TFlops/s/W). In our results, IPUs tend to outperform GPUs at smaller batch sizes. While the GPU supports larger batches thanks to its larger device memory, it also needs to use larger batches for its compute resources to achieve sufficient occupancy. For CNNs whose architectures were designed without GPU efficiency in mind (such as ResNeXt), we observe speedups upward of 700x.

Benchmarking. On each device, we use the manufacturer’s respective optimized convolution primitives: `poplin::convolution` from the Poplar SDK version 1.0.49, and `cudnnConvolutionForward` from cuDNN 7.5.0. All benchmarks use half precision floating point math.

Batch size. On both platforms, we vary batch size over a meaningful range. Note that sufficiently large batches exceed the memory capacity of both IPUs and GPUs. Because of the larger GPU device capacity, it supports larger batch sizes for most layers. Our experiments sweep the range 1 ... 2,048 on the GPU and 1 ... 128 on the IPU.

Raw results. In Tables 5.4 and 5.5 we report in detail the arithmetic throughput achieved by each layer of each CNN, for each batch size considered, on the GPU and IPU respectively. Results show that the GPU prefers larger batch sizes, with most network layers reaching their peak performances at batch size 512 or 1,024. In contrast, the IPU supports smaller batch sizes and tends to achieve peak performance with batch sizes in the 8...32 range. Moreover, for sizes below peak, the IPU still delivers a good fraction of peak throughput.

Comparison at peak. We now present a simpler and more concise analy-

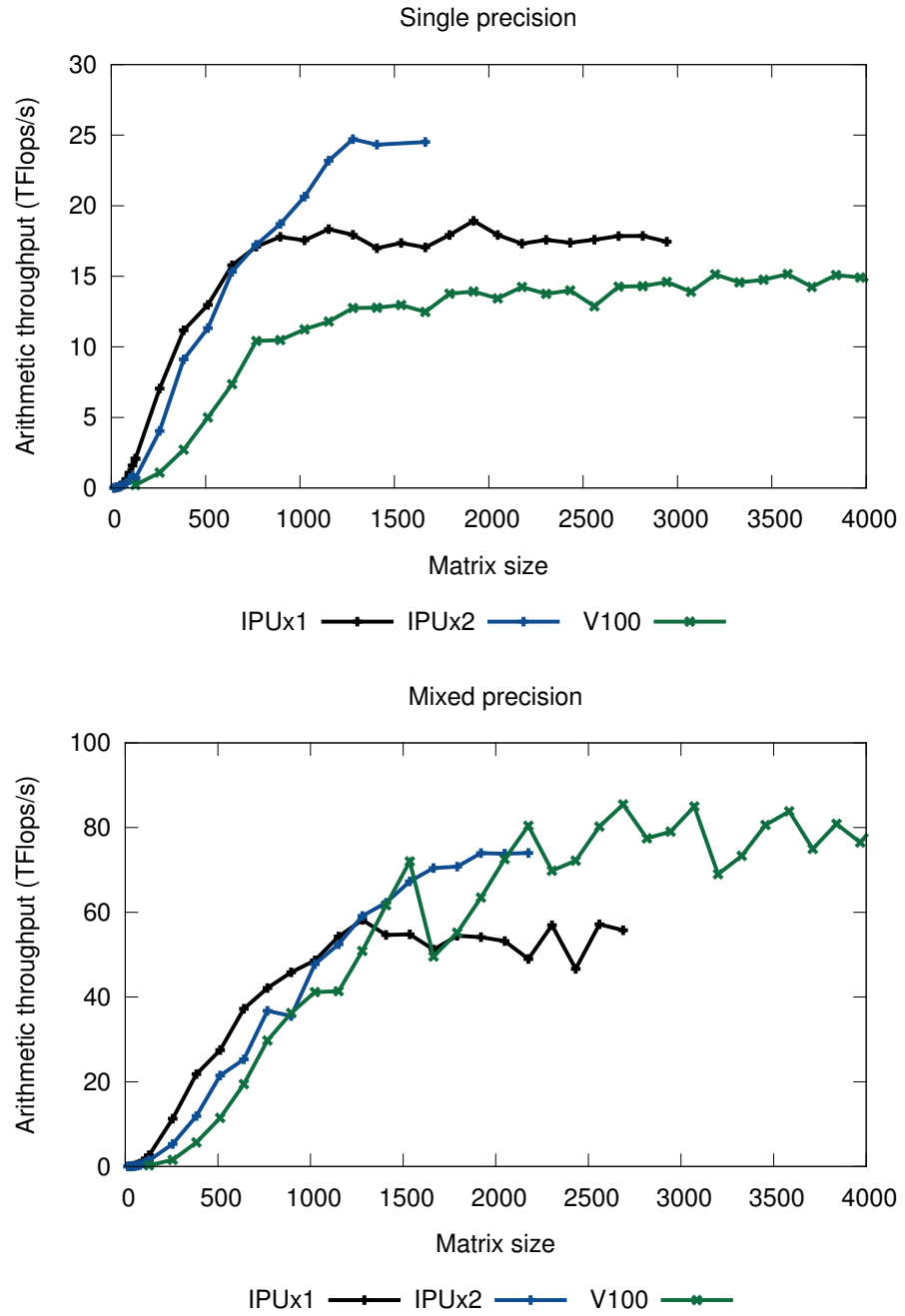


Figure 5.2: Matrix multiplication performance on IPUs and GPUs.

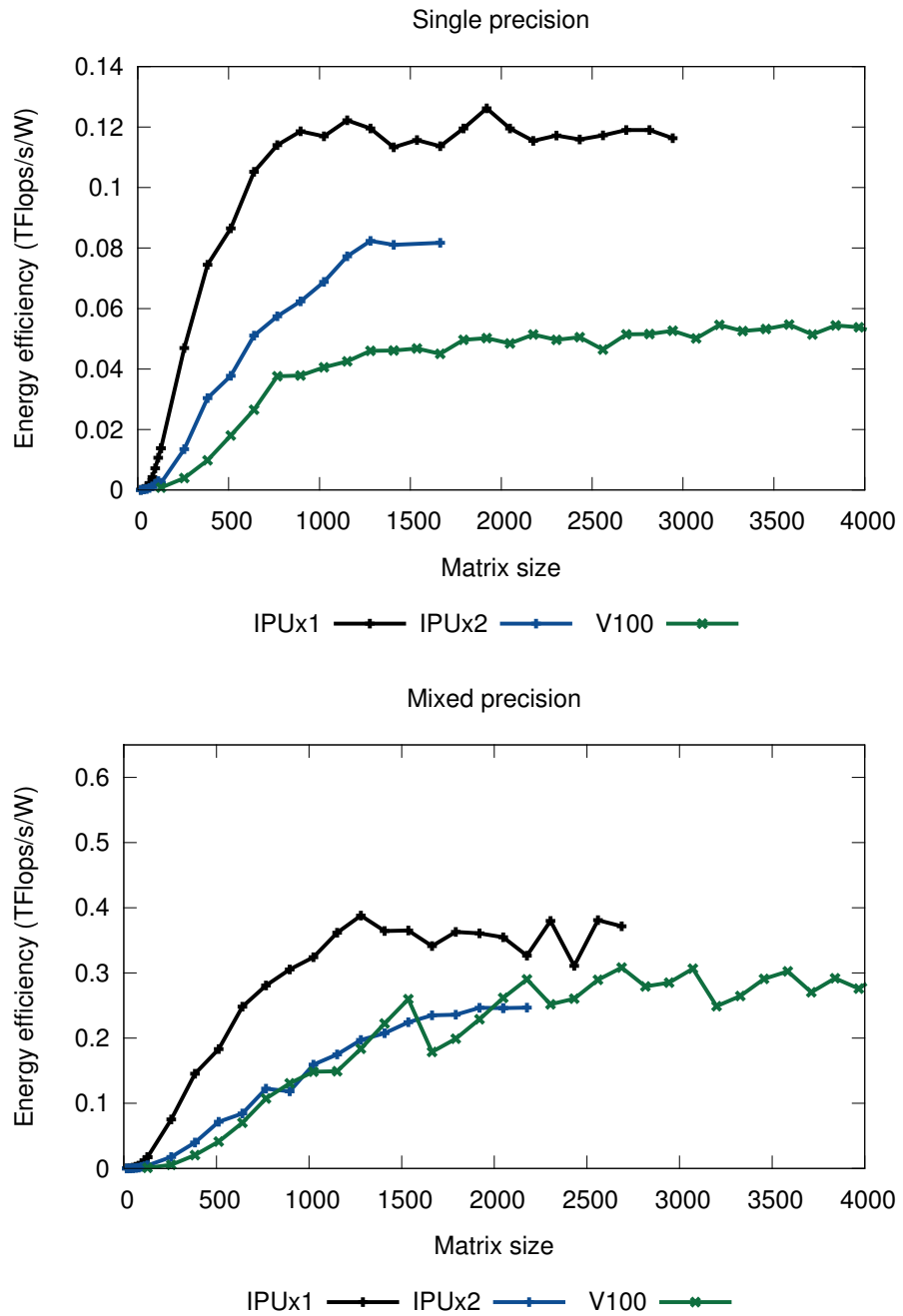


Figure 5.3: Energy efficiency while running matrix multiplication on IPUs and GPUs.

sis that abstracts away from batch size. Specifically, we compare the IPU’s and the GPU’s peak performance at each CNN layer (at the respective peak, whichever batch sizes they correspond to). Table 5.3 shows both arithmetic throughput comparisons and energy efficiency comparisons. We use nominal power figures (250 W for the GPU, 150 W for the IPU). Columns labeled **Ratio** show the IPU/GPU throughput and energy efficiency ratios, with over-unity values indicating an IPU advantage.

Discussion. Results in Table 5.3 support the expectation that the highly parallel fine-grained MIMD architecture of the IPU would provide an advantage in models using group or separable convolutions. When G=32 for the ResNeXt model, the IPU shows >100x advantage for certain convolutions. This advantage is not available in legacy CNN models that were originally optimized for the GPU architecture.

Table 5.3: Comparison between one V100 GPU and one IPU (per chip) in terms of arithmetic throughput and energy efficiency (i.e., arithmetic throughput normalized over nominal power). Benchmark: reference basket of convolutional neural networks [9, 10, 11, 12, 13, 14]. The **ratio** column reports IPU-over-GPU ratios; over-unity values mean that the IPU is performing better than the GPU; below-unity, vice versa. Parameters: F_s : filter size (height = width); I_s : input size (height = width); I_c : input channel; O_c : output channel; S : stride; G : group.

Layer	Parameters						Arithmetic Throughput (TFlops/s)			Energy Efficiency (TFlops/s/W)		
	F_s	I_s	I_c	O_c	S	G	IPU	V100	Ratio	IPU	V100	Ratio
ResNeXt												
Conv1	7	224	3	64	2	1	15.04	6.26	2.40	0.10	0.03	4.00
Conv2.1	3	112	64	64	2	1	62.07	22.85	2.72	0.41	0.09	4.53
Conv2.2	1	56	64	128	1	32	0.32	0.04	8.11	0.00	0.00	13.51
Conv2.3	3	56	128	128	1	32	2.58	0.44	5.86	0.02	0.00	9.77
Conv2.4	1	56	128	256	1	32	1.14	0.15	7.59	0.01	0.00	12.65
Conv3.1	1	28	256	256	1	32	6.90	0.02	344.96	0.05	0.00	574.94
Conv3.2	3	28	256	256	1	32	36.13	0.75	48.17	0.24	0.00	80.29
Conv3.3	1	28	256	512	1	32	10.22	0.03	340.59	0.07	0.00	567.66
Conv4.1	1	14	512	512	1	32	28.21	0.04	705.23	0.19	0.00	1175.38
Conv4.2	3	14	512	512	1	32	45.69	1.38	33.11	0.30	0.01	55.18
Conv4.3	1	14	512	1024	1	32	31.57	0.06	526.23	0.21	0.00	877.05
Conv5.1	1	7	1024	1024	1	32	28.05	0.08	350.61	0.19	0.00	584.35
Conv5.2	3	7	1024	1024	1	32	37.14	4.74	7.84	0.25	0.02	13.06
Conv5.3	1	7	1024	2048	1	32	33.41	0.11	303.76	0.22	0.00	506.27
ResNet-50 v1.5												
Conv1	7	224	3	64	2	1	15.04	6.13	2.45	0.10	0.02	4.09
Conv2.1	3	112	64	64	2	1	62.32	23.27	2.68	0.42	0.09	4.46
Conv2.2	1	56	64	64	1	1	52.39	8.48	6.18	0.35	0.03	10.30
Conv2.3	3	56	64	64	1	1	73.43	47.74	1.54	0.49	0.19	2.56
Conv2.4	1	56	64	256	1	1	58.55	12.09	4.84	0.39	0.05	8.07
Conv3.1	1	28	256	128	1	1	54.87	20.71	2.65	0.37	0.08	4.42
Conv3.2	3	28	128	128	1	1	58.13	64.07	0.91	0.39	0.26	1.51
Conv3.3	1	28	128	512	1	1	62.39	21.38	2.92	0.42	0.09	4.86
Conv4.1	1	14	256	256	1	1	44.41	26.61	1.67	0.30	0.11	2.78
Conv4.2	3	14	256	256	1	1	52.78	78.29	0.67	0.35	0.31	1.12
Conv4.3	1	14	256	1024	1	1	60.92	33.67	1.81	0.41	0.13	3.02
Conv5.1	1	7	512	512	1	1	41.43	37.73	1.10	0.28	0.15	1.83
Conv5.2	3	7	512	512	1	1	52.71	85.48	0.62	0.35	0.34	1.03
Conv5.3	1	7	512	2048	1	1	57.72	48.69	1.19	0.38	0.19	1.98
Inception v3												
Conv1	3	299	3	32	2	1	7.08	3.91	1.81	0.05	0.02	3.02

Layer	Parameters						Arithmetic Throughput (TFlops/s)			Energy Efficiency (TFlops/s/W)		
	F_s	I_s	I_c	O_c	S	G	IPU	V100	Ratio	IPU	V100	Ratio
Conv2	3	149	32	32	1	1	71.59	24.05	2.98	0.48	0.10	4.96
Conv3	3	147	32	64	1	1	70.25	38.33	1.83	0.47	0.15	3.05
Conv4	3	147	64	64	2	1	57.36	23.39	2.45	0.38	0.09	4.09
Conv5	3	73	64	80	1	1	65.66	37.49	1.75	0.44	0.15	2.92
Conv6	3	71	80	192	2	1	61.90	32.77	1.89	0.41	0.13	3.15
Conv7	3	35	192	288	1	1	62.12	61.78	1.01	0.41	0.25	1.68
Conv8	3	35	288	768	2	1	50.85	59.17	0.86	0.34	0.24	1.43
Conv9	3	17	768	1280	2	1	45.56	72.17	0.63	0.30	0.29	1.05
Conv10	3	8	1280	2048	1	1	49.27	87.92	0.56	0.33	0.35	0.93
VGGG16												
Conv1_1	3	224	3	64	1	1	7.20	3.83	1.88	0.05	0.02	3.13
Conv1_2	3	224	64	128	1	1	75.04	52.01	1.44	0.50	0.21	2.40
Conv2_1	3	112	128	128	1	1	72.60	64.59	1.12	0.48	0.26	1.87
Conv2_2	3	112	128	256	1	1	71.79	70.46	1.02	0.48	0.28	1.70
Conv3_1	3	56	256	256	1	1	70.20	78.75	0.89	0.47	0.32	1.49
Conv3_2	3	56	256	512	1	1	72.10	81.35	0.89	0.48	0.33	1.48
Conv4_1	3	28	512	512	1	1	58.53	87.22	0.67	0.39	0.35	1.12
Conv4_2	3	28	512	512	1	1	58.54	87.28	0.67	0.39	0.35	1.12
Conv5_1	3	14	512	512	1	1	49.92	87.02	0.57	0.33	0.35	0.96
SSD v1.1												
Conv1	3	38	512	1024	2	1	53.35	71.51	0.75	0.36	0.29	1.24
Conv2	1	19	1024	1024	1	1	54.83	53.46	1.03	0.37	0.21	1.71
Conv3	1	19	1024	512	1	1	57.01	47.1	1.21	0.38	0.19	2.02
Conv4	3	10	512	512	2	1	46.76	63.02	0.74	0.31	0.25	1.24
Conv5	1	10	512	128	1	1	35.19	24.09	1.46	0.23	0.10	2.43
Conv6	3	10	128	256	2	1	31.83	52.52	0.61	0.21	0.21	1.01
Conv7	1	5	256	128	1	1	16.21	16.07	1.01	0.11	0.06	1.68
Conv8	3	5	128	256	1	1	30.16	63.86	0.47	0.20	0.26	0.79
Conv9	1	3	256	128	1	1	8.81	10.12	0.87	0.06	0.04	1.45
Conv10	3	3	128	256	1	1	17.56	45.51	0.39	0.12	0.18	0.64
AlexNet												
Conv1	11	227	3	96	4	1	20.04	14.7	1.36	0.13	0.06	2.27
MaxPool1	3	55	96	96	2	1	51.73	33.12	1.56	0.34	0.13	2.60
Conv2	5	27	96	256	1	1	64.34	86.46	0.74	0.43	0.35	1.24
MaxPool2	3	27	256	256	2	1	49.21	50.37	0.98	0.33	0.20	1.63
Conv3	3	13	256	384	1	1	53.70	82.07	0.65	0.36	0.33	1.09
Conv4	3	13	384	256	1	1	52.91	82.02	0.65	0.35	0.33	1.08
Conv5	3	13	256	256	2	1	41.77	54.93	0.76	0.28	0.22	1.27

Table 5.4: Convolution performance (arithmetic throughput, TFlops/s) of one NVidia V100 GPU, in half precision, over our reference basket of convolutional neural network architectures. Missing data represents experiments that did not fit in device memory.

Layer name	Batch size											
	1	2	4	8	16	32	64	128	256	512	1024	2048
ResNeXt												
Conv1	2.71	3.75	4.05	5.01	5.89	6.02	6.10	6.14	6.21	6.24	6.26	6.25
Conv2.1	5.89	9.92	15.04	17.91	18.42	21.02	22.25	22.68	22.85	22.79	22.72	22.63
Conv2.2	0.00	0.01	0.01	0.03	0.04	0.04	0.04	0.04	0.04	0.04	0.04	0.04
Conv2.3	0.11	0.20	0.32	0.40	0.43	0.44	0.44	0.44	0.44	0.44	0.44	0.44
Conv2.4	0.01	0.03	0.05	0.11	0.14	0.15	0.15	0.15	0.15	0.15	0.15	0.15
Conv3.1	0.00	0.01	0.02	0.02	0.02	0.02	0.02	0.02	0.02	0.02	0.02	0.02
Conv3.2	0.10	0.20	0.39	0.75	0.17	0.18	0.18	0.18	0.18	0.18	0.17	0.18
Conv3.3	0.01	0.02	0.02	0.02	0.03	0.03	0.03	0.03	0.03	0.03	0.03	0.03
Conv4.1	0.00	0.01	0.02	0.04	0.04	0.04	0.04	0.04	0.04	0.04	0.04	0.04
Conv4.2	0.10	0.20	0.36	0.73	1.38	0.34	0.36	0.35	0.36	0.35	0.36	0.35

Layer name	Batch size											
	1	2	4	8	16	32	64	128	256	512	1024	2048
Conv4_3	0.01	0.02	0.03	0.04	0.05	0.05	0.06	0.06	0.05	0.06	0.06	0.06
Conv5_1	0.00	0.01	0.02	0.04	0.07	0.07	0.08	0.08	0.08	0.08	0.08	0.08
Conv5_2	0.09	0.19	0.37	0.74	1.44	2.80	0.70	4.74	0.72	0.72	0.73	0.73
Conv5_3	0.01	0.02	0.03	0.07	0.09	0.10	0.11	0.11	0.11	0.11	0.11	0.11
ResNet v1.5												
Conv1	4.66	3.70	4.10	4.94	5.78	5.91	5.98	6.02	6.09	6.13	6.13	6.13
Conv2_1	4.71	10.00	15.45	18.15	18.70	21.38	22.72	23.13	23.27	23.23	23.14	23.07
Conv2_2	1.00	2.00	3.99	6.40	6.30	7.12	7.79	8.15	8.32	8.42	8.46	8.48
Conv2_3	6.02	11.79	17.47	29.06	32.83	37.18	42.50	44.11	45.32	46.58	47.41	47.74
Conv2_4	4.00	7.92	8.29	9.76	10.65	11.22	11.69	11.91	12.01	12.07	12.08	12.09
Conv3_1	2.11	4.16	7.77	12.23	15.95	16.02	18.36	19.93	20.33	20.53	20.61	20.71
Conv3_2	3.97	7.94	15.51	28.79	40.58	42.01	53.38	61.81	62.70	63.32	63.44	64.07
Conv3_3	4.07	8.28	13.90	14.69	17.34	19.04	19.88	20.59	20.97	21.21	21.33	21.38
Conv4_1	1.03	2.01	4.00	7.94	13.61	18.80	19.62	22.74	25.24	25.85	26.22	26.61
Conv4_2	2.38	4.67	9.18	18.04	34.50	48.05	50.21	65.12	76.76	77.85	78.10	78.29
Conv4_3	3.56	8.04	14.87	21.85	23.42	28.51	32.23	31.85	32.38	32.94	33.36	33.67
Conv5_1	0.85	1.68	3.15	6.10	11.46	20.43	28.45	29.07	34.73	36.68	37.27	37.73
Conv5_2	1.06	2.10	4.12	8.35	16.80	32.97	51.04	54.24	70.48	82.64	84.69	85.48
Conv5_3	3.28	6.51	12.10	21.96	31.54	33.78	42.23	48.69	47.44	43.98	44.33	44.76
Inception v3												
Conv1	1.43	1.02	1.15	1.30	1.42	1.46	1.50	1.52	1.53	1.54	1.54	3.91
Conv2	10.47	14.26	16.71	19.13	21.09	22.43	23.29	23.67	23.89	23.99	24.04	24.05
Conv3	18.47	23.19	26.73	30.21	33.03	34.69	36.28	37.27	37.94	38.05	38.33	
Conv4	9.02	14.25	17.35	18.12	20.40	22.21	23.21	23.28	23.39	23.44	23.24	
Conv5	12.14	18.11	20.81	26.57	31.35	34.52	36.46	36.68	37.23	37.25	37.49	37.49
Conv6	7.10	13.68	19.25	21.16	24.51	28.09	30.42	31.59	32.39	32.77	32.55	32.72
Conv7	14.95	28.98	40.86	43.01	56.34	57.85	58.77	61.21	61.52	61.67	61.75	61.78
Conv8	9.21	18.02	28.60	53.40	57.41	59.17	52.52	55.04	56.74	57.43	57.19	57.56
Conv9	3.68	7.29	14.62	24.16	47.03	52.68	71.49	72.17	59.45	61.66	62.97	62.78
Conv10	4.11	8.15	16.04	32.20	55.52	65.78	72.01	84.09	87.92	73.27	67.99	64.01
VGG16												
Conv1_1	2.30	2.72	3.22	3.43	3.60	3.72	3.79	3.81	3.83	3.83		
Conv1_2	41.87	48.67	49.97	50.68	51.28	51.58	52.01	51.78	51.96			
Conv2_1	40.21	42.06	53.15	62.04	62.83	63.37	63.57	64.28	64.59	64.59	64.58	
Conv2_2	43.70	53.64	66.60	68.17	68.78	69.18	69.96	70.40	70.43	70.46		
Conv3_1	34.34	48.55	50.16	65.04	76.28	76.92	77.02	77.34	78.27	78.73	78.71	78.75
Conv3_2	45.16	50.56	66.90	78.72	79.38	79.92	79.88	80.80	81.29	81.35	81.28	
Conv4_1	16.99	33.27	51.54	54.48	70.34	82.23	84.11	85.05	85.60	86.61	87.22	87.14
Conv4_2	16.94	33.23	51.53	54.48	70.33	82.30	84.10	85.03	85.59	86.59	87.17	87.28
Conv5_1	4.13	8.37	16.86	33.07	51.28	54.29	70.73	82.92	84.59	85.56	86.00	87.02
SSD v1.1												
Conv1	13.35	26.03	40.11	46.52	61.36	71.51	60.11	62.62	64.01	64.19	64.71	64.86
Conv2	11.12	20.92	37.38	37.73	46.92	52.85	49.97	51.73	52.71	53.00	53.25	53.46
Conv3	7.49	14.27	25.34	32.57	31.91	41.13	43.66	44.40	45.70	46.48	46.89	47.10
Conv4	0.54	1.07	2.14	4.17	8.33	13.23	25.46	47.36	49.94	63.00	62.44	63.02
Conv5	0.43	0.82	1.62	3.11	5.91	9.94	12.75	19.01	19.58	22.23	23.87	24.09
Conv6	0.26	0.51	1.03	2.04	3.91	7.57	11.21	20.49	35.59	37.91	46.05	52.52
Conv7	0.07	0.13	0.26	0.52	1.06	1.75	3.96	7.19	11.24	14.82	15.02	16.07
Conv8	0.26	0.52	1.03	2.02	3.98	7.84	15.22	28.90	39.35	48.53	54.89	63.86
Conv9	0.02	0.05	0.10	0.18	0.38	0.63	1.31	2.63	4.50	6.70	8.91	10.12
Conv10	0.09	0.19	0.38	0.75	1.47	2.84	5.52	10.56	19.66	33.61	42.98	45.51
AlexNet												
Conv1	3.65	7.32	8.62	11.78	12.19	13.42	14.13	14.51	14.57	14.67	14.68	14.70
MaxPool1	2.71	5.32	10.07	13.88	23.14	24.09	28.85	32.18	32.43	32.83	32.87	33.12
Conv2	9.04	17.87	34.83	48.31	50.03	63.49	78.25	79.18	83.13	85.21	86.36	86.46
MaxPool2	2.39	4.59	8.96	16.13	29.04	41.23	42.44	45.37	48.62	49.93	49.59	50.37
Conv3	2.97	5.81	11.57	22.43	42.98	59.82	63.38	65.26	74.03	79.92	80.39	82.07
Conv4	2.18	4.29	8.52	16.72	31.74	44.33	46.29	59.59	70.69	77.62	81.80	82.02
Conv5	0.60	1.19	2.37	4.61	9.03	16.13	29.33	41.50	42.93	48.96	54.35	54.93

Table 5.5: Convolution performance (arithmetic throughput, TFlops/s) of one IPU, in half precision, over our reference basket of convolutional neural network architectures. Missing data represents experiments that did not fit in device memory.

Layer name	Batch size							
	1	2	4	8	16	32	64	128
ResNeXt								
Conv1	7.45	14.23	15.04	11.95		7.75	17.82	
Conv2_1	30.60	39.87	47.74	55.50	62.07	55.93		
Conv2_2	0.18	0.23	0.28	0.30	0.32	0.32	0.49	0.49
Conv2_3	0.87	1.32	1.62	1.86	2.10	2.58	0.71	0.51
Conv2_4	0.37	0.75	0.92	1.03	1.10	1.14	0.46	
Conv3_1	1.57	2.62	3.90	5.19	6.23	6.90	2.17	1.83
Conv3_2	5.81	10.97	16.30	21.39	27.70	36.13	10.78	1.87
Conv3_3	2.54	4.27	6.19	7.99	9.33	10.22	3.91	1.72
Conv4_1	3.22	5.85	9.88	15.12	22.02	28.21	33.75	37.18
Conv4_2	10.28	15.78	20.59	33.03	41.61	45.69	45.26	50.12
Conv4_3	5.91	9.66	14.12	20.20	25.63	31.57	35.93	37.87
Conv5_1	2.74	4.82	8.74	14.41	20.22	28.05	35.76	45.81
Conv5_2	7.77	11.16	15.91	25.60	31.31	37.14	45.06	51.85
Conv5_3	4.84	8.45	13.36	18.98	27.61	33.41	41.51	47.44
ResNet-50 v1.5								
Conv1	7.45	14.23	15.04	11.95		7.75	17.82	
Conv2_1	30.58	39.91	47.74	53.98	62.32	55.82		
Conv2_2	11.85	18.92	26.73	36.84	46.03	52.39	55.93	59.29
Conv2_3	34.44	45.79	54.30	65.21	70.79	73.43	72.00	66.37
Conv2_4	27.48	35.51	44.54	51.39	56.99	58.55	43.21	
Conv3_1	16.23	22.59	27.89	35.41	43.79	54.87	60.86	57.06
Conv3_2	29.82	38.20	47.03	53.89	56.63	58.13	55.88	62.66
Conv3_3	23.16	32.72	41.29	51.86	59.07	62.39	45.49	45.58
Conv4_1	10.92	15.88	21.75	28.29	36.09	44.41	55.60	58.85
Conv4_2	26.53	32.99	41.86	47.94	52.66	52.78	50.36	51.51
Conv4_3	20.65	27.09	34.94	45.20	56.45	60.92	57.94	54.69
Conv5_1	10.30	15.56	20.84	26.60	34.44	41.43	51.27	55.72
Conv5_2	22.52	29.48	32.88	44.85		52.71	50.35	49.28
Conv5_3	21.39	27.91	32.84	42.66	49.81	57.72	55.14	53.44
Inceptionv3								
Conv1	2.90	2.66	2.82	3.17	5.70	7.08		
Conv2	44.61	58.19	70.92	71.59				
Conv3	55.98	69.61	70.25	67.43				
Conv4	37.05	45.06	51.92	57.36		49.85		
Conv5	43.30	52.82	61.51	65.65	65.66	63.77	63.55	
Conv6	32.79	41.10	46.42	55.94	61.90	50.70	35.80	
Conv7	51.80	58.89	59.99	62.12		58.10	61.71	
Conv8	44.93	50.85				49.13	49.05	
Conv9	36.64	45.56				43.23	43.58	
Conv10			49.27	41.35		42.81	45.57	
VGG16								
Conv1_1	6.33	5.36	7.20	7.08				
Conv1_2	75.04	74.89	69.21					
Conv2_1	68.90	72.60	70.71	70.41				
Conv2_2	71.79	70.87	69.25					
Conv3_1	64.05	69.31	70.20	69.03		66.61		
Conv3_2	65.29	72.10	69.13	69.07				
Conv4_1	57.55	58.53			56.39	56.07		
Conv4_2	57.56	58.54			56.39	55.88		
Conv5_1	41.40	46.76				49.92	46.93	
SSD v1.1								
Conv1				47.72	47.58	53.35		
Conv2	40.53	47.34				54.83	56.07	
Conv3	32.90	40.36	48.38	57.01		55.19	56.07	
Conv4	14.78	22.21	30.26	35.26	46.76	42.77		

Layer name	Batch size							
	1	2	4	8	16	32	64	128
Conv5	6.62	10.49	16.08	22.04	28.92	35.19	43.25	
Conv6	5.30	8.37	12.45	18.04	26.01	31.83	38.45	
Conv7	1.08	2.09	3.88	7.13	11.23	16.21	22.95	
Conv8	4.51	7.07	10.51	14.83	23.64	30.16	37.25	
Conv9	0.43	0.81	1.53	2.94	5.51	8.81	13.24	
Conv10	1.47	2.77	4.62	6.68	11.68	17.56	23.35	
AlexNet								
Conv1	8.40	9.75	11.14	11.15		20.04	17.07	
MaxPool1	20.22	28.43	37.38	43.72	51.12	51.73	47.83	
Conv2	44.03	57.30	62.83	64.34		61.69	60.52	
MaxPool2	24.40	28.69	36.60	44.66	49.21	46.32	42.26	
Conv3	28.05	37.17	45.68	52.25		53.70	51.04	
Conv4	28.62	34.72	42.61	51.43		52.91	50.10	
Conv5	12.20	16.15	20.35	26.10	33.43	41.77	44.11	

5.3 Pseudo-Random Number Generation

We compare IPU and GPU performance at bulk pseudo-random number generation (PRNG) in terms of aggregate throughput on a per-chip basis. We find that, thanks to its dedicated, in-core PRNG hardware units, the IPU generates up to 944 billion random samples per second (Gsamples/s), whereas a V100 GPU generates up to 192 Gsamples/s. While the IPU offers $4.9\times$ more aggregate throughput than a V100 GPU, it employs a PRNG algorithm that delivers a lower quality of randomness than the fastest algorithm we benchmarked on the GPU. The IPU’s performance advantage over the GPU doubles in a per-board comparison. We are not qualified to judge which platform the performance-quality trade-off favors. All details follow.

For simplicity, our benchmarks focus only on the generation of pseudo-random numbers extracted from a uniform distribution.

PRNG on the IPU. On the IPU, each tile includes PRNG acceleration circuitry that implements a variant of the *xoroshiro128+* algorithm by David Blackman and Sebastiano Vigna [15]. Details on the algorithm are available upon request from Graphcore. Our benchmark invokes the `poprand::uniform` function from the Poplar SDK. For sufficiently large blocks, the aggregate IPU throughput offered by the function reaches 944 Gsamples/s; see Figure 5.4.

PRNG on the GPU. On the GPUs, our benchmarks exercise PRNG func-

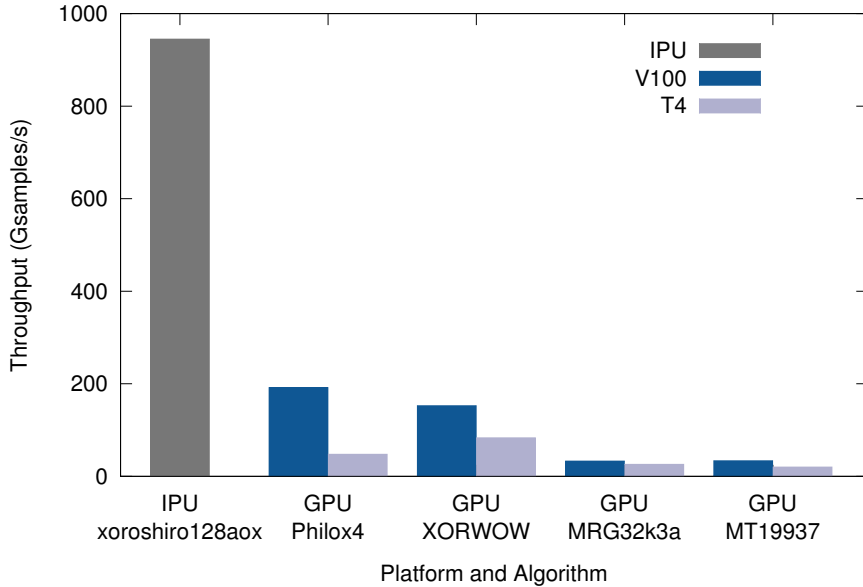


Figure 5.4: Bulk random number generation performance on IPU and GPUs: Peak generation throughput in billions random samples per second, uniform distribution. Per-chip comparison.

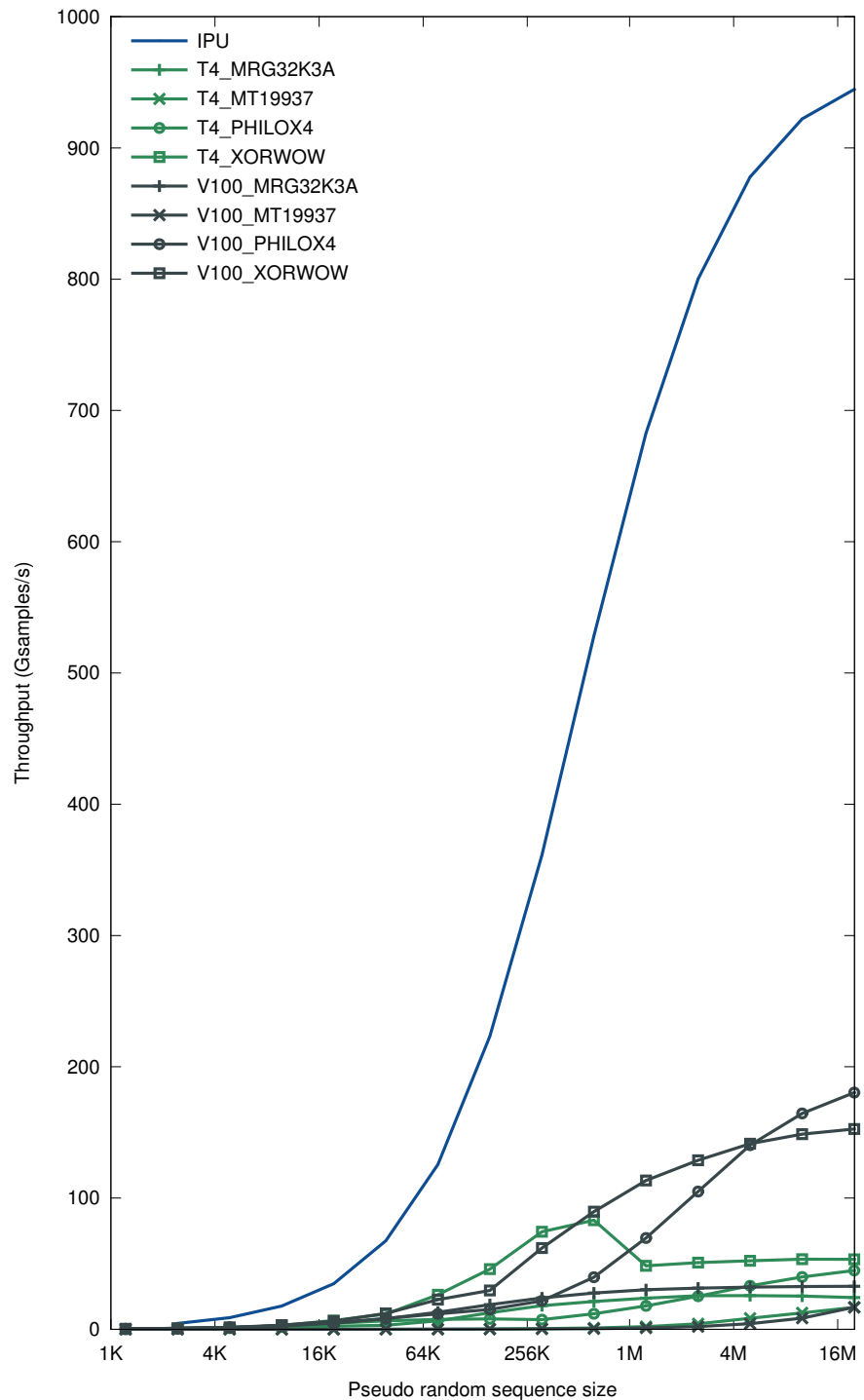


Figure 5.5: Bulk random generation throughput on IPUs and GPUs as a function of block size. Per-chip comparison.

tions offered with NVidia’s cuRand[16] library. cuRand supports multiple PRNG algorithms; we benchmark XORWOW, MRG32K3A, MTGP32, MT19937, Philox4. The fastest algorithm at volume on the V100 GPU is Philox4[17] by John Salmon. We run the experiment on each GPU (V100 and T4) at the maximum clock frequency supported by each device.

A comparison on the quality of randomness provided by PRNG algorithms (e.g., TestU01[18] performance) is beyond the scope of this paper.

Output size. We study how bulk PRNG performance varies as a function of requested output block size. Our results show that both on IPUs and GPUs, the generation of larger output blocks achieves higher throughputs. On the two platforms, performance grows and saturates similarly, as a function of output size (Figure 5.5)

List of Figures

1.1	Simplified block diagram of an IPU processor: the processor features 1,216 tiles (each containing one core and its local memory), the exchange (an on-chip interconnect), IPU link interfaces that provide connectivity to other IPU chips, and PCIe interfaces for host connectivity.	8
2.1	Topology and interconnection of C2 boards and IPU processors in the system that we employed in all our experiments. All IPU numbers in this figure are <i>Device IDs</i> . Board placement in the chassis is depicted accurately (see Fwd and Aft arrows).	18
2.2	Detailed tile layout within an IPU processor, including tile numbering. The logical tile IDs depicted are those exposed to the programmer. Tiles topologically close to each other actually experience shorter communication latencies than tiles farther away (see Section 4.1.2). Source: direct communication with Graphcore.	20
2.3	Topology of Multi-IPU virtual devices (depicted in red) with respect to the physical IPUs (in black). All numbers are Device IDs. For example, IPU16 is a virtual device containing physical IPUs 5 and 7. IPU30 is a virtual device containing all 16 physical IPUs in the server.	22
3.1	Aggregate local memory bandwidth on the entire IPU as a function of block size.	29
4.1	Communication topologies we evaluate in point-to-point latency benchmarks. Data transfers between the source and the destination tiles are depicted with blue arrows. The experiments are designed to exercise both on-chip (a) and off-chip (b,c,d) interconnects.	32
4.2	Minimum latency between all tiles belonging to the same Column on an IPU processor (we first presented columns in Figure 2.2).	34
4.3	Minimum latency between all pairs of tiles on an IPU processor.	35
4.4	Minimum latency between each pair of IPUs in our experimental 16-IPU system, measured in zero-congestion conditions. IPUs are numbered according to their <i>DNC IDs</i> , as discussed in Section 2.2.	36
4.5	The effect of physical proximity on tile-to-tile transfer bandwidth within an IPU is negligible, especially with large messages. In our experiments, the chosen pair of neighboring tiles is (0,1) and the chosen pair of far tiles is (0,644), consistent with the tile enumeration of Figure 2.2.	40

4.6	Peak monodirectional bandwidth between pairs of IPUs, in congestion-free conditions. IPUs are numbered according to their <i>DNC IDs</i> , as discussed in Section 2.2.	43
4.7	Topologies we benchmark in our broadcast and scatter experiments. Different topologies have different connectivity between source and destination tiles and perform differently. We depict data flows from the source to the destination tiles with blue arrows. Reversing all blue arrows depicts the data flows in the gather experiments.	45
4.8	Broadcast latency scaling. Left: scaling within an IPU (on chip). Right: scaling and across multiple IPUs (off chip).	48
4.9	Impact of block size on aggregate broadcast bandwidth. Each line represents a different experiment topology (a)-(j) as illustrated in Figure 4.7.	52
4.10	Impact of block size on broadcast bandwidth per tile. Each line represents a different experiment topology (a)-(j) as illustrated in Figure 4.7.	53
4.11	Effect of operand size on reduction bandwidth in weak scaling conditions. IPU identifiers are DNC IDs.	66
5.1	Floating-point arithmetic throughput achieved by dense matrix multiplication on one IPU. For simplicity, we use square inputs $(n \times n) \times (n \times n)$; the horizontal axis varies n	74
5.2	Matrix multiplication performance on IPUs and GPUs.	76
5.3	Energy efficiency while running matrix multiplication on IPUs and GPUs.	77
5.4	Bulk random number generation performance on IPU and GPUs: Peak generation throughput in billions random samples per second, uniform distribution. Per-chip comparison.	83
5.5	Bulk random generation throughput on IPUs and GPUs as a function of block size. Per-chip comparison.	84

Bibliography

- [1] Z. Jia, M. Maggioni, B. Staiger, and D. P. Scarpazza, "Dissecting the NVidia Volta GPU architecture via microbenchmarking," 2018. [Online]. Available: <https://arxiv.org/abs/1804.06826>
- [2] Z. Jia, M. Maggioni, J. Smith, and D. P. Scarpazza, "Dissecting the NVidia Turing T4 GPU architecture via microbenchmarking," 2019. [Online]. Available: <https://arxiv.org/abs/1903.07486>
- [3] D. Culler, R. Karp, D. Patterson, A. Sahay, K. E. Schauser, E. Santos, R. Subramonian, and T. von Eicken, "Logp: Towards a realistic model of parallel computation," in *Proceedings of the Fourth ACM SIGPLAN Symposium on Principles and Practice of Parallel Programming*, ser. PPOPP '93. New York, NY, USA: ACM, 1993, pp. 1–12. [Online]. Available: <http://doi.acm.org/10.1145/155332.155333>
- [4] A. Alexandrov, M. F. Ionescu, K. E. Schauser, and C. Scheiman, "Loggp: Incorporating long messages into the logp model — one step closer towards a realistic model for parallel computation," Santa Barbara, CA, USA, Tech. Rep., 1995.
- [5] J. Liu, B. Chandrasekaran, W. Yu, J. Wu, D. Buntinas, S. Kini, D. Panda, and P. Wyckoff, "Microbenchmark performance comparison of high-speed cluster interconnects," *IEEE Micro*, vol. 24, pp. 42 – 51, 02 2004.
- [6] M. Kistler, M. Perrone, and F. Petrini, "Cell multiprocessor communication network: Built for speed," *IEEE Micro*, vol. 26, no. 3, pp. 10–23, May 2006. [Online]. Available: <http://dx.doi.org/10.1109/MM.2006.49>
- [7] L. G. Valiant, "A bridging model for parallel computation," *Communications of the ACM*, vol. 33, no. 8, pp. 103–111, Aug. 1990. [Online]. Available: <http://doi.acm.org/10.1145/79173.79181>
- [8] The Ohio State University's Network-Based Computing Laboratory, "Osu micro benchmarks," 2019. [Online]. Available: <http://mvapich.cse.ohio-state.edu/benchmarks/>

- [9] S. Xie, R. Girshick, P. Dollar, Z. Tu, and K. He, "Aggregated residual transformations for deep neural networks," 2016.
- [10] K. He, X. Zhang, S. Ren, and J. Sun, "Deep residual learning for image recognition," 2015.
- [11] C. Szegedy, V. Vanhoucke, S. Ioffe, J. Shlens, and Z. Wojna, "Rethinking the inception architecture for computer vision," 2015.
- [12] K. Simonyan and A. Zisserman, "Very deep convolutional networks for large-scale image recognition," 2014.
- [13] W. Liu, D. Anguelov, D. Erhan, C. Szegedy, S. Reed, C.-Y. Fu, and A. C. Berg, "Ssd: Single shot multibox detector," *Lecture Notes in Computer Science*, pp. 21–37, 2016. [Online]. Available: http://dx.doi.org/10.1007/978-3-319-46448-0_2
- [14] A. Krizhevsky, I. Sutskever, and G. E. Hinton, "Imagenet classification with deep convolutional neural networks," pp. 1097–1105, 2012.
- [15] D. Blackman and S. Vigna, "Scrambled linear pseudorandom number generators," *preprint article*, 2019. [Online]. Available: <http://vigna.di.unimi.it/ftp/papers/ScrambledLinear.pdf>
- [16] NVidia, "cuRand – the API reference guide for cuRand, the CUDA random number generation library," 2019. [Online]. Available: <https://docs.nvidia.com/cuda/curand/index.html>
- [17] J. Salmon, M. Moraes, R. Dror, and D. Shaw, "Parallel random numbers: As easy as 1, 2, 3," 11 2011, p. 16. [Online]. Available: <https://thesalmons.org/john/random123/papers/random123sc11.pdf>
- [18] P. L'Ecuyer and R. Simard, "TestU01: A c library for empirical testing of random number generators," *ACM Transactions on Mathematical Software*, vol. 33, 2007.

The Authors



Zhe Jia is a senior R&D engineer with the High-Performance Computing group at Citadel. Prior to this position, he was a senior R&D engineer with Alicloud, and a software engineering intern at Microsoft, Beijing. He received his B.S. degree in Physics and his M.S. degree in Meteorology from Peking University, China. His interests include the performance optimization of deep learning, numerical modeling, and atmospheric simulation workloads.



Blake Tillman is a Software Engineer with the High-Performance Computing group at Citadel. He joined the firm in July 2019, after receiving a B.S. degree in Computer Science and a B.S. degree in Mathematics. Prior to joining Citadel, Blake completed internships at Google and Apple.



Marco Maggioni is a senior R&D engineer with the High-Performance Computing group at Citadel, Chicago. He received his Ph.D. in Computer Science from the University of Illinois at Chicago, where he focused on sparse linear algebra and convex optimization on GPUs. His research established records for the fastest sparse matrix-vector multiplication GPU kernel in research and industry.



Daniele Paolo Scarpazza leads the High-Performance Computing group at Citadel, Chicago. Prior to this position, he was a Research Scientist with D. E. Shaw Research, a Research Staff Member with the IBM T. J. Watson Research Center, and a Post-Doc with the Pacific Northwest National Laboratory. He received his Ph.D. in Information Engineering from Politecnico di Milano, Italy. He is the co-recipient of a Gordon Bell prize. He focuses on quantitative performance analysis and optimization of algorithms on parallel architectures.